BOLT BERANEK AND NEWMAN INC

CONSULTING • DEVELOPMENT • RESEARCH

NASA CR-114370

AERODYNAMIC SOUND RADIATION FROM LIFTING SURFACES WITH AND WITHOUT LEADING-EDGE SERRATIONS

By Alan S. Hersh and Richard E. Hayden

Prepared under Contract No. NAS2-5974 by
BOLT BERANEK AND NEWMAN INC.
21120 Vanowen Street
Canoga Park, California 91303

for

NATIONAL AERONAUTICS AND SPACE ADMINISTRATION

AMES RESEARCH CENTER

AERODYNAMIC SOUND RADIATION FROM LIFTING SURFACES WITH AND WITHOUT LEADING-EDGE SERRATIONS

By Alan S. Hersh and Richard E. Hayden

Prepared under Contract No. NAS2-5974 by
BOLT BERANEK AND NEWMAN INC.
21120 Vanowen Street
Canoga Park, California 91303

for

NATIONAL AERONAUTICS AND SPACE ADMINISTRATION

AMES RESEARCH CENTER

TABLE OF CONTENTS

TABLE OF CONTENTS (Cont)

LIST OF FIGURES

LIST OF FIGURES (Cont)

LIST OF FIGURES (Cont)

LIST OF FIGURES (Cont)

LIST OF SYMBOLS

A,B,C	Serration dimensions defined in Figure 9
c	Airfoil chord length
c_o	Speed of sound
C_L	Lift coefficient, $L/\frac{1}{2}\rho U^2 S$
d	Maximum thickness of airfoil or propeller
D	Drag
f	Frequency
[f(ω),g(ω)]	Power spectral functions defined by equations B-10 and B-12 respectively
F	Force
$\overline{F}'$	Mean root square flucuating force $\sqrt{\langle F^2 \rangle}$
k	Ratio of chord length to gust wavelength, ωc/2V
L	Lift, also scale of turbulence defined by Eq. B-8
M	Moment
p	Acoustic pressure
P	Aerodynamic static pressure
R_c	Chord based Reynolds number, Vc/ν
R	Airfoil leading edge radius of curvature
R(t),R(x)	Autocorrelation function
r	Distance
S	Surface area, also side force, also Strouhal number, $(\frac{fd}{V})$
t	Time
u,w	Velocity component in x,z directions respectively
V	Mean velocity in x-direction
x_{LE}	Distance of airfoil leading edge from jet exit plane

x,y,z	Cartesian coordinates
α,α_o	Angle of attack
θ,ϕ	Spherical angles defined by Figure 2
ν	Kinematic coefficient of viscosity
τ	Delay time
ω	Circular frequency, $2\pi f$
η	Ratio of chord length to eddy size, $\pi c/L$

Subscripts:

c	Chord length
fj	Free jet
i	Component in i^{th} direction
j	Jet
LE	Leading edge

Superscripts:

$(\dot{})$	Denotes time derivative
$(\bar{})$	Denotes time average

Conventions:

< >	Denotes time average

AERODYNAMIC SOUND RADIATION FROM LIFTING SURFACES WITH AND WITHOUT LEADING-EDGE SERRATIONS

By Alan S. Hersh and Richard E. Hayden*
Bolt Beranek and Newman Inc.

SUMMARY

A series of fundamental studies have been conducted to understand how lifting surfaces radiate sound in both smooth and turbulent flow. The application of leading edge serrations as a device for reducing the sound radiated from these surfaces was studied for the case of smooth inflow.

The directivity pattern radiated by a *small* airfoil (1 in. chord) in flow (268 ft/sec) has been compared with that predicted by Curle's point dipole sound theory, and found to be sufficient to present a partial check on that aspect of his theory.

A theoretical model predicting the sound radiated from a *small* airfoil (2-in. chord) in turbulent flow shows good agreement with experiment over a wide speed range (258 to 804 ft/sec). The good agreement between theory and experiment suggests that for small airfoils in turbulent flow, most of the radiated sound is generated by the time-derivative of the fluctuating lift induced by the turbulent flow.

The effect of leading edge serrations as a noise reduction device has been studied on a NACA 0012 shaped airfoil (6-in. chord) and two-bladed propeller (14-in. diameter) operating in a smooth inflow at chord based Reynolds numbers from 8.33×10^4 to 3.33×10^5. Loud distinct tones were observed to radiate from these surfaces in the Reynolds number range tested, corresponding to a predominantly laminar boundary layer. The tones are generated by vortices being shed into the airfoil and propeller wake at a periodic or near periodic rate. Properly designed and properly located leading edge serrations remove the tones by generating chordwise trailing vortices that change the character of the wake vortex shedding from periodic to broadband resulting in power level reductions up to 37 dB.

---

* The authors gratefully acknowledge helpful conversations with Professor W. C. Meecham, School of Engineering and Applied Science, UCLA, and consultant to BBN, and Dr. D. A. Bies of the Canoga Park, California, office of BBN.

1. INTRODUCTION

Aerodynamic sound generation from lifting surfaces that rotate as propulsive devices or are stationary as lifting surfaces is one of the dominant noise sources for a variety of subsonic aircraft, including helicopters, V/STOL aircraft, propeller driven aircraft, and gliders. Effective reduction of aircraft noise requires identification of the various acoustic sources and understanding of their physical mechanisms.

This report examines three rather fundamental aspects of aerodynamic sound generation from stationary and rotating lifting surfaces. The theory of sound radiation from stationary and rotating lifting surfaces is reviewed in Section 2 of this report. This section provides the basis for the proper interpretation and understanding of the three fundamental studies discussed in Sections 3, 4 and 5.

In Section 3, measurements of the directivity pattern radiated from the fluctuating lift and drag of a small airfoil are compared with theory. In Section 4, a theoretical model predicting the noise radiated from a small, two-dimensional airfoil in turbulent flow is developed and compared with experiment.

Section 5 presents and interprets a series of extensive studies of the application of leading edge serrations as a device for reducing the vortex noise radiated from stationary and rotating lifting surfaces. In these studies, a variety of serrations were attached at selected locations near the leading edge of a two-dimensional airfoil and a two-bladed, variable pitch model propeller. The effects of the serrations on both the acoustic and aerodynamic performance are discussed and a theoretical interpretation of the results given. This novel approach to noise reduction was developed by Paul T. Soderman of the NASA-Ames Research Center [1]. In his pilot experiments, Soderman achieved significant noise reductions by attaching to a propeller small sawtooth serrations near the leading edges. Soderman's studies were motivated by the observation that owls, which fly very quietly, have small comblike feathers located near the leading edge of their wings.

Section 6 summarizes the principal conclusions from this study and offers recommendations for further work.

2. REVIEW OF AERODYNAMIC SOUND THEORY FOR STATIONARY AND ROTATING LIFTING SURFACES

2.1 Curle's Dipole Sound Theory

Curle's dipole sound theory is commonly used to predict the level and directivity of sound radiated from surfaces in flow [2]. Curle's theory represents an extension of Lighthill's aerodynamic sound theory [3]. Lighthill shows that the fluctuating fluid stresses in a turbulent flow can generate sound in the absence of solid surfaces within the flow. These stresses are equivalent to a distribution of volume quadrupoles. Curle shows that whenever surfaces are present in the flow, the volume quadrupoles are supplemented by additional surface sources. These additional sources, which are equivalent to a distribution of acoustic dipoles, are more efficient radiators at subsonic flow speeds than the volume quadrupoles; thus these surface sources are likely to overwhelm any quadrupoles in the nearby flow.

Recent studies by Clark and Ribner [4], Gordon [5], and Heller [6] have established quite conclusively that the surface-generated sound can be correlated directly with the fluctuating force field produced by interaction of the fluid with the surface. Clark and Ribner, in particular, show that the instantaneous sound radiated by a small airfoil (relative to a typical acoustic wavelength) immersed in a turbulent flow and its fluctuating lift are connected by Curle's equation.

Curle supplemented Lighthill's equation with the following expression

$$p(\underline{x},t) = -\frac{1}{4\pi c_o}\frac{\partial}{\partial x_i}\int_S \frac{P_i(\underline{y},t-r/c_o)}{r}\,dS(\underline{y}) \quad , \qquad (1)$$

which represents the radiation of sound $p(\underline{x},t)$ due to the presence of the surface S immersed in a flow. Here, P_i is the reaction force per unit surface area exerted by the surface upon the fluid in the i-direction, $\underline{x}$ is the vector distance to the observation point, $\underline{y}$ is the vector distance to the center of the differential surface area $dS(\underline{y})$, and $r = |\underline{x}-\underline{y}|$.

In the far field, Curle shows that Eq. (1) reduces to

$$p(\underline{x},t) = -\frac{1}{4\pi c_o}\frac{x_i}{x^2}\frac{\partial}{\partial t}\int_S P_i(\underline{y},t-x/c_o)dS(\underline{y}) \quad . \tag{2}$$

If the surface characteristic length is small relative to a typical wavelength of the radiated sound, the retarded time delay over the surface may be neglected in Eq. (2) resulting in the following simplified expression for the sound pressure level,

$$\langle p^2\rangle = \frac{1}{16\pi^2 c_o^2 x^4}\langle(\underline{x}\cdot\dot{\underline{F}})^2\rangle \quad , \tag{3}$$

where $\dot{\underline{F}}$ represents the time derivative of the fluctuating force exerted upon the fluid by the surface.

Equation (3) represents the starting point for most estimates of the level and directivity of the sound radiated from small surfaces in flow. The dipole nature of the sound radiation follows immediately from dimensional analysis. Assuming that the fluctuating force is proportional to $\rho V^2 L^2$ and that the time derivative operator ($\dot{}$) is proportional to V/L where L is a characteristic surface dimension, the radiated sound pressure may be expressed as

$$\langle p^2\rangle \sim \frac{\rho^2 L^2 V^6}{c_o^2 x^2} \tag{4}$$

which is equivalent to the sound pressure radiated from a point dipole.

2.2 Sound Radiation from Stationary Lifting Surfaces

Curle has shown that the sound radiated from rigid surfaces in flow is related to the time derivative of the fluctuating forces imparted to the surrounding fluid. The fluctuating forces arise from (1) upstream turbulence generating a fluctuating angle of attack, (2) boundary-layer (Strouhal) spanwise wake vortex shedding (including stall as a limiting case), and (3) turbulent boundary layers. These three mechanisms are not really independent; they interact through nonlinear fluid mechanical processes. Sharland [7] and Siddon [8] have shown, however, that under certain conditions it is reasonable to separate the three. For example, when the upstream flow approaching

an airfoil is smooth, most of the fluctuating forces arise from wake vortex shedding. Conversely, most of the fluctuating forces arise from a fluctuating incident angle of attack when the flow is highly turbulent.

In smooth flow, stationary lifting surfaces such as aircraft wings radiate sound due to lift and drag fluctuations induced primarily by wake vortices. The wakes of most bodies contain vortices which shed at discrete frequencies over a wide range of Reynolds numbers. These wake vortices are responsible for generating several different kinds of acoustic phenomenon, the most famous being the Aeolian tone. An excellent summary of wake vortex shedding and its connection to the Strouhal number has been given by Ross [9].

It was Strouhal who first observed that the frequency of Aeolian tones is proportional to flow speed and inversely proportional to the diameter of a wire shedding vortices [10]. Rayleigh was the first to use dimensional analysis to show that the Strouhal number should be a function, at low speed flow, only of the Reynolds number [11]. Relf firmly connected the acoustic and hydrodynamic phenomena when he showed that the frequency heard from a wire in flow is the same as the frequency of the shed vortices [12].

Not only do wakes of bluff bodies contain vortices, but so do the wakes of airfoils. Gongwer investigated the effect on the Strouhal number of varying the trailing edge thickness of aerodynamically shaped vanes in water [13]. He found that the Strouhal number was $S \doteq 0.185$ over the range of vane trailing edge thicknesses tested with the characteristic vane diameter defined as the sum of the trailing edge thickness and the local boundary layer momentum thickness. Of particular interest is the study by Bauer who defined the Strouhal number with the characteristic length being the sum of the local trailing edge thickness and the total boundary layer displacement thickness for flat plates and for a NACA 0012 airfoil [14]. He found values of the Strouhal number of the order of 0.20 to 0.26 for both the flat plate and the NACA 0012 airfoil.

Most of the studies of aerodynamic sound radiation from stationary surfaces have been restricted to the case where the characteristic surface dimensions are small relative to a typical acoustic wavelength. When the surface dimensions are small, the contribution of the turbulent boundary layer (TBL) to the total radiated sound is usually negligible relative to the contribution from the wake or, if the flow is highly turbulent, from the angle of attack fluctuations induced by the turbulence. Recent studies by Hayden and Chanaud of the sound radiation from airfoils

having a large chord (relative to a typical acoustic wavelength) show that the interaction of the TBL with the trailing edge imparts momentum fluctuations to the surrounding medium and the total radiated spectrum may be separated into TBL-dominated components and wake-dominated components [15,16]. Hayden and Chanaud found that when the TBL is thin (relative to the airfoil thickness), the wake contribution to the total radiation sound dominates that due to the TBL interaction with the trailing edge.

2.3 Sound Radiation from Rotating Lifting Surfaces

The sound radiated from rotating lifting surfaces such as propellers, rotors, and fans differs from that from stationary surfaces in that periodic or discrete components, historically called rotational noise, appear in the sound spectrum arising from the steady and periodic loads acting upon the fluid in the neighborhood of the rotating blades.

The steady loads are defined as the time-average rotating lift and drag forces. The periodic loads are associated with (1) non-uniform but steady inflow, (2) periodic vibration of the lifting surface blades, and (3) cyclic pitch changes. The steady loads may be modeled by a mean circulation about the lifting surface blades; the periodic loads may be modeled by a periodic circulation about the lifting surface blades. In both cases, the fluid dynamic loads may be characterized as being inviscid. Although the circulation is initially created by the viscosity of the fluid, the circulation may be subsequently modeled by a distribution of bound, shed, and tip vortices.

The nondiscrete or broadband sound components of the sound spectrum, historically called vortex noise, are generated by the randomly fluctuating lift and drag forces (in both amplitude and phase) imparted to the surrounding fluid. The various random forces arise from (1) boundary-layer (Strouhal) spanwise vortex shedding (including stall as a limiting case), (2) upstream turbulence inducing angle-of-attack fluctuations, (3) the blade turbulent boundary layer, (4) vortex shedding interaction between rotating blades, and (5) random blade vibration.

Stowell and Deming were the first to study the relation between vortex wake shedding from a rotating cylindrical rod and the subsequent radiated sound [17]. They showed that the size or scale of the vortices shed was approximately constant along the rod with magnitude 1/5th of

the rod diameter. Later, Yudin observed that a body shedding vortices experiences an alternating force which he related to an acoustic dipole [18]. Originally only a supposition on the part of Yudin, this concept was later confirmed by Curle [2] to be a consequence of Lighthill's basic theory of aerodynamic sound [3].

Hubbard [19] extended Yudin's work on rotating rods to the practical case of rotating airfoils and found that the radiated sound power due to vortex noise was proportional to the blade area and the sixth power of a characteristic blade section velocity. Schlegel et al [20] developed an empirical prediction scheme for vortex noise from a certain class of propellers based on mean lift and drag coefficient and a characteristic velocity to the sixth power. Schlegel's work does not account for vortex noise from symmetrical airfoil sections when the section angle of attack is zero (i.e., no lift or thrust) and thus may not be generally used.

In addition to generating acoustic dipole sources, a rotating blade also generates acoustic monopole and quadrupole sources. The monopole acoustic sources are generated by the blade thickness which imparts a periodic volumetric flow rate to the surrounding fluid. The quadrupole acoustic sources are generated by the fluctuating shear stresses imparted to the surrounding fluid. For thin lifting surfaces operating at moderate subsonic speeds, the sound radiated from the monopole and quadrupole sources is negligible relative to the sound radiated from the dipole sources and, hence, will not be considered in this study.

3. SOUND DIRECTIVITY PATTERN RADIATED FROM SMALL AIRFOILS

Although Curle's dipole sound theory is commonly used to predict the sound pressure level and directivity radiated from surfaces in flow, only the sound pressure level part of his theory has been verified for the case where the characteristic dimensions are small in comparison to a typical wavelength of the radiated sound. The purpose of this section is to provide an additional check on Curle's theory by measuring and comparing with his predictions the sound directivity pattern radiated by a small airfoil in flow. According to Curle's theory, the fluctuating lift and drag of airfoils with characteristic dimensions that are small in comparison to a typical wavelength of the radiated sound may be modeled as point dipoles. The resulting directivity pattern sould, therefore, be dipole in nature.

3.1 Basic Equations

According to Curle, the sound pressure level and directivity radiated from a small airfoil in flow may be estimated from Eq. (3), rewritten here for convenience,

$$\langle p^2 \rangle = \frac{1}{16\pi^2 c_o^2 x^4} \langle (\underline{x} \cdot \mathring{\underline{F}})^2 \rangle \ . \qquad (3)$$

The fluctuating force $\mathring{\underline{F}}$ imparted to an airfoil in flow may be resolved at, say, time $\overline{t}$ into the three orthogonal components $(\mathring{S},\mathring{D},\mathring{L})$ representing a fluctuating side force $\mathring{S}$, drag force $\mathring{D}$, and lift force $\mathring{L}$. The observation point (or microphone location) x may similarly be resolved into the components $(x \sin\theta \sin\phi,\ x \sin\theta \cos\phi,\ x \cos\theta)$. Substituting these into Eq. (3) results in the following expression for the sound pressure level

$$\langle p^2 \rangle = \frac{1}{16\pi^2 c_o^2 x^4} \langle [\mathring{S}x \sin\theta \sin\phi + \mathring{D}x \sin\theta \cos\phi + \mathring{L}x \cos\theta]^2 \rangle . \qquad (5)$$

3.2 Experimental Program

Measurements of the directivity pattern radiated from a small airfoil in flow were conducted in the UCLA free-jet anechoic facility. The facility and the instrumentation used to record the measurements are described in Appendix A.

A symmetrical airfoil was used in this study having a chord length of 1 in., a maximum thickness of 0.24 in., and a span of 4 in. Since the measurements show that the radiated sound is quite insensitive to airfoil angle of attack changes (below stall), the airfoil angle of attack was fixed at zero degrees throughout the tests. The airfoil is supported by a simple yoke apparatus attached to a 1-1/2 in. diameter pipe mounted parallel to the floor of the anechoic room. A schematic of the airfoil, support apparatus, pipe and microphone angular path is shown in Fig. 1. To simplify the analysis, we chose to support the airfoil in the two positions shown in the upper half of Fig. 2. In the horizontal position, the plane of symmetry of the airfoil is parallel to the floor; in the vertical position, the plane of symmetry of the airfoil is perpendicular to the floor. Referring again to Fig. 1, the microphone is rotated through the arc shown and lies in a plane which is parallel to the floor and co-planar with the plane passing through the axis of the jet.

The contribution to the radiated sound from the fluctuating side forces $\dot{S}$ is ignored since it is quite small relative to $\dot{L}$ and $\dot{D}$. When the airfoil is in the horizontal position, the contribution of the fluctuating lift $\dot{L}$ vanishes because it is orthogonal to the microphone path which lies in the $x_3 = 0$ plane (see the lower half of Fig. 2). Thus, Eq.(5) simplifies to

$$\langle p^2 \rangle_{\text{horiz.}} = \frac{\cos^2\phi}{16\pi^2 c_o^2 x^2} \langle (\dot{D})^2 \rangle + \langle p^2 \rangle_{f.j} \quad , \tag{6}$$

where $\langle p^2 \rangle_{f.j}$ represents the background noise of the free jet.

When the airfoil is in the vertical position, however, the fluctuating lift $\dot{L}$ is rotated 90 degrees so that is lies in the $x_3 = 0$ plane. For this case, Eq. (5) reduces to

$$\langle p^2 \rangle_{\text{vert}} = \frac{\cos^2\phi \langle \dot{D}^2 \rangle + \sin^2\phi \langle \dot{L}^2 \rangle}{16\pi^2 c_o^2 x^2} + \langle p^2 \rangle_{f.j} \quad , \tag{7}$$

where by symmetry, at zero angle of attack, we expect $\langle \dot{D}\dot{L} \rangle = 0$.

Since we anticipate that the fluctuating lift is much larger than the fluctuating drag, the radiated sound pressure level should be considerable larger when the airfoil is held in the vertical position rather than in the horizontal position. The experimental data shown in Fig. 3 demonstrates

that this is indeed the case. Here, the center jet velocity at the nozzle exit is 268 ft/sec. The angle of attack is set at zero degrees and the leading edge is located 1 in. from the nozzle exit. Thus, most of the airfoil is located within the jet core--with only a small fraction of its surface within the shear region of the expanding jet. To ensure that the ratio of acoustic wavelength to the chord length is sufficiently large to model the sound source as a classical dipole, we present in Fig. 3 the radiated directivity pattern for the 1250-Hz 1/3-octave band which corresponds to a ratio of acoustic wavelength to airfoil chord of 10.56. Figure 3 contains plots of the sound pressure levels corresponding to the background of the free-jet, the free jet and airfoil in the horizontal position, and the free jet and airfoil in the vertical position. As expected, the noise levels are considerably larger when the airfoil is in the vertical position.

The procedure for determining the radiated sound from the drag and lift dipoles follows immediately from Eqs. (6) and (7). The background noise from the free jet is first subtracted from the $\langle p^2 \rangle_{horiz}$ data which determines the drag dipole, $\langle p^2 \rangle_{drag}$. (Recall from the earlier discussion that in the horizontal position, the lift dipole is orthogonal to the microphone-boom plane; hence its vector product vanishes as $\theta = 90^o$--see Eq. (5).) The experimental drag dipole data are shown in the lower half of Fig. 4. Since we did not measure the values of the fluctuating forces, we fitted, rather arbitrarily, the classical expression for the drag dipole (see Eq. (6)) to the data at the angle $\phi = 70^o$. The comparison is quite good for $\phi \leq 80^o$. We believe the poor agreement between the theory and experiment for $\phi \geq 80^o$ is due primarily to interference (reflection of the radiated sound) by the supporting yoke structure.

The lift dipole $\langle p^2 \rangle_{lift}$ follows immediately from Eq. (7); here we subtract $\langle p^2 \rangle_{drag}$ and $\langle p^2 \rangle_{f.j}$ from the $\langle p^2 \rangle_{vert}$ data. (They are both invariant to angular rotation due to symmetry of the jet exhaust.) Figure 4 shows that the minimum of the experimental drag dipole data and the maximum of the lift dipole data both occur at $\phi = 80^o$ instead of at the theoretical angle $\phi = 90^o$. This result is perhaps due to refraction effects arising from the sheared jet. In addition, the lift dipole data show that for $\phi < 70^o$, sound pressure levels of the data are greater than that predicted by theory, but for $\phi > 90^o$ they are less. We believe this difference may be due to residual convection of the fluid volume sources by the jet velocity, because the sound pressure levels would be increased by convection effects when the sources are directed towards the microphone and decreased when they are directed away from the microphone.

Figure 5 shows a comparison between theory and data for the 8000-Hz 1/3-octave band center frequency, which corresponds to a ratio of acoustic wavelength to airfoil chord of 1.65. For this case, the agreement between theory and data is poor. This result is to be expected from Eq. (3) which is valid only for large ratios of wavelength to chord.

We believe the comparison between theory and experiment, for the sound angular distribution, to be sufficient to present a partial check on the validity of Curle's equation for the case of a surface whose dimensions are small relative to the wavelength of the radiated sound.

4. THEORY OF SOUND RADIATION FROM SMALL AIRFOILS IN TURBULENT FLOW

In this section, we present and compare with experiment a theoretical model of the sound radiated from a small two-dimensional airfoil in turbulent flow. We assume that virtually all the fluctuating forces are caused by variations of angle of attack due to upstream turbulence.

4.1 Theoretical Model

The lift and drag of a small, thin two-dimensional airfoil of chord c moving with velocity V through a turbulent fluid will fluctuate because of angle-of-attack fluctuations. Liepmann [21] proposed a simple analytical model of the mean square lift fluctuations $\langle L^2 \rangle$ for application to airfoil flutter and fatigue. (The mean square drag fluctuations $\langle D^2 \rangle$ are small relative to $\langle L^2 \rangle$, hence are ignored.) Liepmann's model can be immediately extended to predict airfoil sound radiation by using Curle's equation to connect the time derivative of the mean square lift $\langle L^2 \rangle$ to the radiated sound.

Liepmann assumed that the relationship between the fluctuating angle of attack of the airfoil and the resulting lift is given by thin airfoil theory. The airfoil is located at the origin of a coordinate system x,y,z where the mean flow is V-directed along the positive x-axis. The airfoil is infinitely extended in the y-direction. Within the frame of unsteady thin wing theory, the airfoil is replaced by a *lifting point* at the origin responding to angle-of-attack fluctuations in the x-z plane. The effect of the finite airfoil chord c is absorbed in an admittance function which relates the frequency and magnitude of the lift to the frequency and magnitude of the angle-of-attack fluctuations at the origin.

A detailed derivation of Liepmann's model and its extension to predict sound radiation from small airfoils in turbulent flow is given in Appendix B. The overall sound pressure radiated at a distance x from a small airfoil to chord c immersed in turbulent flow of intensity $\langle w^2 \rangle / V^2$ and characteristic eddy scale L is given from Eq. (B.17) of Appendix B as

$$\langle p^2 \rangle = \frac{\langle w^2 \rangle}{V^2} \cdot \frac{\rho^2 S^2 V^6}{16\pi^2 c^2 c_o^2 x^2} \left[\frac{\eta^2(4\eta+3\pi)}{4\pi(\eta^2+1)} + \frac{5\eta^2(1-\eta^2)}{4(\eta^2+1)^2} + \frac{(3\eta^2+5)}{\pi(\eta^2+1)^2} \eta^3 \log\eta \right], \tag{8}$$

where $\eta = \pi c/L$. Equation 8 shows that the overall sound pressure radiated from small airfoils in turbulent flow is independent of mean angle-of-attack below stall.

We note that Eq. (8) diverges for large values of η which corresponds to an airfoil of large chord in small-scale turbulence. We believe that the model breaks down for large η because we have neglected to account for time delay effects along the airfoil surface. Since Liepmann applied his theory to airfoil buffeting and fatigue, he did not have to be concerned about time delay effect. In Eq. (1) of Section 2.1, we showed that the sound radiated from a small rigid surface may be written as

$$p(\underline{x},t) = -\frac{1}{4\pi c_o}\frac{\partial}{\partial x_i}\int_S \frac{P_i(\underline{y},t-r/c_o)}{r}\, dS(\underline{y}) \,, \qquad (1)$$

repeated here for convenience. If the airfoil chord $c << c_o/\omega$, where ω is a typical sound frequency, then, in Eq. (1), we may neglect the time delay r/c_o, and Eq. (1) simplifies to

$$p \doteq \frac{1}{4\pi c_o}\,\frac{x_i}{x^2}\,\frac{\partial}{\partial t}\,F_i(t) \doteq \frac{\dot{L}(t)}{4\pi c_o x^2} \,. \qquad (9)$$

Thus, time delay is important when ω is large. Large ω, however, corresponds to small eddy sizes (recall that under our assumption of frozen turbulent flow--see Appendix B-- $\omega \sim 2\pi/\tau = 2\pi c_o/L$). Thus, the model is valid only when the ratio of eddy size L to airfoil chord c is of order unity or larger.

4.2 Experimental Program

A series of experiments were conducted in the UCLA free-jet anechoic facility to verify Eq. (8). The experiments consisted of placing a small 2-in. chord, 8-in. span, NACA 0012 section airfoil in the turbulent mixing region of the jet exhaust. The leading edge of the airfoil was located 10.25 in. downstream of the jet exit plane well into the intense turbulent mixing region of the jet exhaust. Sound pressure measurements were recorded for local jet centerline velocities of 258 ft/sec, 393 ft/sec, and 804 ft/sec with the airfoil oriented in the vertical position at a zero angle-of-attack (see Appendix A and Section 3 for a description of the facility and the experimental set-up). The measurements showed that the radiated sound was quite insensitive to

angles-of-attack changes below stall which is consistent with the derivation of Eq. 8. The microphone was located at $\phi = 90$ degrees. Figure 6 shows 1/3-octave band sound pressure levels and overall sound pressure levels for the three velocities tested. We note that most of the sound energy occurs at frequencies sufficiently low to warrant using the point dipole model of Eq. (8).

Measurements of the turbulent intensity $\sqrt{\langle w^2 \rangle}/V$ and eddy size L of a subsonic circular jet by Davies *et al* [22] show that in the turbulent mixing region of a subsonic jet,

$$\frac{\langle w^2 \rangle}{V_c^2} \doteq 2.25 \times 10^{-2} \text{ and } L \doteq 1 \text{ in.} \quad , \qquad (10a,b)$$

where $V_c = 0.6\ V$ is the average convection velocity of the eddies.[c] Using these values and assuming that an effective surface area is $S \doteq 1.5$ in. by 2 in. (since the jet velocity decays in the radial direction from its maximum value at the jet axis), we show in Fig. 7 a comparison between Eq. (8) and the data. Considering the approximations made, the comparison is reasonably good.

The good agreement between the theoretical model and the experimental data supports the ideas of Sharland [7] and Siddon [8] that for airfoils in highly turbulent flow, most of the radiated noise is generated by the time-derivative of the fluctuating lift induced by the turbulent flow.

5. STUDIES OF LEADING-EDGE-SERRATIONS AS A DEVICE FOR REDUCING AERODYNAMIC SOUND RADIATION FROM LIFTING SURFACES

In this section, we present and interpret a series of extensive studies of the application of leading-edge-serrations as a device for reducing vortex noise radiated from stationary and rotating lifting surfaces. The tests were made in the BBN quiet wind tunnel on a stationary two-dimensional NACA 0012 profile airfoil and on a NACA 0012 profile, two-bladed, variable pitch propeller. The present study has been motivated by Soderman's pilot experiments [1,23] which are reviewed below.

5.1 Review of Soderman's Studies

Soderman [1] attached serrations of various size and shape to the leading edge of a 5-ft diameter, two-bladed, model tail rotor. The rotor blade had a NACA 0012 section with a constant 2-3/4 in. chord and a square tip. The rotor was tested in hover condition with the thrust axis horizontal. Noise measurements were made with and without the serrations at rotational speeds between 840 and 1440 rpm. The serrations reduced the overall sound pressure levels from about 4 to 8 dB. Spectral measurements clearly showed that the serrations substantially reduced the high-frequency sound by eliminating a high-frequency "sing" generated by the unmodified rotor.

In another study, Soderman investigated the effects of serrations on the flow over lifting surfaces [23]. This study consisted of wind-tunnel tests of the flow field over and the aerodynamic performance of a two-dimensional NACA 66_1-012 airfoil. The airfoil chord and span were 30 in. and 40 in., respectively. End plates were attached to increase the region of two-dimensional flow. Serrated brass strips of various sizes and shapes were attached at several locations near the airfoil leading edge. Force and moment data were recorded, and photographs were taken of tuft patterns and oil flow patterns. The Reynolds number based on the chord was 2.3×10^6.

The flow visualization photographs show that the serrations generate chordwise trailing three-dimensional vortices over the airfoil upper surface which resemble Taylor-Göertler vortices. These vortices bring higher energy air into the boundary layer, thereby delaying the leading-edge and trailing-edge flow separation to higher angles of attack thereby increasing maximum lift. The flow visualization photographs also suggest that the vortices decrease the airfoil wake thickness. These results

strongly suggest that the vortices play an important role in the rotor noise reductions achieved with the serrations. Measurements show that the maximum lift is quite sensitive to serration size and position on the airfoil and spacing between serrations.

5.2 Study of the Effects of Leading-Edge Serrations on a NACA 0012 Airfoil

5.2.1 Acoustic Tests

A series of tests were conducted to study the effects of leading-edge serrations on sound radiation from a two-dimensional NACA 0012 airfoil of 6-in. chord and 30-in. span in smooth flow. The tests were conducted in the BBN free-jet acoustic wind tunnel. The BBN facility and the instrumentation used in these tests are described in Appendix C.

The airfoil was mounted in the simple support structure shown in Fig. 8a. A typical serration attached near the airfoil leading-edge is shown in Fig. 8b. Figure 9 is a schematic of the geometry and location of the serrations.

A protractor was used to measure the angle-of-attack α. Noise measurements were made for α varying between 0 and 16 degrees and for flow speeds V of 60 ft/sec and 100 ft/sec. These speeds correspond to chord-based Reynolds numbers R_c of 2×10^5 and 3.33×10^5, respectively. The free-jet background sound power levels for these velocities are shown in Fig. 10.

Four different serrations were tested. The serrations were placed on the airfoil lower surface (pressure side) slightly behind the leading-edge. The details of their location and size are tabulated in Table I.A. In the column entitled "Serration Location Number", the unprimed numbers mean that the serrations are attached flush against the airfoil surface as shown in Fig. 9; the primed numbers mean that they extend out somewhat from the airfoil surface. The serrations were attached with a depth gauge using double-backed masking tape.

Comparison of sound power measurements made with and without the serrations show, in almost all cases, that the serrations reduce noise. The measurements also show that the magnitude of the relative noise reduction is extremely sensitive to serration size and location. This is consistent with Soderman's earlier findings [1,23].

The sound power measurements show that the greatest noise reduction was achieved by serration No. 4, the largest serration. The measurements also show that the "best" location is 3′, where the serration sticks out from the surface. Figures 11 and 12 show the effect of serration size and location, respectively, on the radiated sound for $\alpha = 4$ degrees and $V = 60$ ft/sec. The sensitivity of the radiated sound to serration size is clearly demonstrated in Fig. 11. Figure 12 shows the effect on the radiated sound of placing serration No. 4 at different locations near the airfoil leading-edge. Of particular interest is the large difference in radiated sound between serration No. 4 at Location 3 (serration flush against the airfoil surface) and the same serration at Location 3′ (serration sticking out from the surface).

In Figs. 13 through 17, we compare sound power levels of the unmodified airfoil with those of the airfoil modified by serration No. 4 at Location 3′ for $V = 60$ ft/sec and for $\alpha = 0$, 4, 8, 12, and 16 degrees, respectively. Figures 13 and 14 are unusual in that large peaks in the spectrum are generated by the unmodified airfoil at the 1/3-octave band center frequency of 800 Hz. Oscilloscope traces of both acoustic and wake velocity signals showed that the peaks in the spectrum represent essentially sinusoidal tones. Figure 13 shows that for $\alpha = 0$ degrees, the serration shifts the peak from $f = 800$ Hz to the two neighboring 1/3-octave bands. (The tones were often observed to be unstable between neighboring 1/3-octave bands.) Figure 14 shows that for $\alpha = 4$ degrees, the serration eliminates the tone completely. In Fig. 15, we see that for $\alpha = 8$ degrees, the intensity of the tone radiated from the unmodified airfoil is much weaker than its intensity at the lower angles. Again, the tone disappears when serration No. 4 is attached. In this figure, the spectra of the serrated airfoil is cut off beyond the center frequency of 1000 Hz because the sound levels approached the background noise of the wind tunnel. In Figs. 16 and 17, corresponding to $\alpha = 12$ and 16 degrees, respectively, the tones disappear even for the unmodified airfoil. Here, spectra are broadband and the differences between unmodified airfoil and serrated airfoil sound radiation are small.

In Figs. 18 through 22, we compare again the sound power levels of the unmodified airfoil with those of the serrated airfoil, but this time for $V = 100$ ft/sec. Here, tones occur at a center frequency of 1600 Hz for $\alpha = 0$, 4, and 8 degrees as shown in Figs. 18, 19, and 20, respectively. Thus, the frequency of the tones increases when the flow speed increases. We note, but cannot explain, that the intensity of the tone which appears in Fig. 20 is much stronger than its counterpart

shown in Fig. 15. The tone again disappears between Figs. 20 and 21, i.e., between α = 8 and 12 degrees. In Figs. 21 and 22, the spectrum is again broadband but here the serrations are more effective in reducing the noise than they were at V = 60 ft/sec (see Figs. 16 and 17 for comparison). For example, at α = 12 degrees (Fig. 21), the peak of the sound spectra for the unmodified airfoil is reduced more than 7 dB by the serration.

To summarize, the 1/3-octave band peaks associated with the unmodified airfoil represent tones which were observed to be nearly "pure" but were often unstable between neighboring 1/3-octave band center frequencies. It is evident that the serrations remove virtually all the tones. Without the serrations, however, the tones disappear at angles of attack above 10 degrees.

We believe the disappearance of the tones above 10 degrees is related to the stalling characteristics of the NACA 0012 airfoil. Studies by McCullough and Gault [24] of the low-speed ($M < 0.4$) stalling characteristics of the NACA 0012 airfoil show that stall is initiated by the bursting of a short laminar separation bubble formed at low angles of attack on the airfoil upper surface near its leading edge and by a trailing-edge separation. Little is known, however, about the interaction between the leading-edge separation and the trailing-edge separation. As the angle of attack increases, the bubble tends to contract and the region of separation begins to grow. At some angle of attack, the leading-edge bubble suddenly bursts; there is no subsequent flow reattachment and stall occurs.

The change from a short leading-edge bubble to complete turbulent boundary layer separation occurs at an effective Reynolds number* R_{eff} of 16×10^6 according to the data of Ref. 25. Figure 23, taken from Ref. 25, shows the behavior of the lift coefficient C_L vs α for different Reynolds numbers. At Reynolds numbers $R_c < 0.33 \times 10^6$ ($R_{eff} < 0.9 \times 10^6$), the NACA 0012 airfoil has a laminar trailing-edge separation. (Recall that for the 6-in. NACA 0012 airfoil used in our tests, the Reynolds number is 0.2×10^6 for V = 60 ft/sec and 0.33×10^6 for V = 100 ft/sec.) The laminar trailing-edge shedding suggests a periodic (or near periodic) vortex shedding which, according to Curle, would generate a tone such as the measurements in Figs. 13 through 22 exhibit. Figure 23 also

---

*R_{eff} includes the effect of unstream turbulence and is defined as $R_{eff} = K R_c$ where $K > 1$ and R_c is the chord-based Reynolds number. Since the turbulence levels in the BBN free jet are extremely low, $K \doteq 1$ and $R_{eff} \doteq R_c$.

shows that for $R_c < 0.33 \times 10^6$, stall occurred at $\alpha \approx 9$ degrees. If the tones, indeed, are generated by the laminar trailing-edge separation, their disappearance at $\alpha > 8^0$ is consistent with the results of Fig. 23. The laminar trailing-edge separation also suggests an expanation of how the serrations remove the tones. We believe that at low angles of attack, the vortices generated by the serrations destroy the laminar trailing-edge separation by changing the character of the boundary layer from laminar to turbulent.

5.2.2 Diagnostic Tests

Two diagnostic tests were undertaken to verify our understanding that the tones are generated by laminar trailing-edge vortex shedding and that the serrations remove the tones by generating vortices that change the character of the trailing-edge vortex shedding from laminar to turbulent.

The first test, which consisted of recording spectral measurements of the fluctuating forces and moments imparted to the airfoil by the flow, was undertaken to locate the aerodynamic source of the acoustic tone on the airfoil surface and to connect the spectra of the unsteady forces to the acoustic spectra. The measurements were made with and without serrations.

The second test, a recording of the spectral measurements of the fluctuating horizontal and vertical velocity components near the airfoil trailing edge, was conducted to determine if periodic or near periodic vortex shedding occurs in the airfoil wake and if the serrations change the character of the vortex shedding from periodic to broadband.

Force and moment measurements. - To locate the aerodynamic source of the acoustic tone, we measured the fluctuating lift, drag, and moment on a lightweight isocyanate foam version of the NACA 0012 airfoil. The measurements were made with a six-degree-of-freedom, eight-component force balance designed and built by BBN. The force balance is described in Appendix C.

Figure 24 shows experimental curves of fluctuating lift, drag, and pitching moment for V = 25 ft/sec and $\alpha = 0$ degrees on the unmodified airfoil. Only low-speed measurements were made because it is difficult to interpret the data at the higher speeds where the frequency of the tones are near the resonance of the airfoil/force-balance combination. Figure

24 shows that the acoustic tone and the mean square fluctuating life $\langle L^2 \rangle$, moment $\langle M^2 \rangle$, and drag $\langle D^2 \rangle$ are concentrated at the 1/3-octave band center frequency of 250 Hz. The location of $\langle L^2 \rangle$ on the airfoil is determined from the expression

$$(\Delta x)^2 = \frac{\langle M^2 \rangle}{\langle L^2 \rangle} \quad , \tag{11}$$

where x is measured from the airfoil aerodynamic center. From Fig. 24, we see that $\langle L^2 \rangle$ is equal to -29 dB re 1 lb_f, and $\langle M^2 \rangle$ is equal to -16 dB re 1 lb_f-in. Inserting these values into Eq. (11), we find $\Delta x = 4.47$ in.

Since the aerodynamic center of the NACA 0012 airfoil is, by definition, located at the airfoil quarter chord (i.e., 1.5 in. from the leading edge, the airfoil chord being 6 in.), the flutuating lift, which is the dipole source of the acoustic tones, is located 5.97 in. from the airfoil leading edge. The chord-based Reynolds number for V = 25 ft/sec is 8.33×10^4. For this Reynolds number, the boundary layer, according to the measurements of Ref. 25, is laminar (see Fig. 23). A narrow-band fluctuating force located near the trailing edge is just the behavior expected from vortices being shed at a periodic rate from the trailing edge of a laminar boundary layer at low angles of attack.

Figure 25 shows experimental curves of fluctuating lift, drag, and pitching moment for V = 25 ft/sec and α = 0 degrees with serration No. 4 attached at location 3'. Comparison of Fig. 25 with Fig. 24 shows that the fluctuating lift, drag, and pitching moment levels are reduced considerably with the serration. Of special interest is the lift fluctuation which is concentrated at the 250 Hz 1/3-octave center band frequency for the unmodified airfoil (see Fig. 24) and virtually eliminated in this band on the serrated airfoil (see Fig. 25).

Measurements show that at low angles of attack, the tones are concentrated in the 250 Hz, 800 Hz, and 1600 Hz 1/3-octave band center frequencies for flow speeds of 25 ft/sec, 60 ft/sec, and 100 ft/sec, respectively. The relationship between the frequency of the tones and the flow speed is most conveniently expressed in terms of the Strouhal number (S) defined as

$$S = \frac{fd}{V} \quad , \tag{12}$$

where for the 6-in. NACA 0012 airfoil tested, d = 0.06 ft, the maximum thickness of the airfoil*. For low-speed flow, the Strouhal number should be a function only of Reynolds number. Figure 26 shows the relationship between Strouhal number and chord-based Reynolds number (R_c) for the acoustic tones. Also shown in Fig. 26 is an empirical curve defined as

$$S = 0.6 \log R_c - 2.35 \quad , \qquad (13)$$

which fits the data in the Reynolds number range $8.33 \times 10^4 \leq R_c \leq 3.33 \times 10^5$ corresponding to the velocity range 25 ft/sec $\leq V \leq$ 100 ft/sec. (Equation (13) shows the dependence of S on viscosity and will be useful in analyzing the propeller data discussed in Section 5.3.)

To summarize, the measurements show that the fluctuating lift (the source of the acoustic tone) is concentrated in a narrowband and is located in the immediate vicinity of the airfoil trailing edge. The effect of serration No. 4 attached at Location 3 is to reduce considerably the level of the fluctuating lift in the narrowband, thereby reducing considerably the level of the tone.

Velocity measurements. - The results of the fluctuating force and moment measurements show that the fluctuating lift (the dipole source of the tones) is located near the trailing edge of the airfoil. Thus, a limited series of measurements was undertaken to investigate (1) the fluctuating velocity field around the airfoil and (2) how the leading-edge serrations affect the fluctuating velocity field.

---

*A major drawback in defining the Strouhal number with a characteristic dimension based, in part, on a trailing-edge viscous length (viz, δ^* or θ) rather than, say, the maximum body dimension is that it is extremely difficult to calculate δ^* or θ because the flow is almost always separated near the trailing edge. Boundary-layer theory is invalid in a separated flow region; thus, the complete (and most difficult) Navier-Stokes equation must be solved or, alternately, θ and/or δ^* must be measured if these quantities are to be determined. Since extensive velocity surveys were not the object of this study, Strouhal number of the observed acoustic tone is defined using the airfoil maximum thickness as the characteristic dimension.

Velocity fluctuations, in the 1/3-octave band center frequency of 800 Hz corresponding to the acoustic tone for V = 60 ft/sec, were measured at various locations near the airfoil surface using a single 0.00025-in. diameter hot-wire probe attached to a traversing mechanism. Only near the trailing edge and in the wake were strong velocity fluctuations observed. The small fluctuations (on the order of 0.001 V), which were observed far from the airfoil surface, seem to represent weak circulation fluctuations induced by the wake.

Figure 27 shows typical measurements in the 800 Hz 1/3-octave band center frequency of the root-mean square velocity fluctuations (i.e., $\sqrt{u^2 + v^2}$) near the airfoil trailing edge. Of particular interest are the "double rows of vortices" shown in Figs. 27(a) and 27(b) which are characteristic of the wake shedding observed behind cylinders. The various letters referred to in Fig. 27 identify the locations of the spectral measurements discussed below. Traverse positions 2 in Fig. 27(a) and 3 in Fig. 27(b) are located 0.1 in. and 1 in. behind the airfoil trailing edge (Fig. 33 shows a schematic of these traverse positions).

Figures 28 through 30 show comparisons at several locations near the trailing edge of the velocity fluctuations in the wake of the unmodified airfoil with those of the airfoil modified by serration 4 attached at Location 3′. Measurements of the velocity fluctuations at the three locations in the wake, shown in Figs. 28, 29 and 30, show that most of the energy of the shed vortices is concentrated at the 800 Hz 1/3-octave band center frequency, the frequency of the tones. The effect of the serrations, a reduction of the peak velocity fluctuation in this band, is consistent with the earlier observations which showed that the serrations either reduce or eliminate both the acoustic tones and the fluctuating lift. No measurements were made to assess the effect of the serration on the spanwise correlation of the velocity fluctuations in the various 1/3-octave bands.

The measurements of the velocity fluctuations and the corresponding acoustic measurements apparently explain the noise reduction achieved with properly designed and located leading-edge serrations. The serration evidently "trips" the boundary layer on both the pressure and suction sides of the airfoil, thus preventing the development of a coherent, intense wake. In support of this hypothesis, Figs. 28 through 30 show that with serration No. 4 attached to the airfoil at Location 3′, the wake tone no longer dominates the spectrum.

5.2.3 Steady-State Aerodynamic Performance Tests

A series of tests were conducted to determine the effects of serrations on the steady-state aerodynamic performance of the airfoil. The tests were conducted with and without the "best" serration (No. 4 at Location 3′) and consisted of (1) measurements of the steady-state lift and drag, (2) steady-state velocity surveys at selected locations on the airfoil upper surface and in the wake, and (3) flow visualization photographs of the airfoil upper surface.

Lift and drag measurements. - Mean lift and drag data were obtained to investigate the effects of serrations on airfoil performance. To increase the region of two-dimensional flow, end plates were attached to the airfoil at both ends. The flow was found to be two-dimensional only at low angles of attack; at high angles of attack, the flow was observed to be still three-dimensional. No significant improvements in aerodynamic performance (viz, C_L vs α, C_D vs α, etc.) were observed by attaching the serrations. The C_L vs α curve was slightly extended by attaching serration 4 at Location 3′, but only by 1-2%. Similarly, the drag was reduced but only by 1-5%.

If the serrations do indeed remove the tones by changing the character of the boundary layer from laminar to turbulent, then any device which creates a turbulent field should also remove the tones. Therefore, we placed a 0.09-in. diameter trip wire at several locations on the airfoil. As expected, attaching the trip wire reduced or removed the airfoil tone. However, the trip wires had a detrimental effect upon aerodynamic lift with stall often occurring abruptly. Figure 31 shows the effect of a single trip wire on aerodynamic lift for various locations on the airfoil surface. When placed on the suction side of the airfoil (Fig. 31a), the trip wire did not substantially reduce the tone but induced stall prematurely, in most cases, at relatively low angles of attack. When placed on the pressure side (Fig. 31b), the trip wire reduced or eliminated the tone but degraded aerodynamic performance near stall, although to a much lesser extent than when placed on the suction side.

Figure 32a shows the effect of placing a single trip wire at the center of the leading edge (i.e., the stagnation point when $\alpha = 0^\circ$); the result is a dramatic *improvement* of the stall characteristics of the airfoil. However, the tone is reduced only for $\alpha < 2^\circ$ (i.e., a 6-dB reduction for $\alpha = 0^\circ$, but 0 dB at $\alpha = 2^\circ$). Figure 32b shows the effect of placing "double trip" wires at the aerodynamic center (i.e., one on

the pressure side and one on the suction side); the result is almost complete reduction of the tone but again degradation of the near-stall performance of the airfoil.

We conclude from these studies that trip wires when placed on the pressure side of the airfoil reduce the acoustic tone but generally degrade aerodynamic performance near stall. Properly placed leading-edge serrations (i.e., on pressure side), on the other hand, can result in slight improvements in aerodynamic performance as well as significantly reducing or eliminating the tones at the Reynolds numbers tested.

Steady-state velocity measurements. - Mean velocity profiles for the unmodified airfoil were measured over the entire region from the leading edge to two chord lengths (12 in.) downstream from the trailing edge. The measurements show that the flow is accelerated in the vicinity of the airfoil aerodynamic center and that a velocity deficit exists in the wake behind the airfoil.

The effect of leading-edge serrations on the mean flow was observed to be rather insignificant at low angles of attack ($\alpha \leq 4^{\circ}$). (All angles up to stall were not studied.) Figure 33 shows a representative comparison of mean velocity profiles in the vicinity of the trailing edge with and without leading-edge serrations. The effect of the serrations on the mean flow is to thin slightly both the boundary layer near the trailing edge and the velocity profile in the wake. The slightly reduced wake is consistent with the 1-5% reductions in drag observed from the force measurements.

Flow visualization study. - Oil visualization photographs were taken of the airfoil upper surface to study the effect of serrations on the behavior of the leading-edge bubble with varying angle of attack. This test was motivated by Soderman's work [23], which shows that with properly designed serrations stall can be delayed to extremely high angles of attack. Since stall is initiated on the NACA 0012 airfoil with bursting of the leading-edge bubble, obviously the serrations must affect the bubble behavior.

We applied a mixture of kerosene, titanium-dioxide, and motor oil to the upper surface of the airfoil so that we could study the behavior of the airfoil leading-edge bubble. For the unmodified airfoil, the leading-edge bubble was not observed until an angle of attack of 5 degrees. Figure 34 shows a photograph of the leading-edge bubble formed at

α = 5 degrees. The arrows indicate the direction of the flow near the airfoil surface; the dotted line is the reattachment point. When the serrations were attached, no such bubble was observed - the flow appeared to be in the direction of the free stream at all points.

Since we did not significantly improve the airfoil aerodynamic performance with the serrations tested, we cannot offer any definitive explanation of how or why serrations can delay stall, as Soderman showed [23], to high angles of attack. The results of these tests do, however, support the explanation put forth by Soderman to explain how serrations delay stall. We offer the following tentative explanation based in part on Soderman's earlier findings.

It is well-known that the laminar boundary layer over the nose of a thin airfoil at high angle of attack fails to remain attached to the upper surface in the region of the high adverse pressure gradient that exists just downstream of the suction peak. A leading-edge bubble forms when the separated flow reattaches to the upper surface.

Under proper excitation, the bubble may "burst" to form an unattached free shear layer representing the onset of stall. We believe that the vortices generated by the serrations augment the momentum in the boundary layer by mixing high energy air from the potential flow above the boundary layer sufficiently to prevent the flow from separating locally from the upper surface, thereby eliminating the separation bubble. If the momentum augmentation if sufficiently strong, the character of the stall may change from a leading-edge bubble stall to a trailing-edge stall characterized by a separated trailing region growing inward towards the leading edge. Soderman's study [23] shows that the serrations delay even the trailing edge separation to higher angles of attack. We note that trailing-edge stall occurs on thick airfoils which generally stall at higher angles of attack than do thin airfoils [24].

5.3 Study of the Effects of Leading-Edge Serrations on a Two-Bladed NACA 0012 Propeller

A series of tests were conducted to study the effects of leading-edge serrations on vortex sound radiation from a two-bladed, variable pitch NACA 0012 section propeller of chord 2 in. and diameter 14 in. Sound power measurements, with and without serrations, were made in the laminar core of the free jet. Photographs of the propeller with a typical serration attached near the leading edge are shown in Fig. 35. The propeller was spun at rotational speeds of 2000 and 4000 rpm

for a constant jet inflow speed of 40 ft/sec. The Reynolds numbers based upon chord length and flow speed at the three-quarter propeller span are 1.16 x 10^5 for 2000 rpm and 2.18 x 10^5 for 4000 rpm - well within the previously discussed airfoil Reynolds number range. The background sound power levels with the spinner attached are shown in Fig. 36.

The size and location of the serrations tested are shown in Table I.B. Measurements of the sound power radiated from the propeller, with and without the serrations described in Table I.B., show that serration No. 5 attached at Location 2′ yielded the greatest reduction in noise. Figures 37 through 40 show the noise reductions achieved with serration No. 5 attached at Location 2′ for base angles α_B = 20, 22.5, 25, and 27.5 degrees. The base angle α_B is the angle at which the base (or hub) or the propeller is rotated relative to its zero lift angle for no inflow. Thus, for a given inflow velocity and rotational speed, the local angle of attack incident to the propeller is a function of the local spanwise position along the propeller; the angle-of-attack distribution is partially offset, however, by a negative one degree per inch spanwise twist. The angle-of-attack distribution along the propeller is expressed analytically as

$$\alpha = \alpha_B - \frac{(r-1)}{12} - \tan^{-1}\left[\frac{V}{2\pi r\ rpm/720}\right] , \qquad (14)$$

where V is the jet inflow velocity, r is the propeller spanwise distance in inches and the middle term represents the one degree per inch negative twist along the propeller. (Although the propeller radius is 7 in., the hub radius is 1 in., which explains the (r-1) expression - see Fig. 35.) The angle-of-attack distribution along the propeller, defined by Eq. (14), is tabulated in Tables II.A and II.B for an inflow of 40 ft/sec and rotational speeds of 2000 and 4000 rpm, respectively.

Figures 37 through 40 are of special interest for three reasons. First of all, the measurements show that the unmodified propeller generates a loud tone primarily at the 4000-Hz, 1/3-octave center band frequency, although Fig. 38 suggests that the tones are unstable between neighboring 1/3-octave bands in much the same way as the airfoil tones. This tone dominates the spectrum, being larger than the fundamental blade passing rate tone of the propeller. The fundamental tone and its higher harmonics are not shown in Figs. 37 through 40 because they are overwhelmed by the tunnel background noise levels shown in Fig. 36. Thus, only propeller vortex noise is considered. Second, the tore is

virtually eliminated when serration No. 5 is attached at Location 2′. Figures 37 through 40 demonstrate that the serrations produce less noise reduction at high angles of attack than at low angles of attack. Third, to isolate the sound-producing region of the blade, we cut the serration span progressively in half and made comparative measurements. Little or no effect upon the tones was found until 1/4 of the original serration length remained at the tip. For lengths less than 1/4 of the original serration length, the level of the tones increased as shown in Figs. 37 through 40. Thus, to clarify some long-standing speculation on the subject, we conclude that the dominant region of non-rotational or vortex noise generation is the outer 1/4 of the blade radius.

We believe that the propeller tones are generated in precisely the same way that the airfoil tones discussed earlier are generated. To support this conclusion, we have plotted the Strouhal number corresponding to the propeller tone on the airfoil Strouhal curve shown in Fig. 26. The propeller Strouhal number is determined from Eq. (13) where $V \doteq 104$ ft/sec and $R_c = 1.16 \times 10^5$ are based on the local velocity at the 3/4 radius station and d = 0.02 ft, the propeller maximum thickness.

Figures 41 through 43 show the effects of attaching serration No. 5 at Locations 1′ and 2′ for the higher rotational speed of 4000 rpm. Tones are again generated from the unmodified propeller but at the higher 1/3-octave center frequency of 8000 Hz. The tones are virtually eliminated with serration No. 5 attached at Location 2′. The Strouhal number of the tones where V = 196 ft/sec and $R_c = 2.18 \times 10^5$ is plotted in Fig. 26. Thus, we believe that the tones at the higher rotational speed of 4000 rpm are also generated by vortices shed at a periodic or near periodic rate into the propeller wake.

6. CONCLUSIONS AND RECOMMENDATIONS

The principal conclusions from this study are:

(1) Loud, distinct tones are generated by NACA 0012 shaped airfoils and propellers operating at low angles of attack in smooth flow with chord based Reynolds numbers ranging from $8.33 \times 10^4 \leq R_c \leq 3.33 \times 10^5$. The tones are generated by periodic or near periodic fluctuating forces, located on the airfoil and propeller near the trailing edge and induced by laminar boundary-layer wake vortex shedding. We suspect, although we have not verified, that the fluctuating forces are well-correlated along the airfoil and propeller span. At higher angles of attack, corresponding to stall where the wake vortex shedding is broadband, the tones disappear.

(2) The tones are reduced or eliminated by attaching properly designed and properly located serrations near the leading edge of the airfoil and propeller *pressure* side. The serrations generate chordwise trailing vortices which trip the laminar boundary layer on both the pressure and suction surfaces thereby changing the character of the wake vortex shedding from periodic or almost periodic to broadband --hence the reduction or elimination of the tones. At high angles of attack corresponding to stall, the serrations also reduce the broadband noise.

(3) The directivity pattern radiated by *small* airfoils in flow has been compared with that predicted by Curle's point dipole sound theory. We believe the comparison between theory and experiment to be sufficient to present a partial check of the validity of Curle's theory.

(4) A theoretical model predicting the sound radiated from *small* airfoils in turbulent flow shows good agreement with experiment over a large velocity range. The good agreement between theory and experiment suggests that for small airfoils in turbulent flow, most of the radiated sound is generated by the time-derivative of the fluctuating lift induced by the turbulence.

The present study has investigated the behavior of the tones and their subsequent removal with leading-edge serrations for only a limited Reynolds number range. For low angles of attack, the boundary layer over the unmodified airfoil and propeller surface is predominantly laminar. Since the tones are generated by vortices shed at a periodic or near periodic rate into the airfoil or propeller wake,

they should be sensitive to the local flow conditions near the trailing edge. Thus, the behavior of the tones and their effective removal with serrations should be investigated over a Reynolds number range sufficiently large to include a turbulent boundary layer over most of the airfoil and propeller surface.

Curle's dipole sound equation is commonly used to predict the sound radiation from *small* lifting surfaces in flow. Little is known, however, about the validity of his general model for *large* lifting surfaces in flow--i.e., large with respect to a typical wavelength of the radiated sound. Since there are many situations where the dimensions of the lifting surfaces are large (e.g., the airfoil blades on a high rpm compressor or lift fan), a comparison of his theory with experiments is important. The experiments should be designed to isolate the various surface dipole distributions. For example, it is commonly believed that for airfoils in smooth flow, most of the dipole source strength is concentrated near the airfoil trailing edge [8, 15, 16]. Conversely, for airfoils in turbulent flow, most of the dipole source strength is believed to be concentrated near the airfoil leading edge. It would be desirable to understand the conditions under which both the leading and trailing edge dipole sources are important contributors to the sound field.

REFERENCES

1. Soderman, P.T.: A Device for Reducing Airfoil Noise Modeled After the Leading Edge Comb of the Owl. NASA TN to be published.

2. Curle, N.: The Influence of Solid Boundaries Upon Aerodynamic Sound. *Proc. Roy. Soc.* 231A, 1955, pp. 505-517.

3. Lighthill, M. J.: On Sound Generated Aerodynamically I. General Theory. *Proc. Roy. Soc.* 211A, 1952, pp. 564-587.

4. Clark, P. J. F.; and Ribner, H. S.: Direct Correlation of Fluctuating Lift with Radiated Sound for an Airfoil in Turbulent Flow. *J. Acoust. Soc. Amer.* 46, 1969, pp. 802-805.

5. Gordon, C. G.: Influence of Upstream Power Flow Discontinuities on the Acoustic Power Radiated by a Model Air Jet. NASA CR-679, January 1967.

6. Heller, H. H.: Correlation of Fluctuating Forces with the Sound Radiation of Rigid Flow-Spoilers. BBN Report 1734, Bolt Beranek and Newman Inc., Cambridge, Massachusetts, 17 October 1968.

7. Sharland, I. J.: Sources of Noise in Axial Flow. *J. Sound Vib.*, vol. 1, no. 3, July 1964, pp. 302-322.

8. Siddon, T. E.: Surface Dipole Strength for Flow Past Airfoils. Presented at the 79th Meeting of the Acoustical Society of America (Atlantic City, New Jersey), April 1970.

9. Ross, D.: Vortex-Shedding Sounds of Propellers. BBN Report 1115, Bolt Beranek and Newman Inc., Cambridge, Massachusetts, March 1964.

10. Strouhal, V.: Ueber eine Besondere Art der Tonerregung. *Annalen der Physik and Chemie* 5, 1878, pp. 216-251.

11. Rayleigh, Lord: Aeolian Tones. *Phil. Mag.* 29, 1915, p. 433.

12. Relf, E. F.: On the Sound Emitted by Wires of Circular Section when Exposed to an Air Current. *Phil. Mag.* 42, 1921, pp. 173-176.

13. Gongwer, C. A.: A Study of Vanes Singing in Water. *J. Appl. Mech.* 19, 1952, p. 432.

14. Bauer, A. E.: Vortex Shedding from This Flat Plates Parallel to the Free Stream. *J. Aero. Sci.* 28, 1961, pp. 340-341.

15. Hayden, R. E.: Sound Generation by Turbulent Wall Jet Flow Over a Trailing Edge. M.S. Thesis, Purdue University, 1969. Also Paper FF-10 with R.C. Chanaud, 1970 Spring Meeting of the Acoustical Society of America, Atlantic City, New Jersey.

16. Chanaud, R. C.; and Hayden, R. E.: Edge Sound Produced by Two Turbulent Wall Jets. Paper FF-11, 1970 Spring Meeting of the Acoustical Society of America, Atlantic City, New Jersey.

17. Stowell, E. Z.; and Deming, A. F.: Vortex Noise from Rotating Cylindrical Rods. National Advisory Committee for Aeronautics, NACA 519, 1935.

18. Yudin, E. Y.: On the Vortex Noise from Rotating Rods. Washington, D.C., NACA TM 1136, March 1947.

19. Hubbard, H. H.: Propeller Noise Charts for Transport Airplanes. Washington, D.C., NACA TN 2968, June 1953.

20. Schlegel, R.; King, R.; and Mull, F.: Helicopter Rotor Noise Generation and Propagation. Ft. Eustis, Virginia, USAVLABS TR 66-4, Oct. 1966.

21. Liepmann, H. W.: On the Application of Statistical Concepts to the Buffeting Proglem. *J. Aero. Sci.* 19, 1952, p. 793.

22. Davies, P. O. A. L.; Barrett, M. J.; and Fisher, M. J.: Turbulence in the Mixing Region of a Round Jet. ARC 23, 728-N200-FM 3181, 1962.

23. Soderman, P.T.: Effects of Leading Edge Serrations on a Two-Dimensional Airfoil, NASA TN to be published.

24. McCullogh, G. B.; and Gault, D. E.: Examples of Three Representative Types of Airfoil-Section Stall at Low Speed. NACA TN 2502, 1951.

25. Jacobs, E. N.; and Sherman, A.: Airfoil Section Characteristics as Affected by Variations in the Reynolds Number. NACA Tech. Report 586, 1937.

Table I. Summary of Serration Size and Location

A. Airfoil Serrations (R = 0.095 in.)

Serration no.	Location no.	A/R	B/R	C/R	x/R
1	1	0.35	0.17	0.53	0
	2				-0.53
	3				0.26
	4				0.53
2	1	0.67	0.34	0.67	0.53
	2				0.79
	3				1.05
	3′				1.05
3	1′	1.05	0.53	1.05	0.53
	2′				0.79
	3′				1.05
4	1	1.40	0.70	1.40	0.79
	2				1.05
	3				0.53
	3′				0.53

B. Propeller Serrations (R = 0.0317 in.)

Serration no.	Location no.	A/R	B/R	C/R	x/R
5	1′	0.98	0.47	0.98	0.51
	2′				0.76
	3′				1.01
6	1′	2.11	1.07	2.11	1.01
	2′				0.76
	3′				1.42

TABLE II

ANGLE-OF-ATTACK DISTRIBUTION

ALONG PROPELLER SPAN FOR V = 40 FT/SEC

A. 2000 RPM

α_B \ r	1"	2"	3"	4"	5"	6"	7"
20°	-46.5°	-30°	-19.5°	-13°	-8.7°	-8°	-4.2°
22.5°	-44°	-27.5°	-17°	-10.5°	-6.2°	-5.5°	-1.7°
25°	-41.5°	-25°	-14.5°	-8°	-3.7°	-3°	0.8°
27.5°	-39°	-22.5°	-12°	-5.5°	-1.2°	1.5°	3.3°

B. 4000 RPM

α_B \ r	1"	2"	3"	4"	5"	6"	7"
17.5°	-31.5°	-13.5°	-5.5°	-1.5°	0.5°	1.7°	2.2°
20°	-29°	-11°	-3°	1°	3°	4.2°	4.7°
22.5°	-26.5°	-8.5°	-0.5°	3.5°	5.5°	6.7°	7.2°

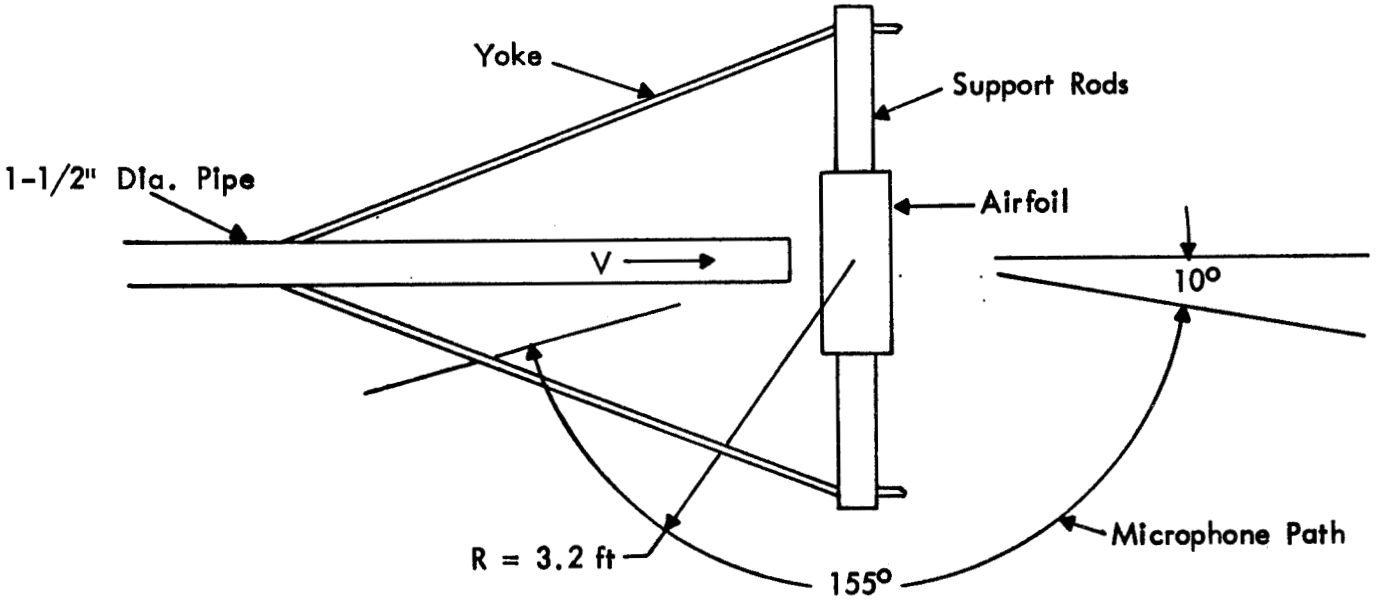

FIGURE 1. SCHEMATIC OF AIRFOIL SUPPORT APPARATUS AND MICROPHONE ANGULAR PATH

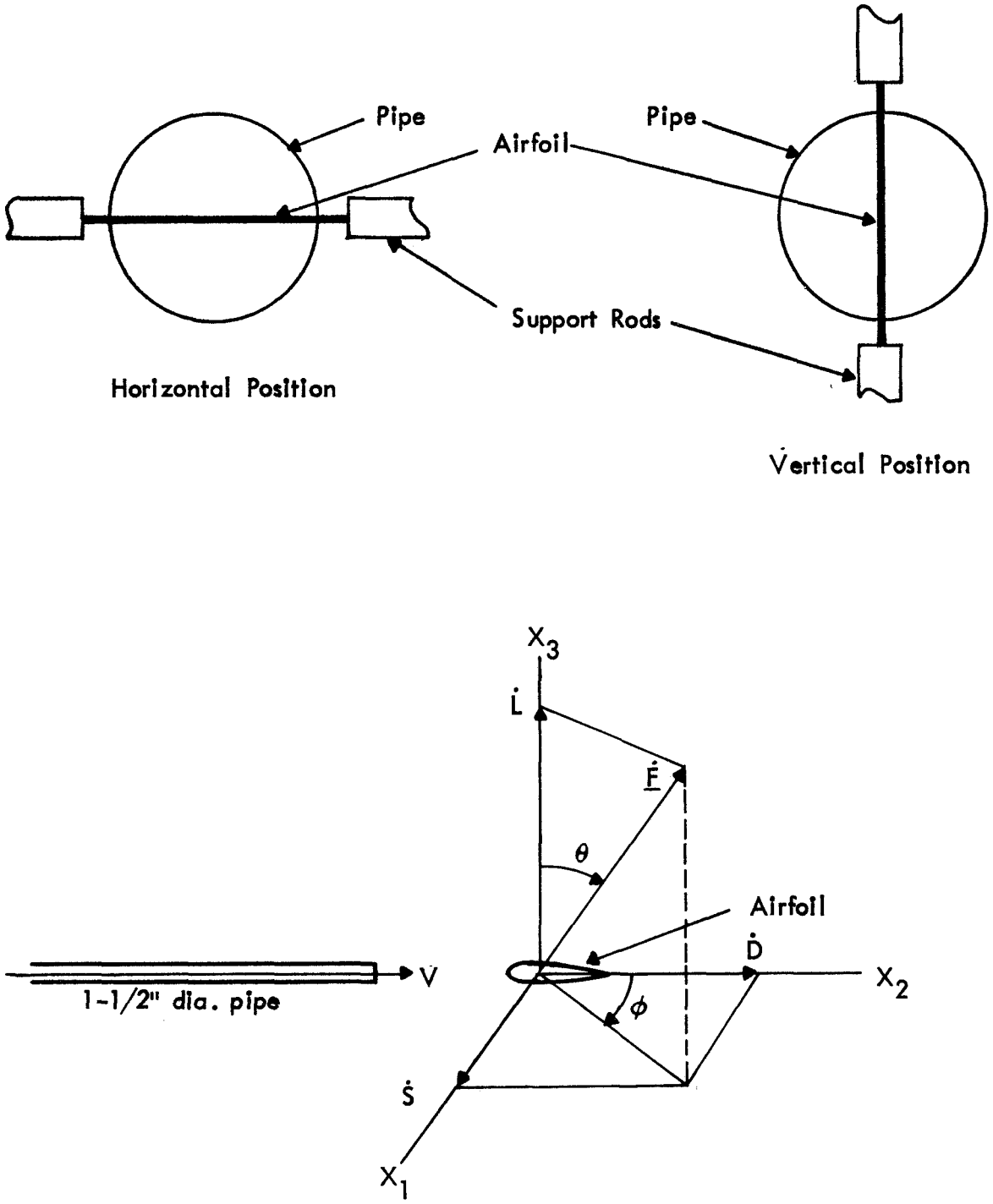

FIGURE 2. SCHEMATIC OF TEST SET-UP AND DEFINITION OF COORDINATE SYSTEM

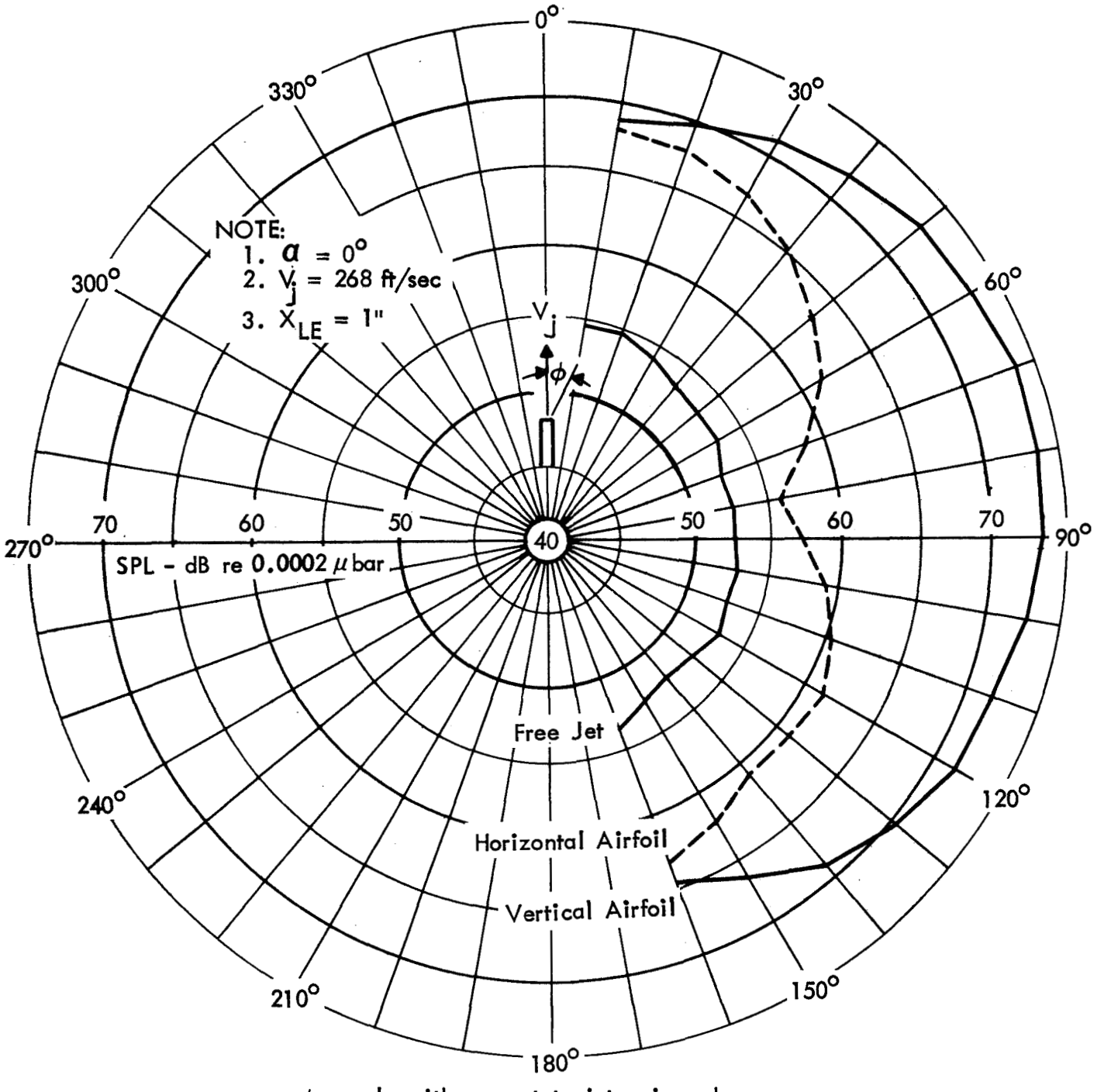

FIGURE 3. AIRFOIL DIRECTIVITY PATTERN
f = 1250 Hz - 1/3 Octave Band

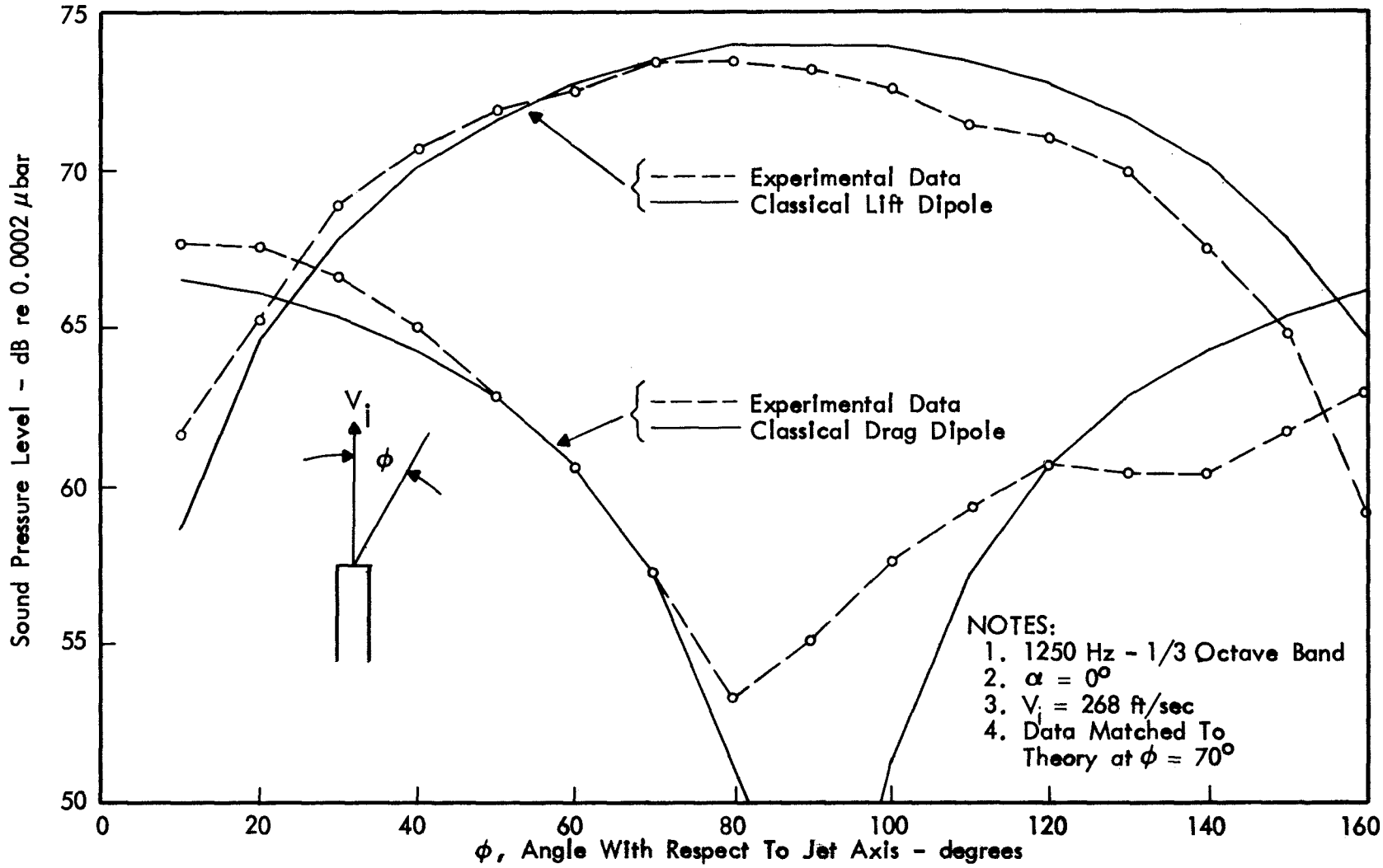

FIGURE 4. COMPARISON OF CURLE'S DIPOLE DIRECTIVITY PATTERN WITH EXPERIMENT

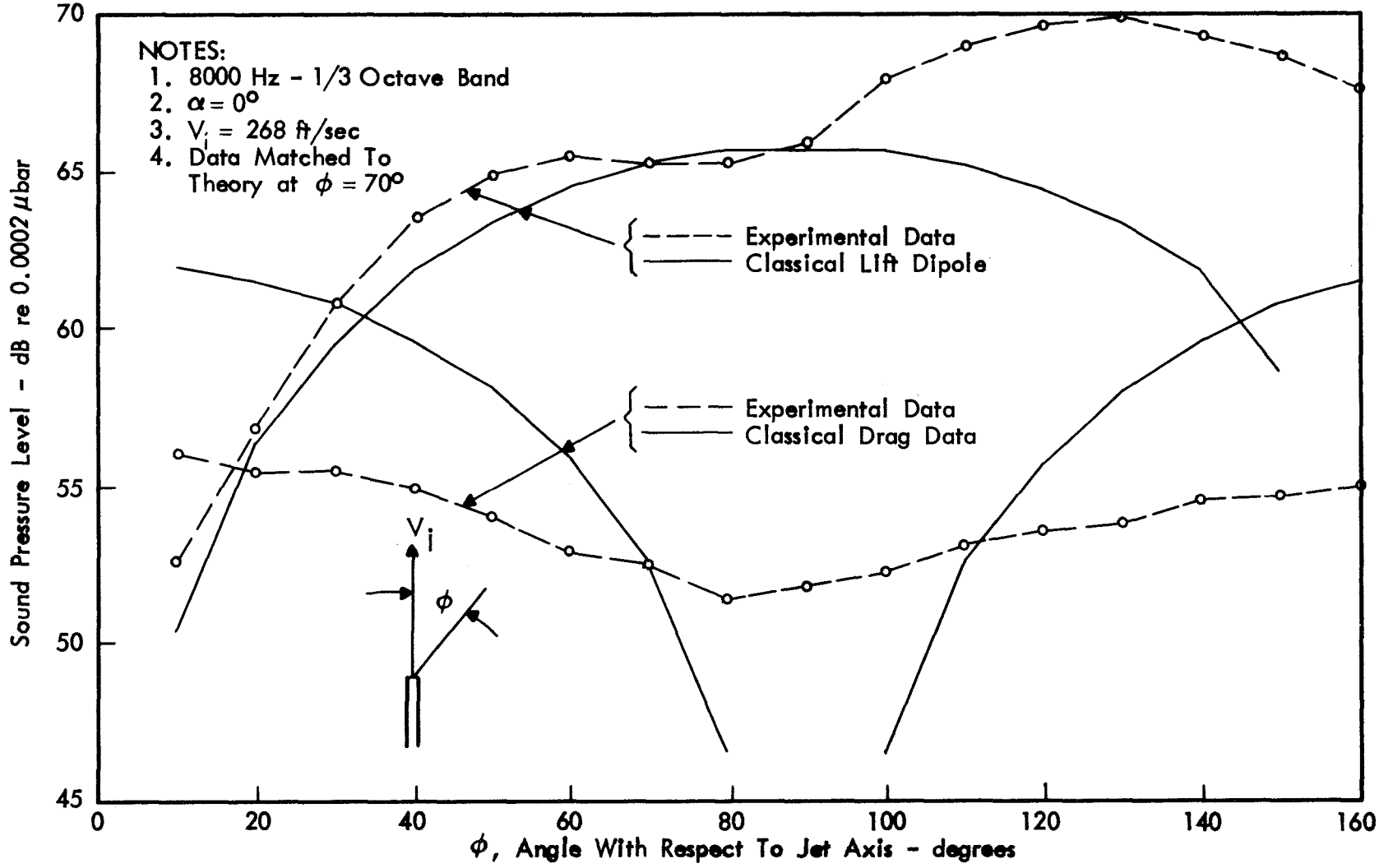

FIGURE 5. COMPARISON OF CURLE'S DIPOLE DIRECTIVITY PATTERN WITH EXPERIMENT

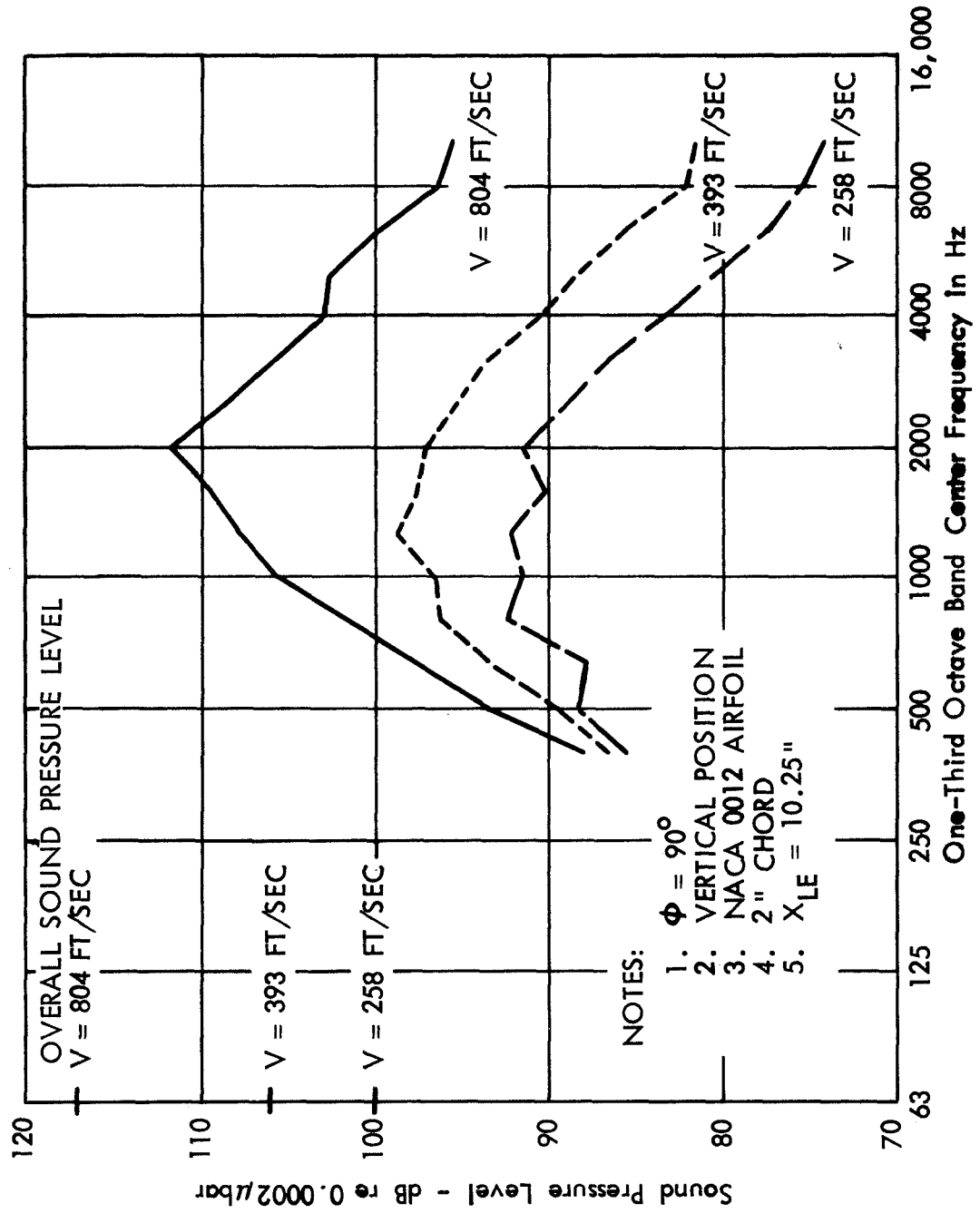

FIGURE 6. AIRFOIL SOUND RADIATION ONE-THIRD OCTAVE BAND SPECTRUM

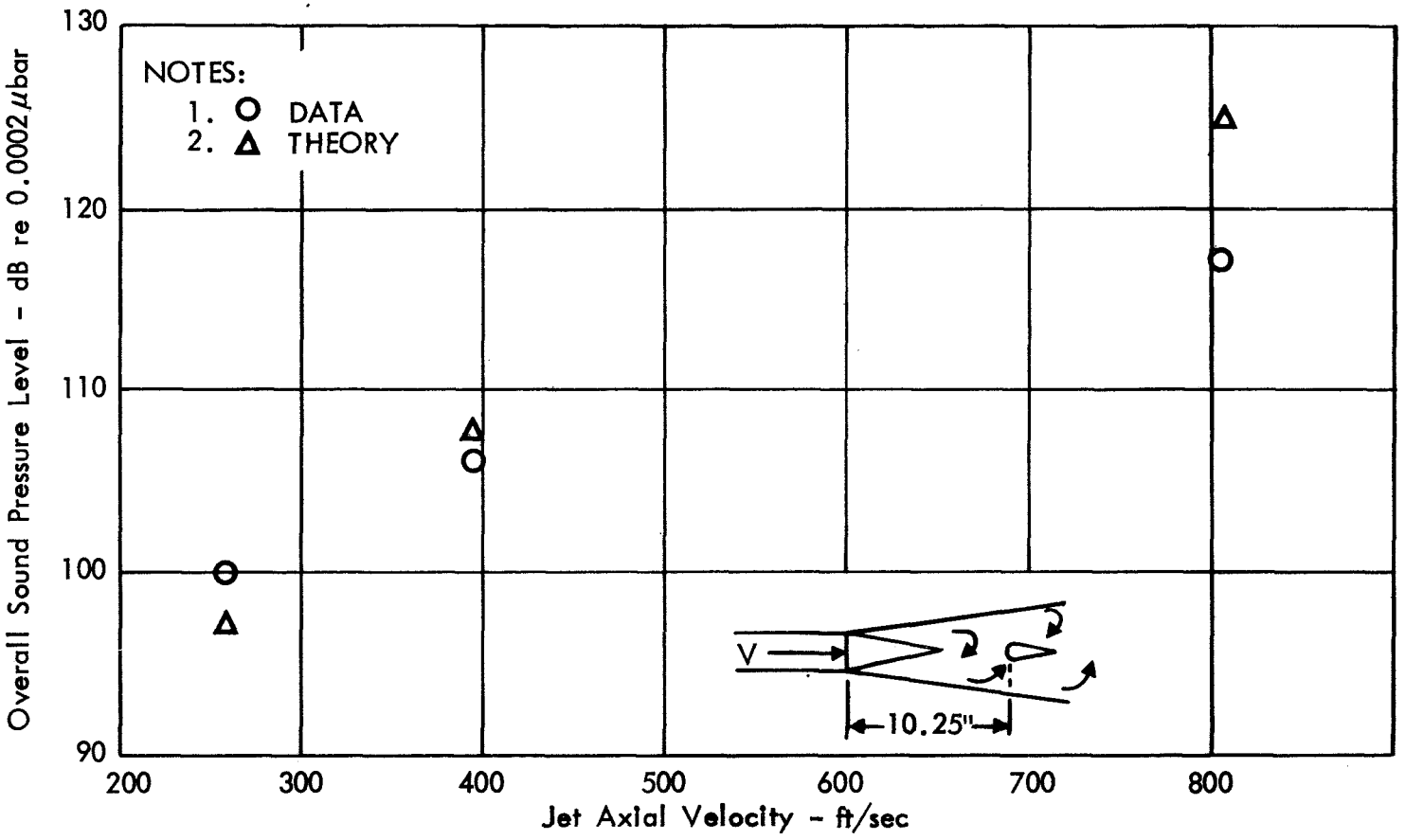

FIGURE 7. AIRFOIL SOUND RADIATION IN TURBULENT FLOW-COMPARISON BETWEEN THEORY AND EXPERIMENT

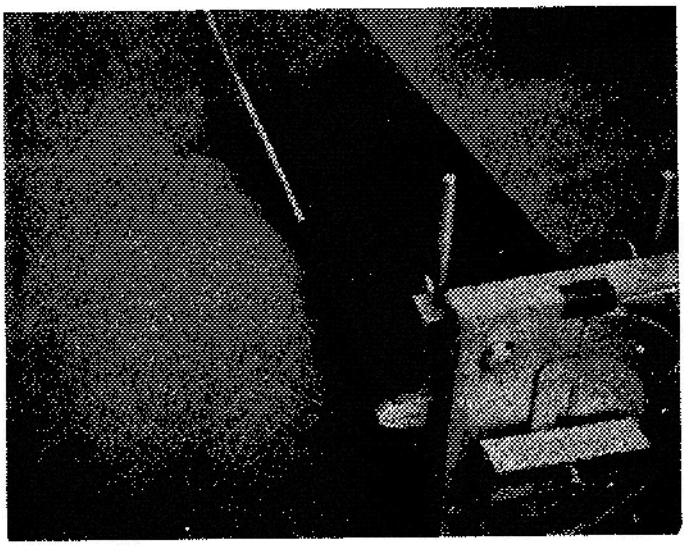

FIGURE 8a. PHOTOGRAPH OF NACA 0012 AIRFOIL SUPPORT APPARATUS USED IN BBN QUIET WIND TUNNEL

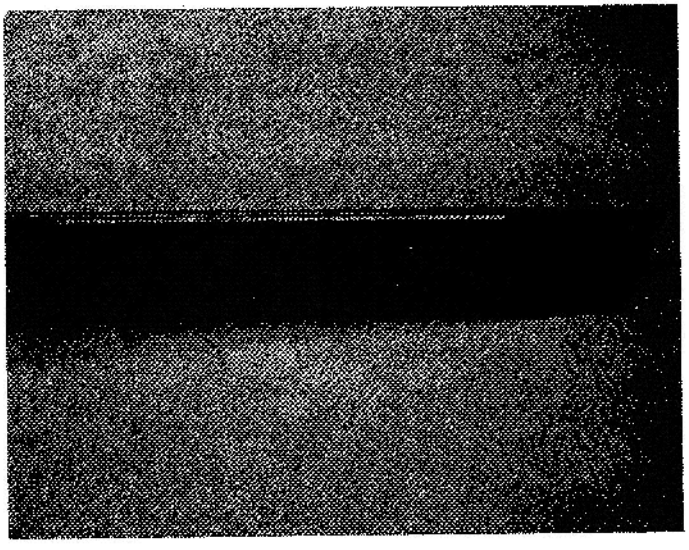

FIGURE 8b. PHOTOGRAPH OF NACA 0012 AIRFOIL WITH LEADING EDGE SERRATION; 6 IN. CHORD, 30 IN. SPAN

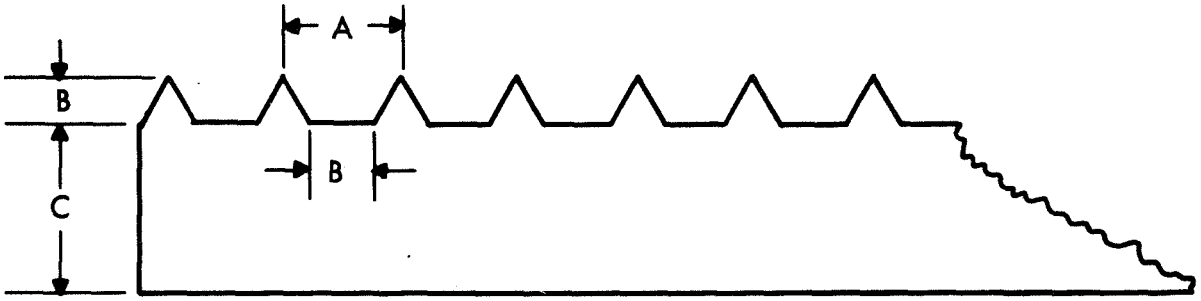

a) Serration Geometry

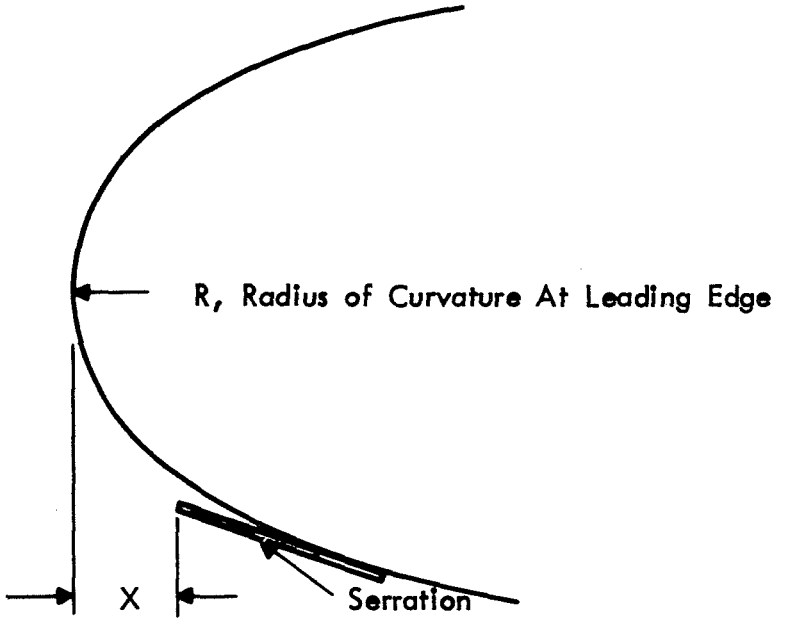

b) Serration Location (Serration Extends Away From Surface)

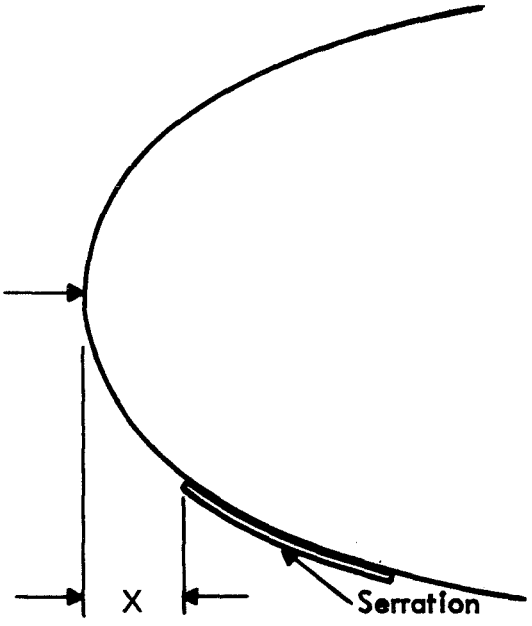

c) Serration Location (Flush Against Surface)

FIGURE 9. SCHEMATIC AND LOCATION OF SERRATIONS (SEE TABLE I)

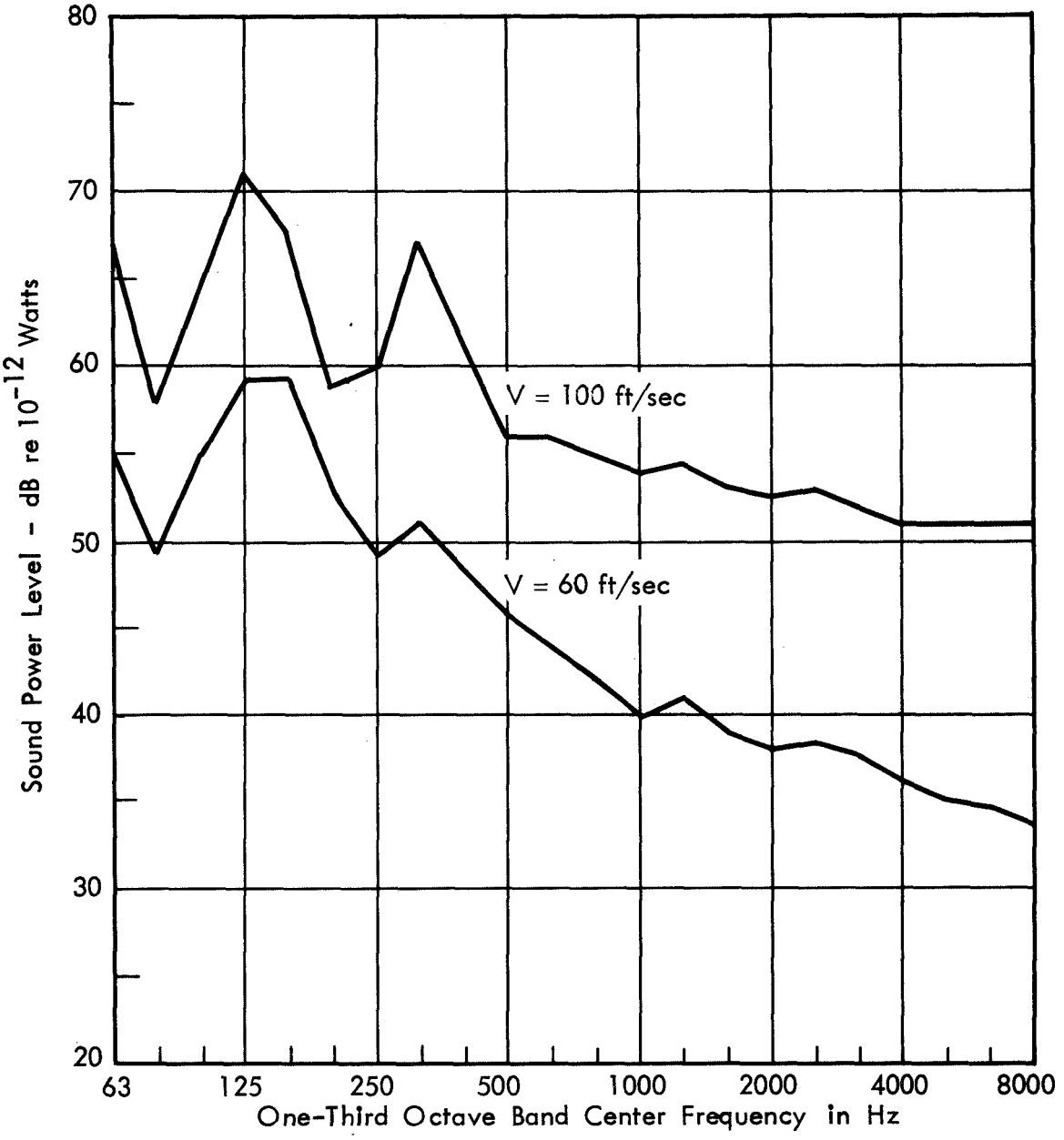

FIGURE 10. BBN FREE-JET BACKGROUND SOUND POWER LEVELS

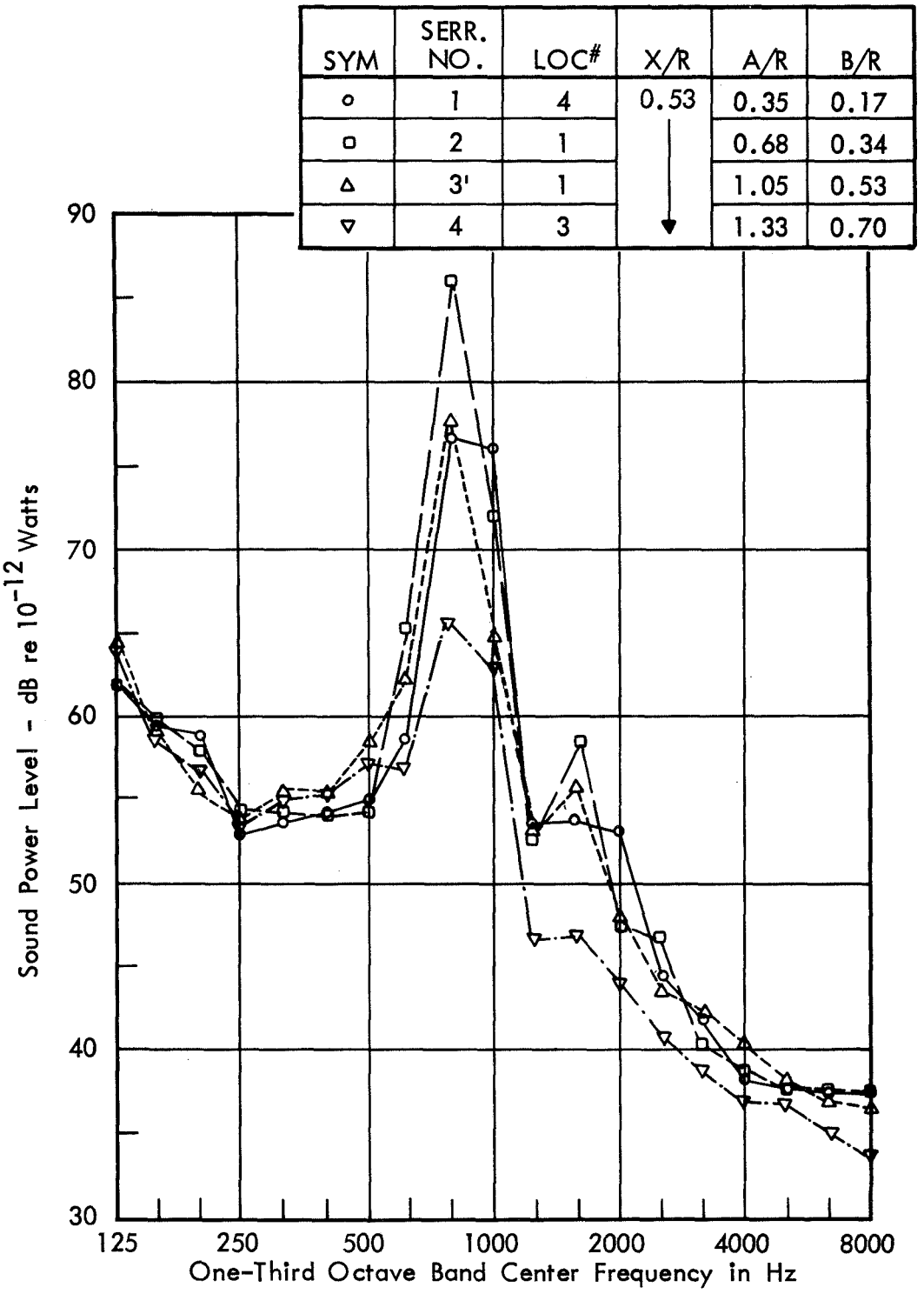

FIGURE 11. EFFECT OF SERRATION SIZE ON AIRFOIL SOUND RADIATION FOR $\alpha = 4^{\circ}$, V = 60 FT/SEC

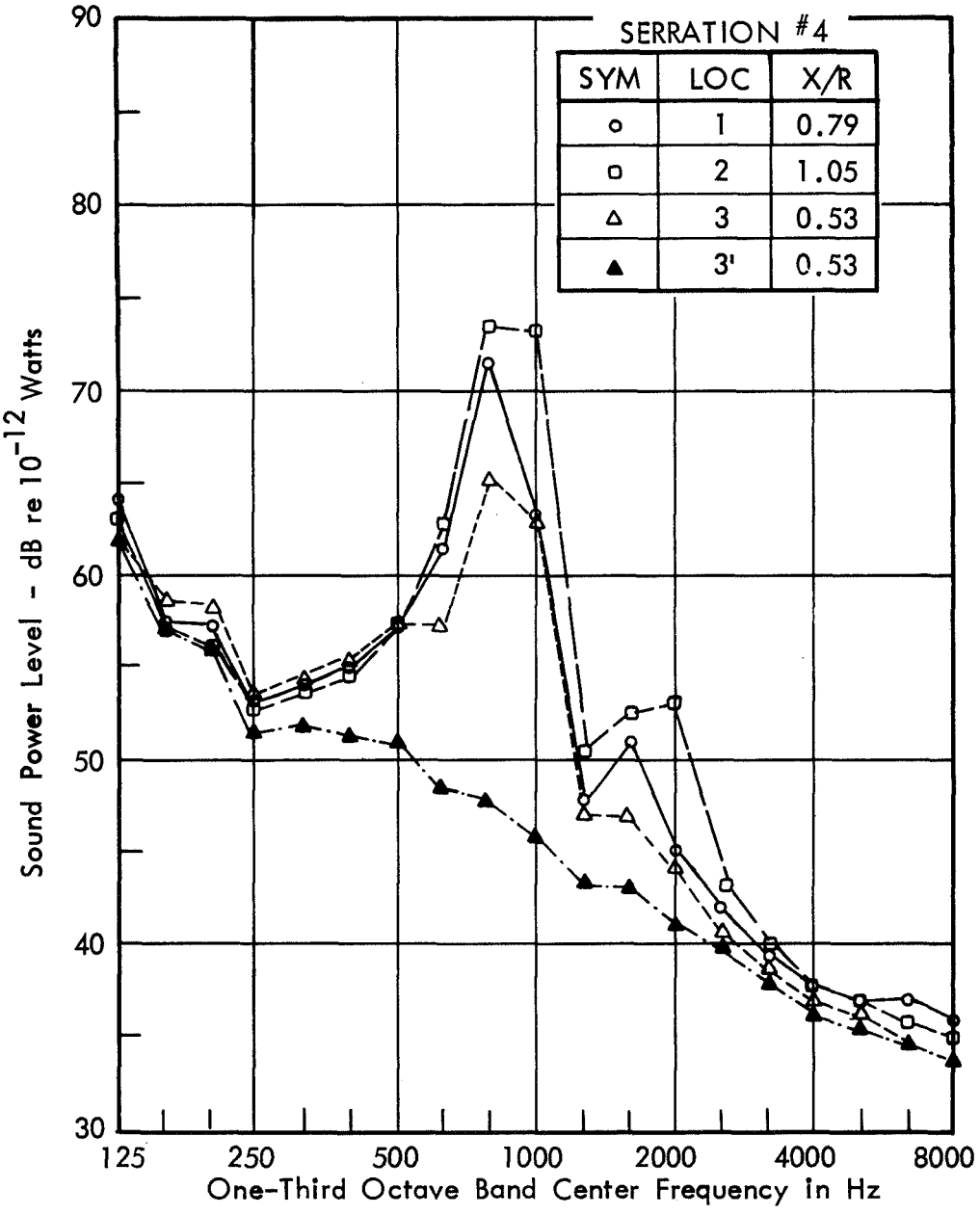

FIGURE 12. EFFECT OF SERRATION LOCATION ON AIRFOIL SOUND RADIATION FOR $\alpha = 4^{\circ}$, V = 60 FT/SEC

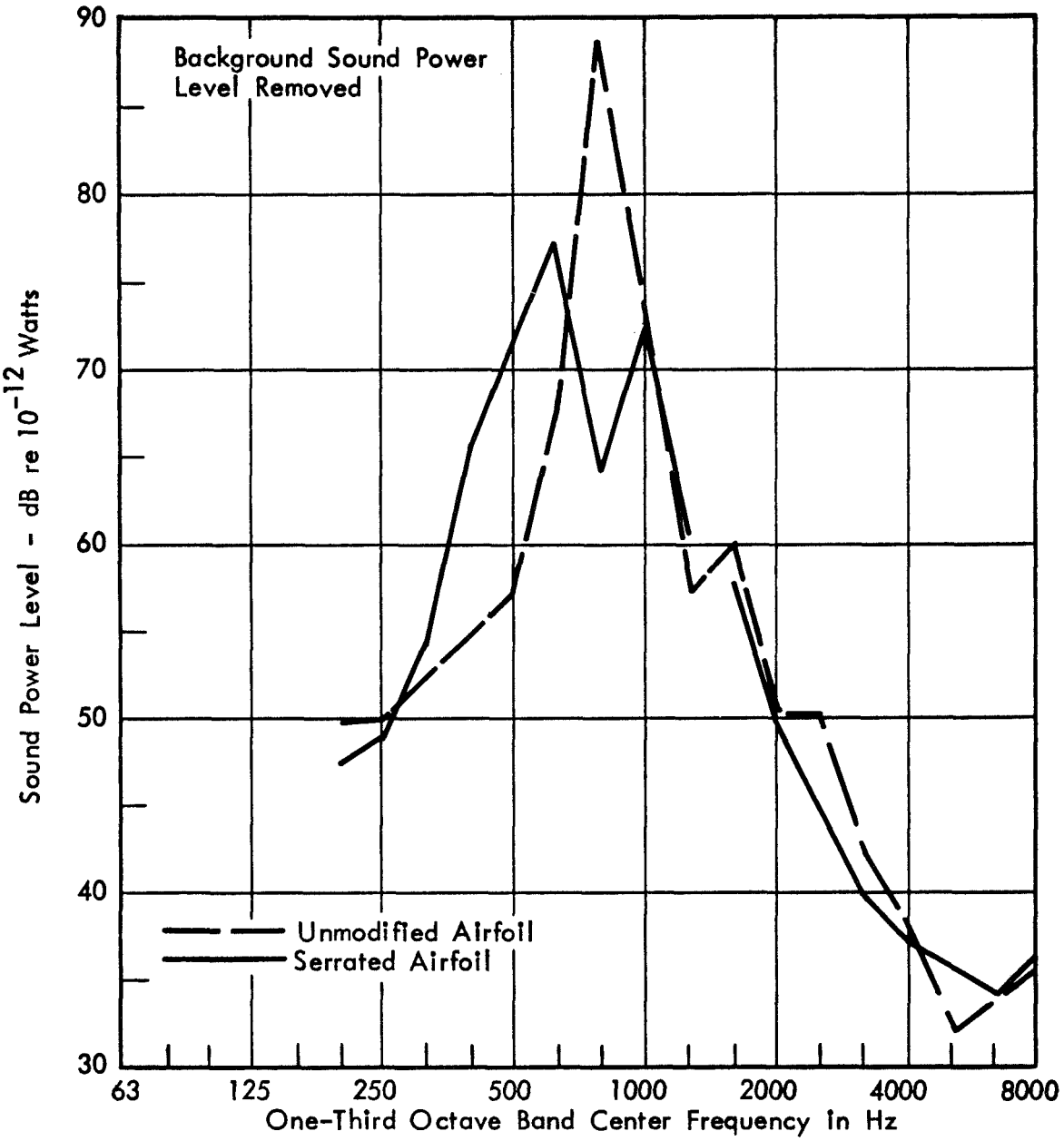

FIGURE 13. EFFECT OF SERRATION 4, LOC 3' ON AIRFOIL SOUND RADIATION FOR $\alpha = 0°$, V = 60 FT/SEC

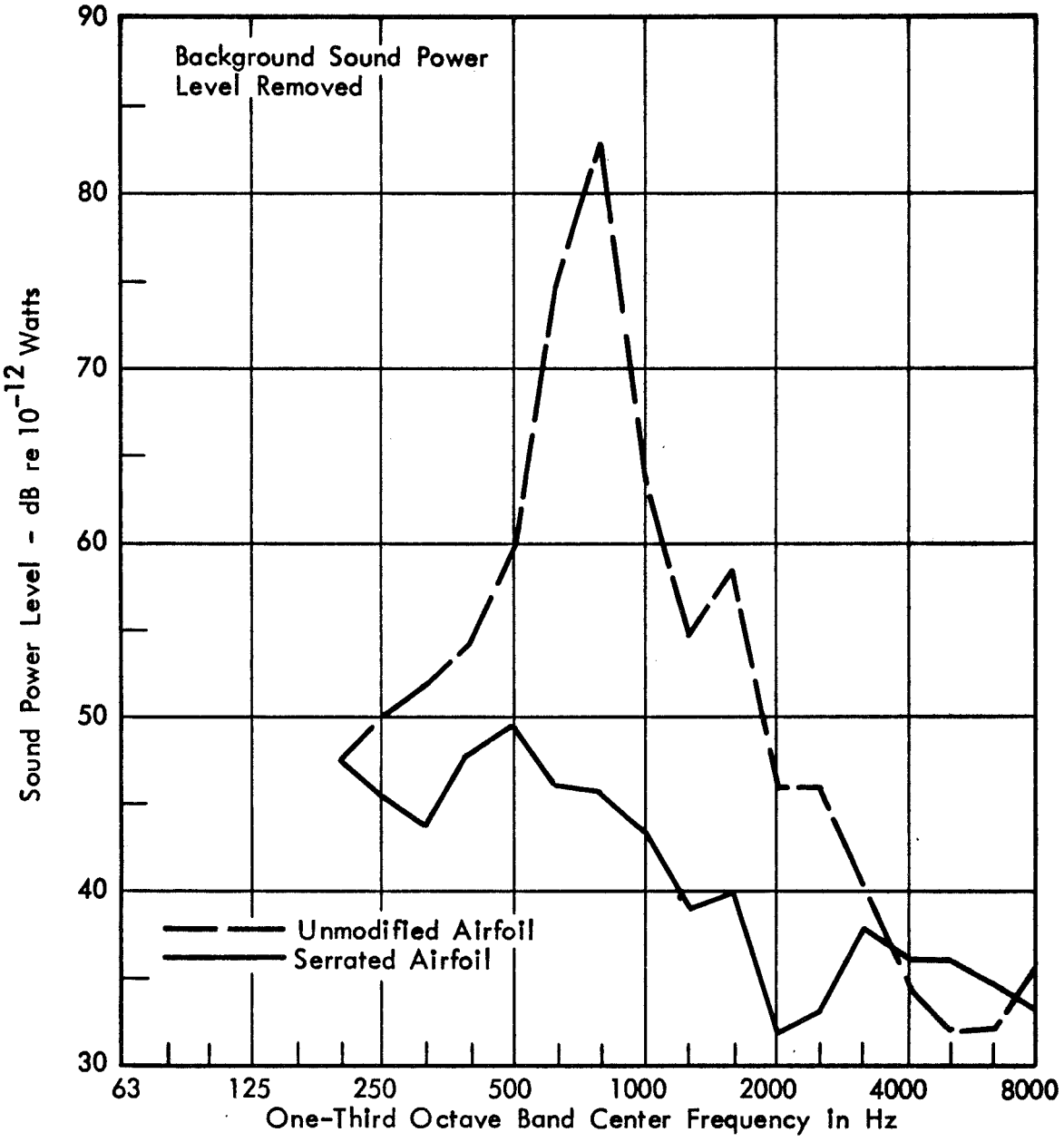

FIGURE 14. EFFECT OF SERRATION 4, LOC 3' ON AIRFOIL SOUND RADIATION FOR α = 4°, V = 60 FT/SEC

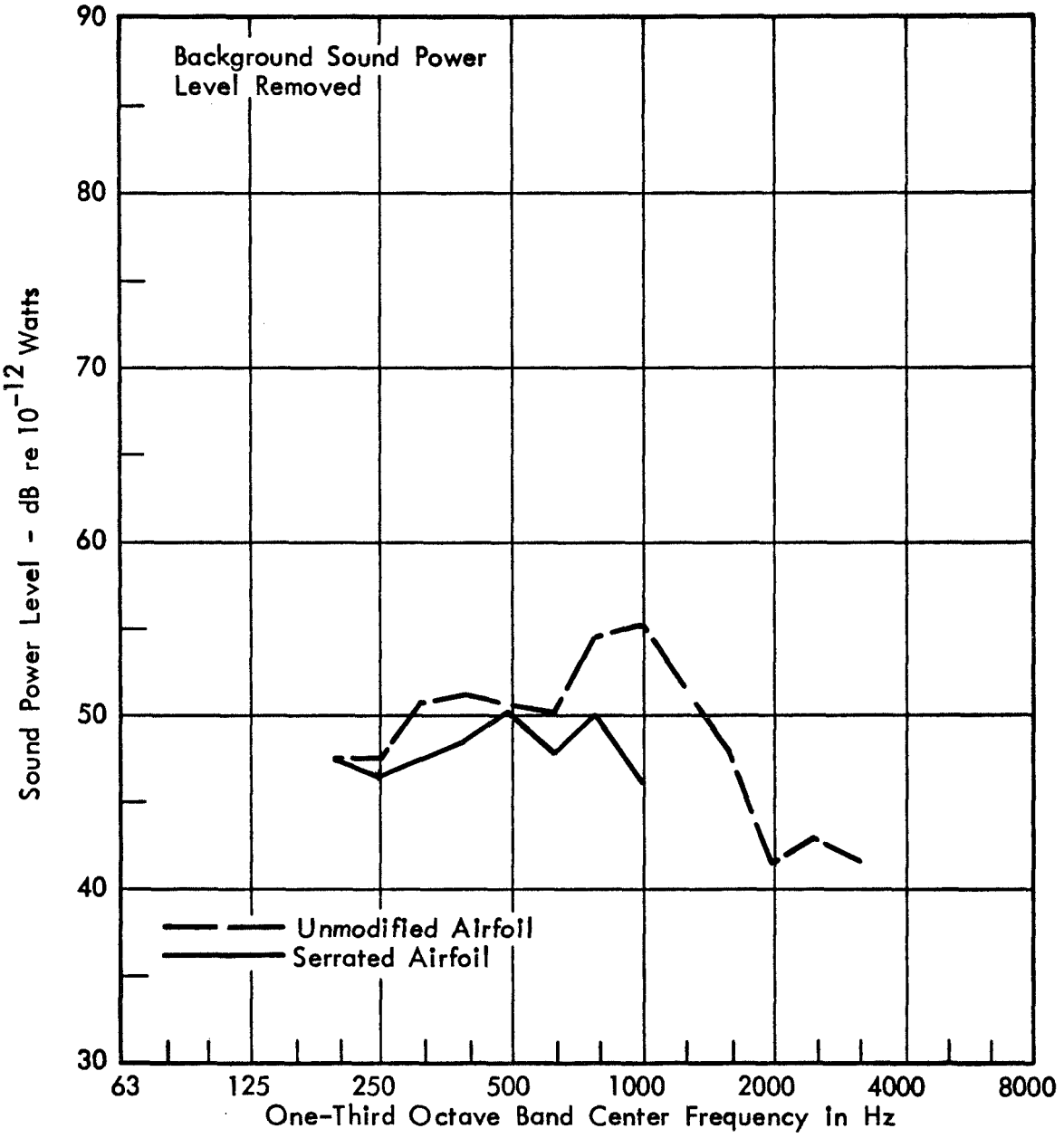

FIGURE 15. EFFECT OF SERRATION 4, LOC 3' ON AIRFOIL SOUND RADIATION FOR $\alpha = 8^{\circ}$, V = 60 FT/SEC

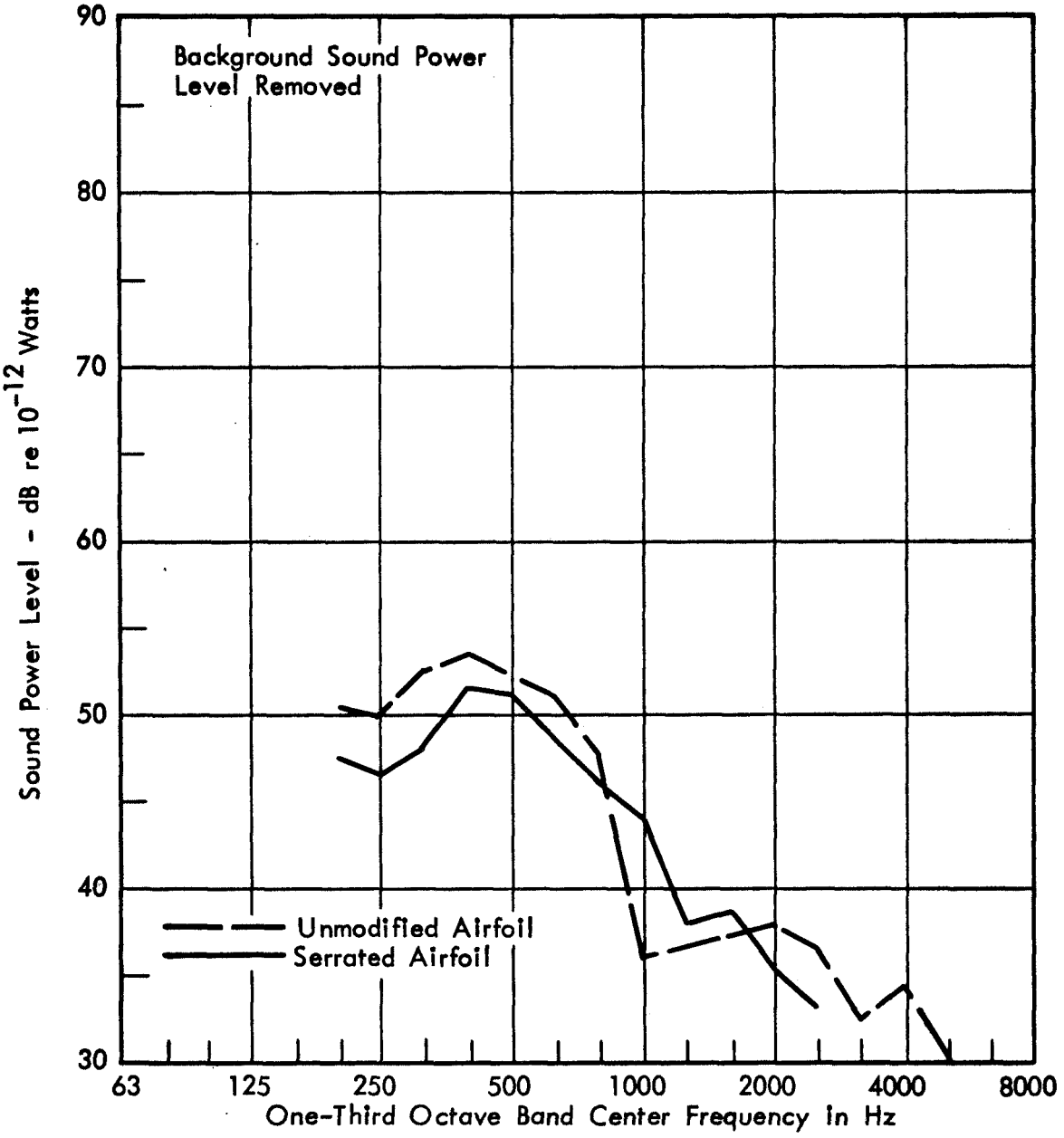

FIGURE 16. EFFECT OF SERRATION 4, LOC 3' ON AIRFOIL SOUND RADIATION FOR α = 12°, V = 60 FT/SEC

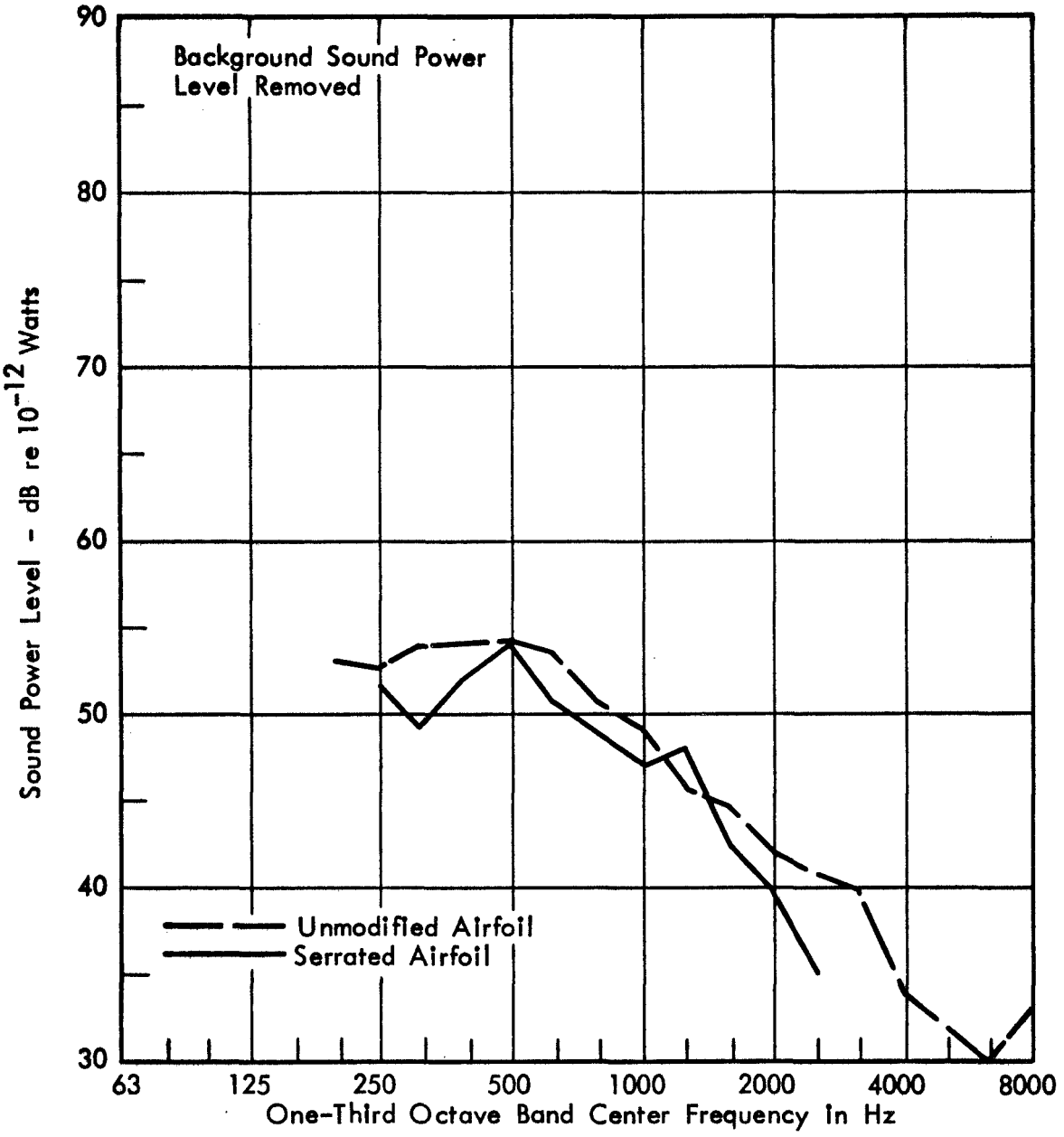

FIGURE 17. EFFECT OF SERRATION 4, LOC 3' ON AIRFOIL SOUND RADIATION FOR $\alpha = 16°$, V = 60 FT/SEC

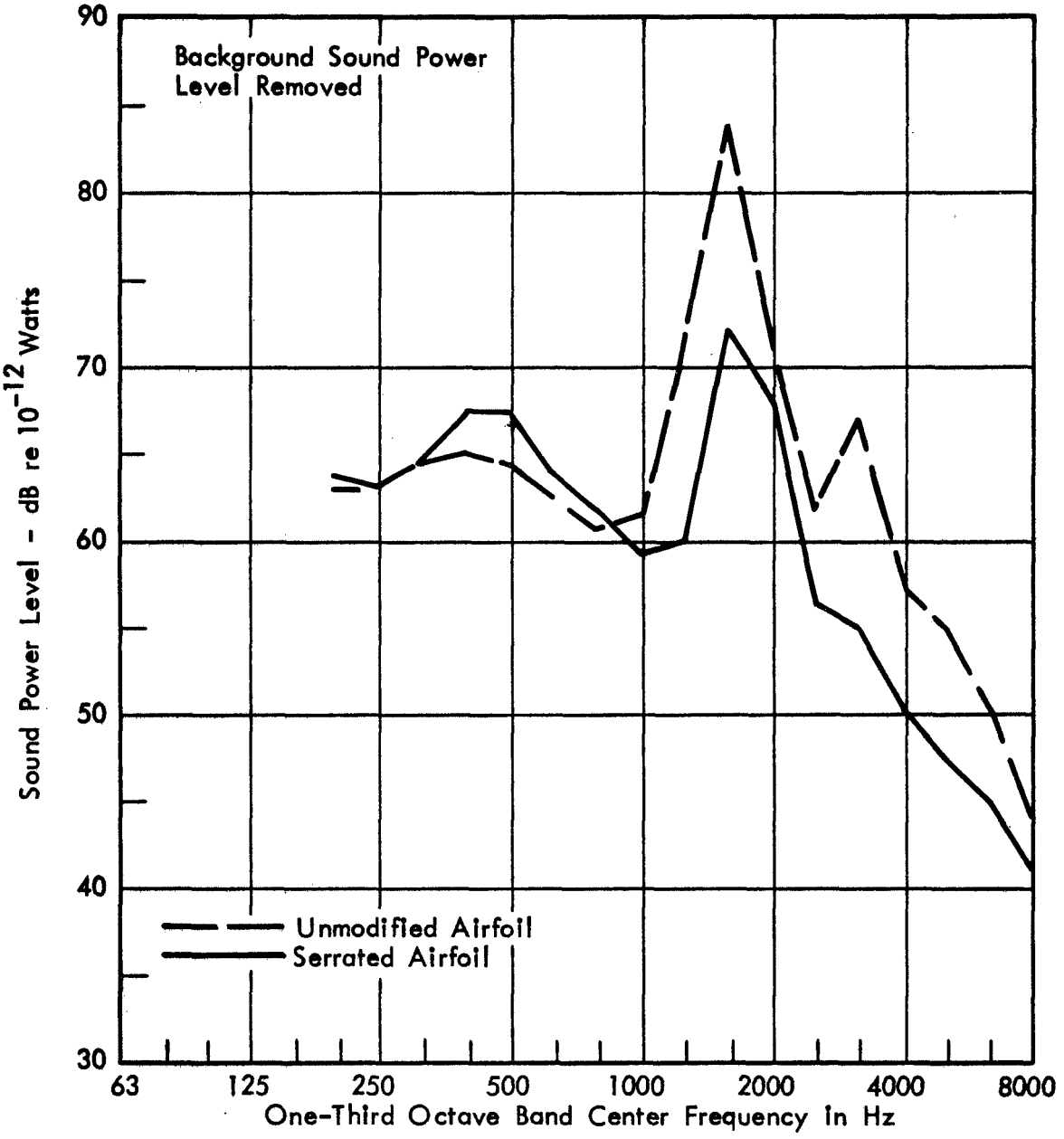

FIGURE 18. EFFECT OF SERRATION 4, LOC 3' ON AIRFOIL SOUND RADIATION FOR α = 0°, V = 100 FT/SEC

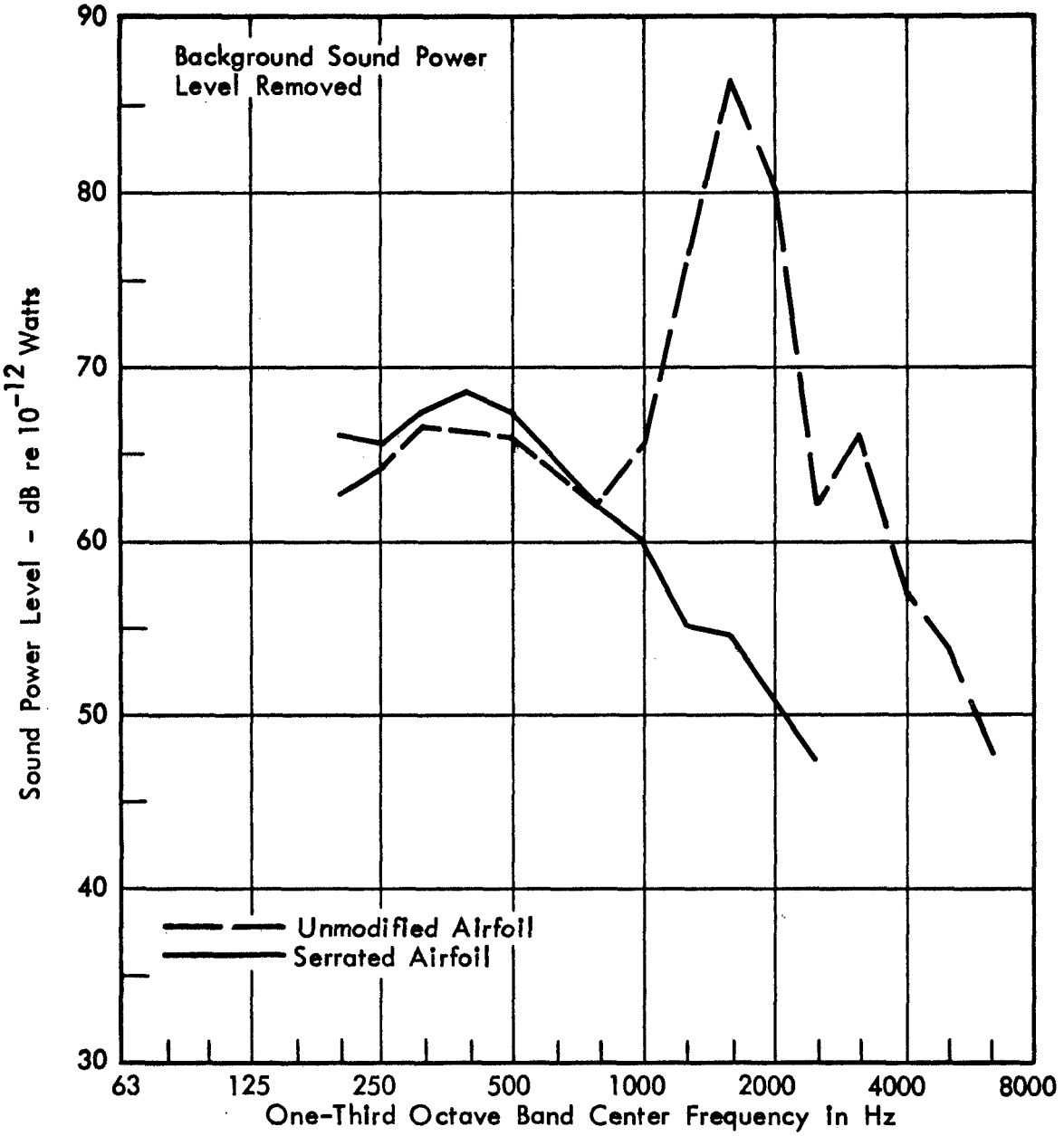

FIGURE 19. EFFECT OF SERRATION 4, LOC 3' ON AIRFOIL SOUND RADIATION FOR $\alpha = 4^{\circ}$, V = 100 FT/SEC

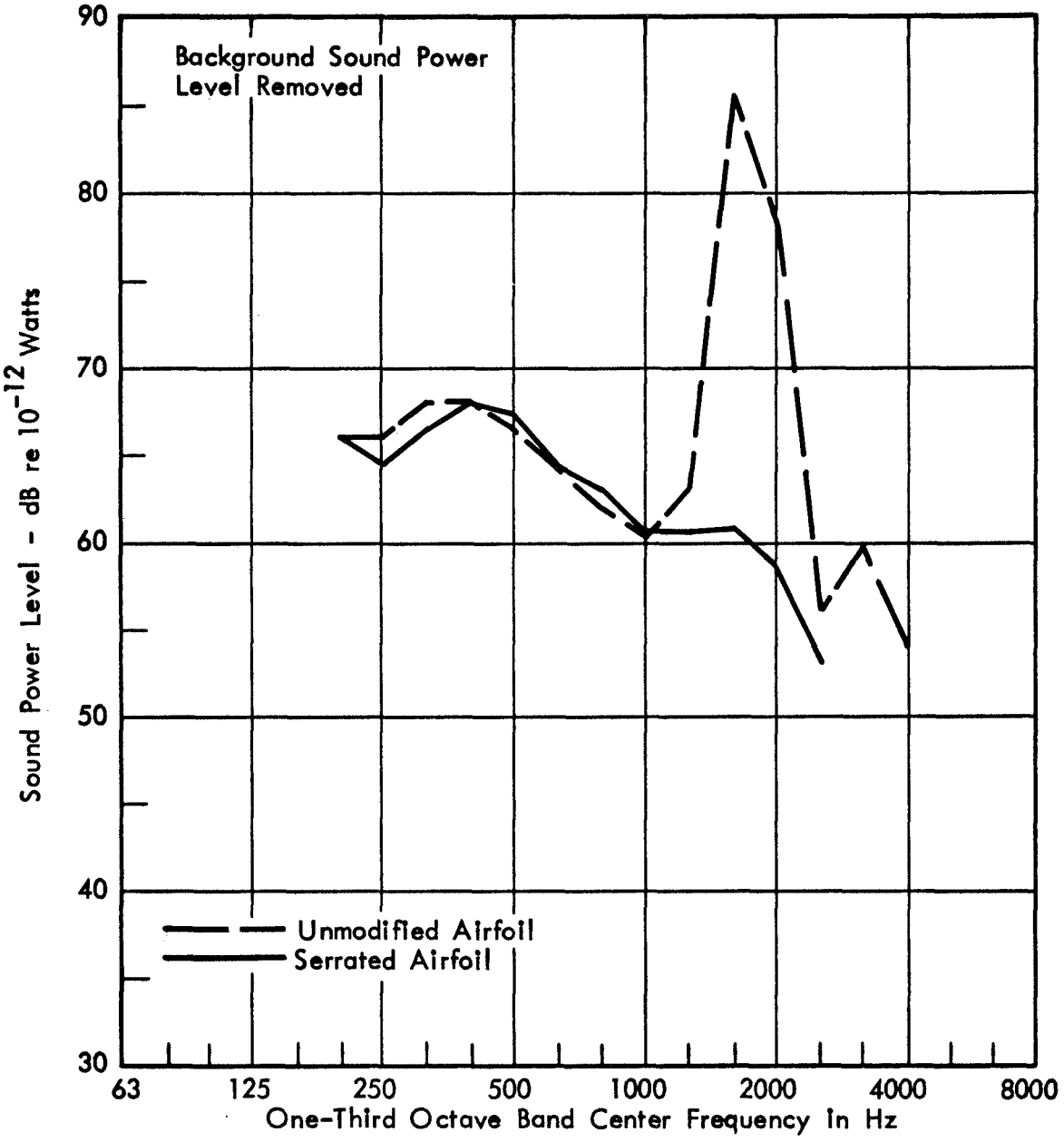

FIGURE 20. EFFECT OF SERRATION 4, LOC 3' ON AIRFOIL SOUND RADIATION FOR $\alpha = 8°$, V = 100 FT/SEC

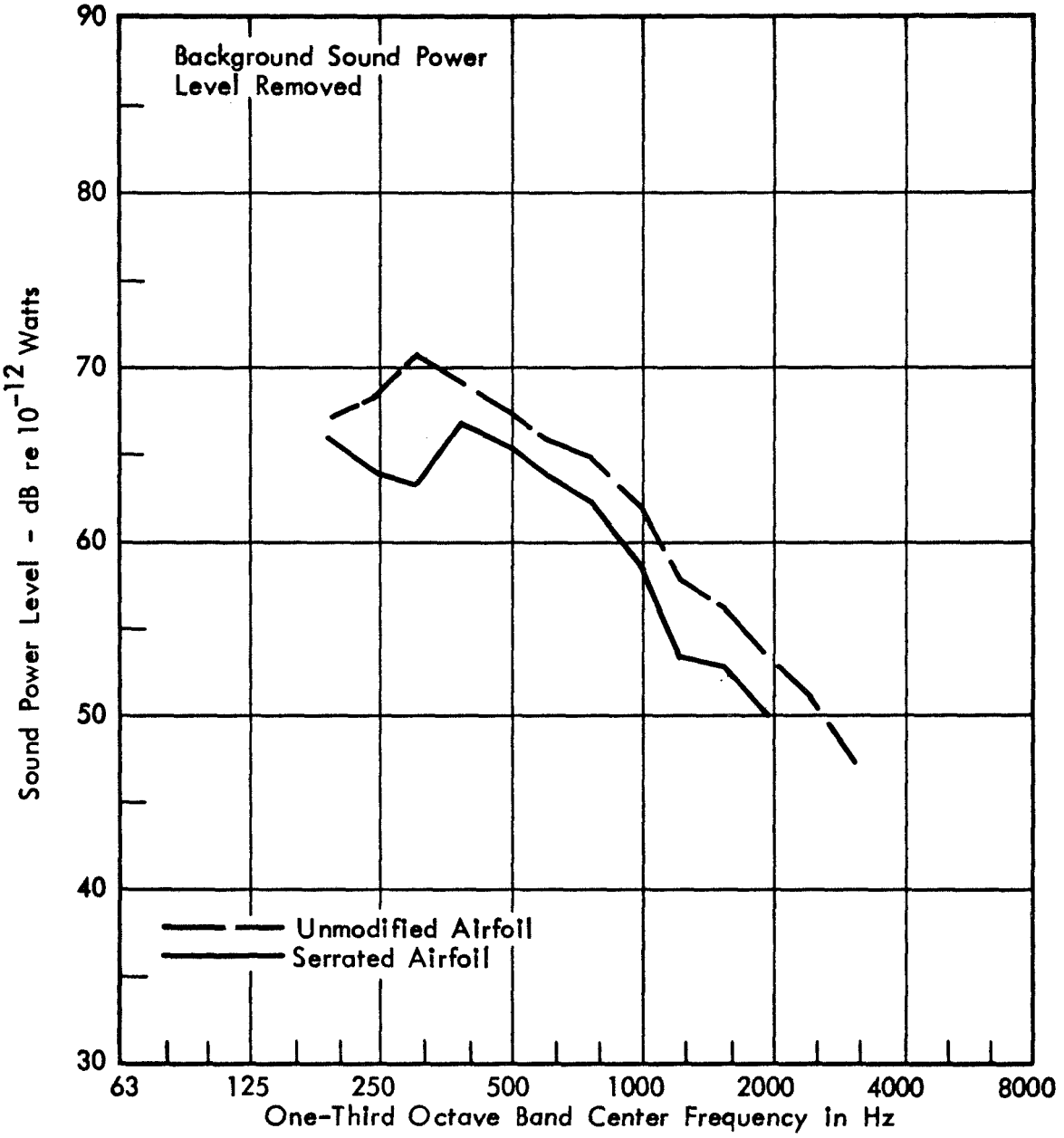

FIGURE 21. EFFECT OF SERRATION 4, LOC 3' ON AIRFOIL SOUND RADIATION FOR α = 12°, V = 100 FT/SEC

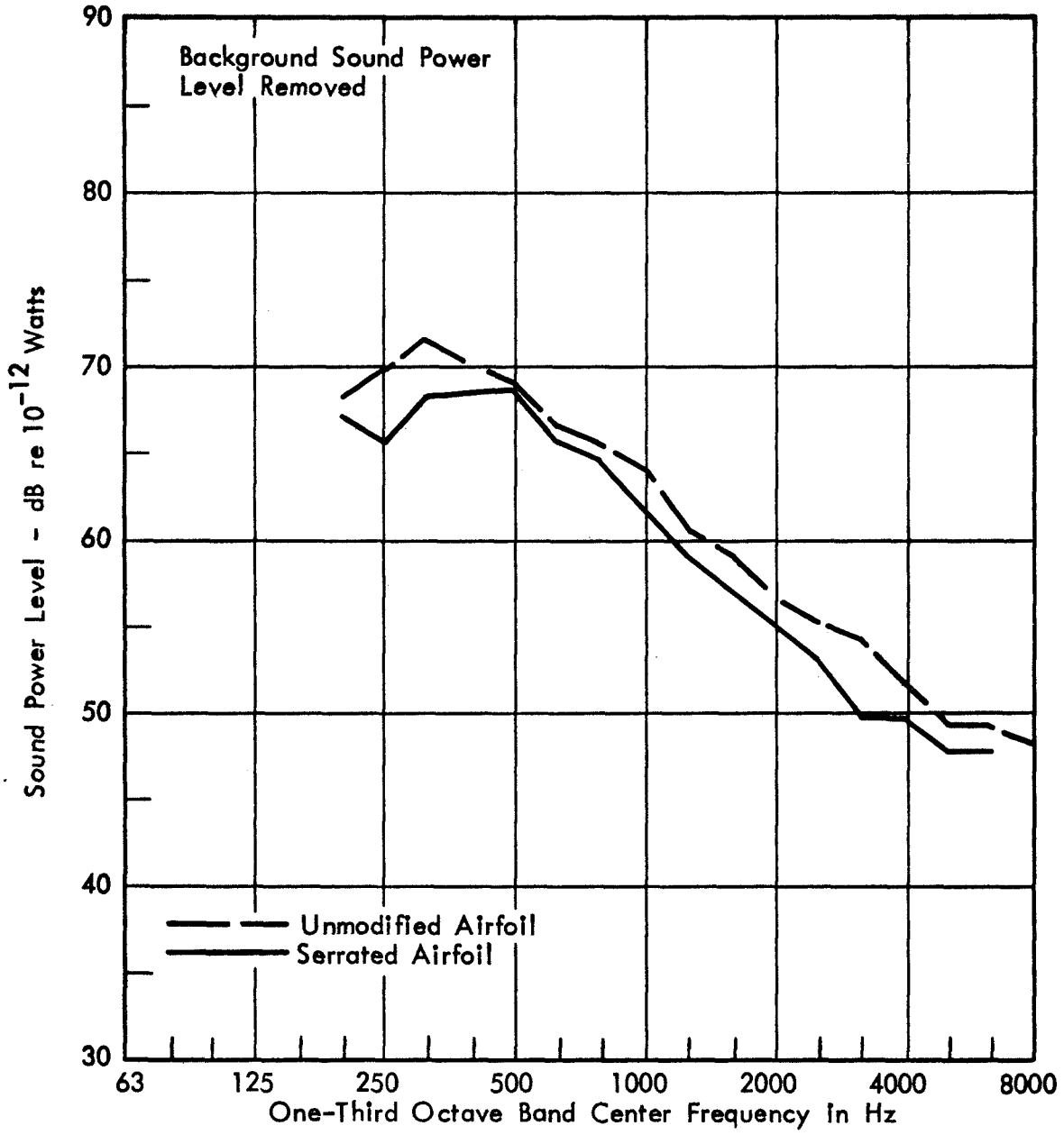

FIGURE 22. EFFECT OF SERRATION 4, LOC 3' ON AIRFOIL SOUND RADIATION FOR α = 16°, V = 100 FT/SEC

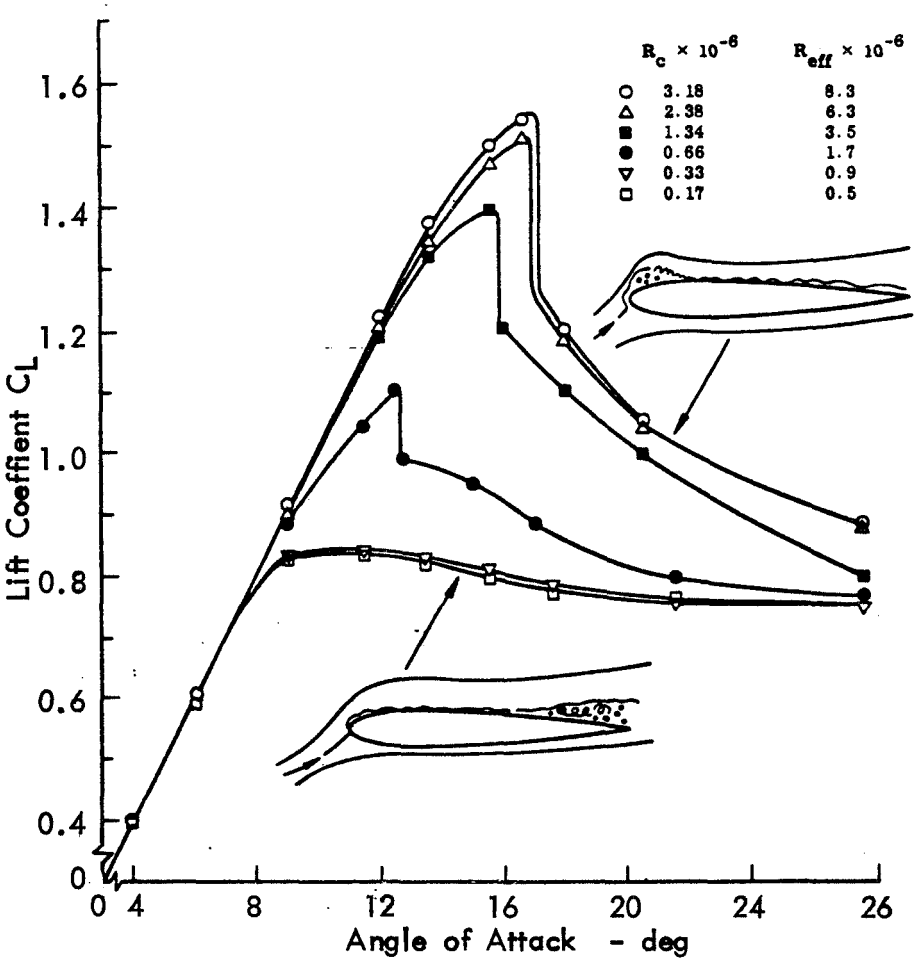

FIGURE 23. EFFECT OF REYNOLDS NUMBER ON NACA 0012 AIRFOIL CHARACTERISTICS (REF 25)

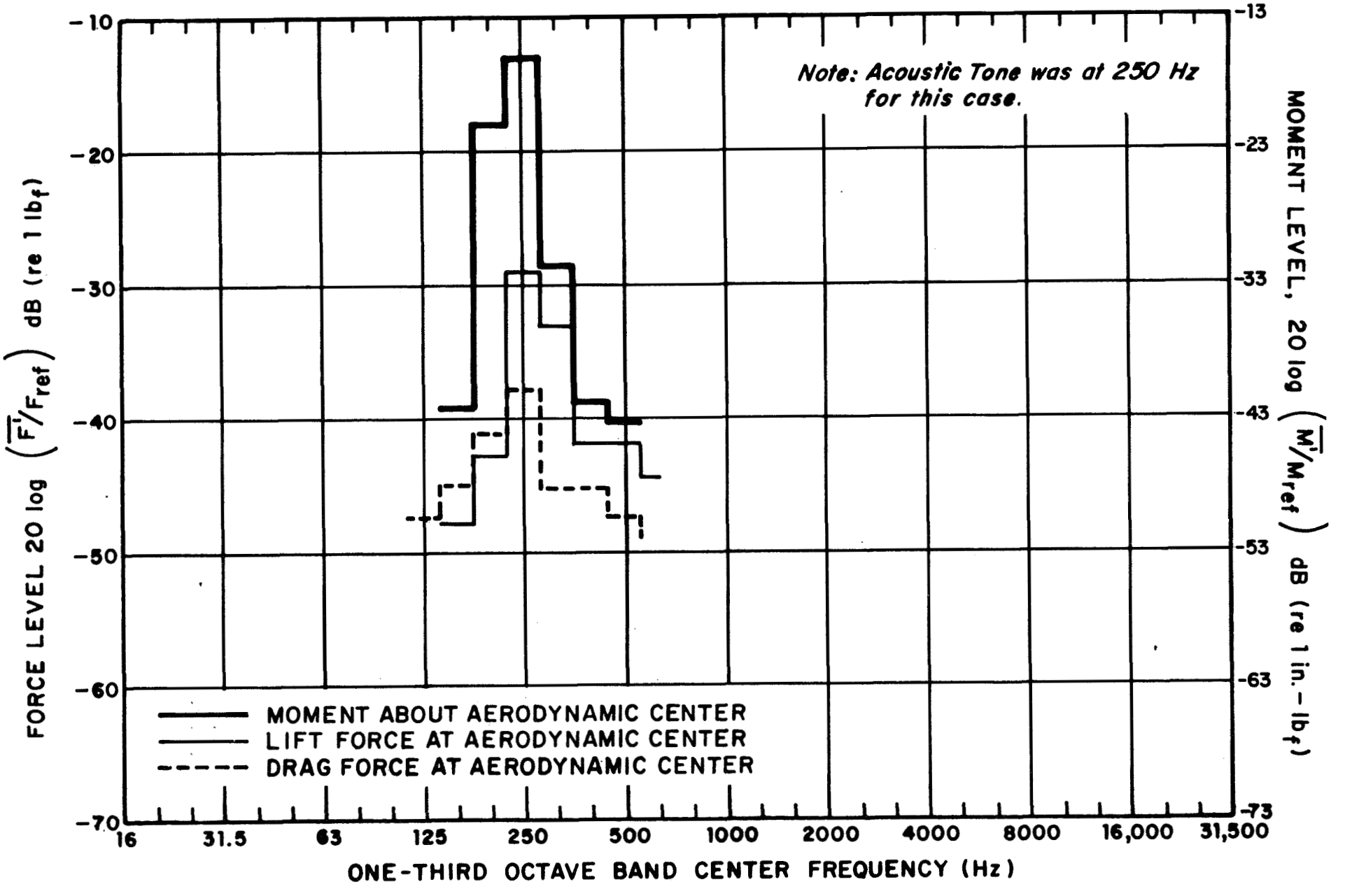

FIGURE 24. FLUCTUATING LIFT, DRAG AND MOMENT ABOUT AERODYNAMIC CENTER OF UNMODIFIED NACA 0012 AIRFOIL FOR $\alpha = 0°$, V = 25 FT/SEC

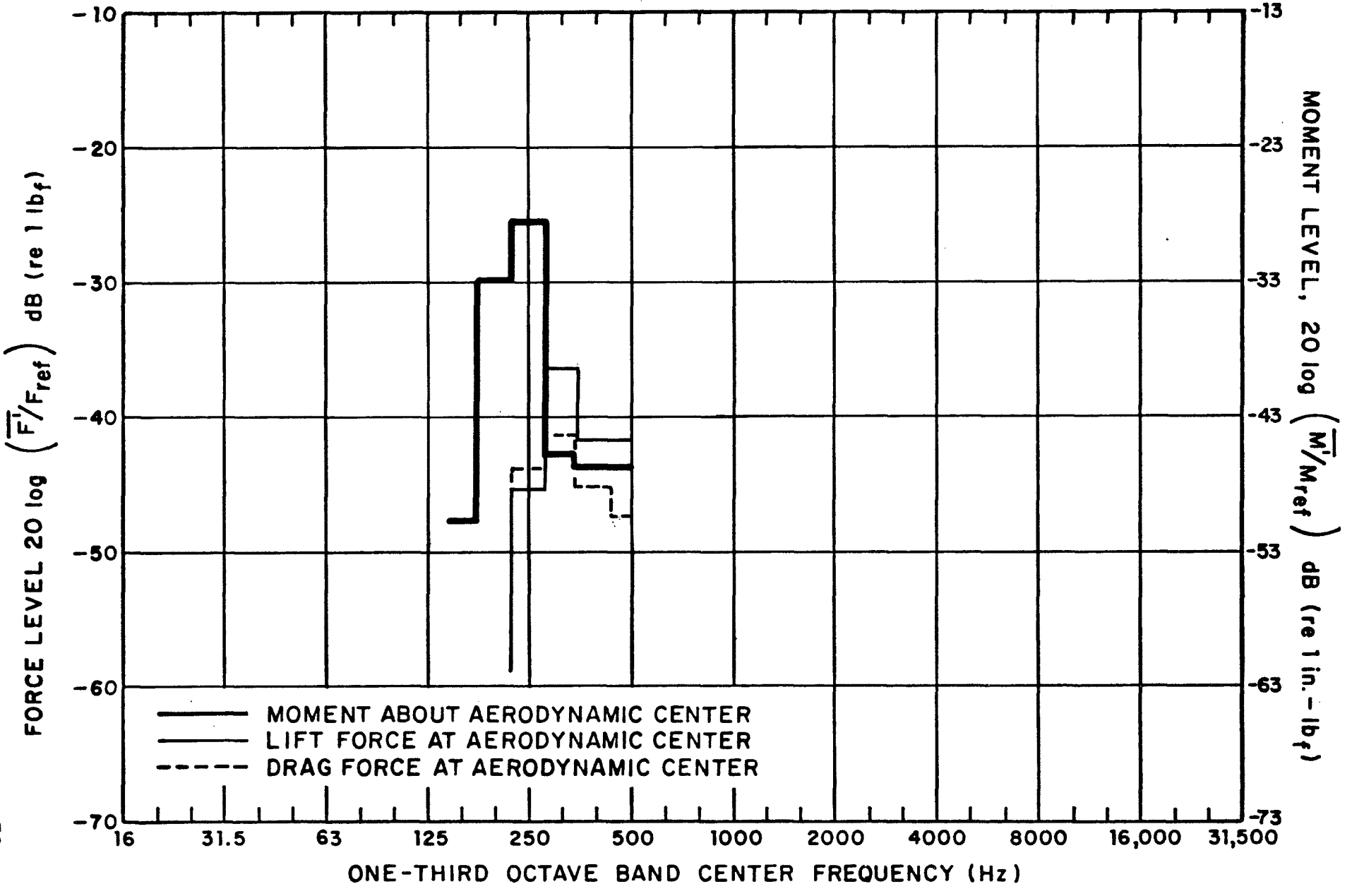

FIGURE 25. FLUCTUATING LIFT, DRAG AND MOMENT ABOUT AERODYNAMIC CENTER OF NACA 0012 AIRFOIL WITH SERRATION 4, LOC 3' FOR $\alpha = 0°$, V = 25 FT/SEC

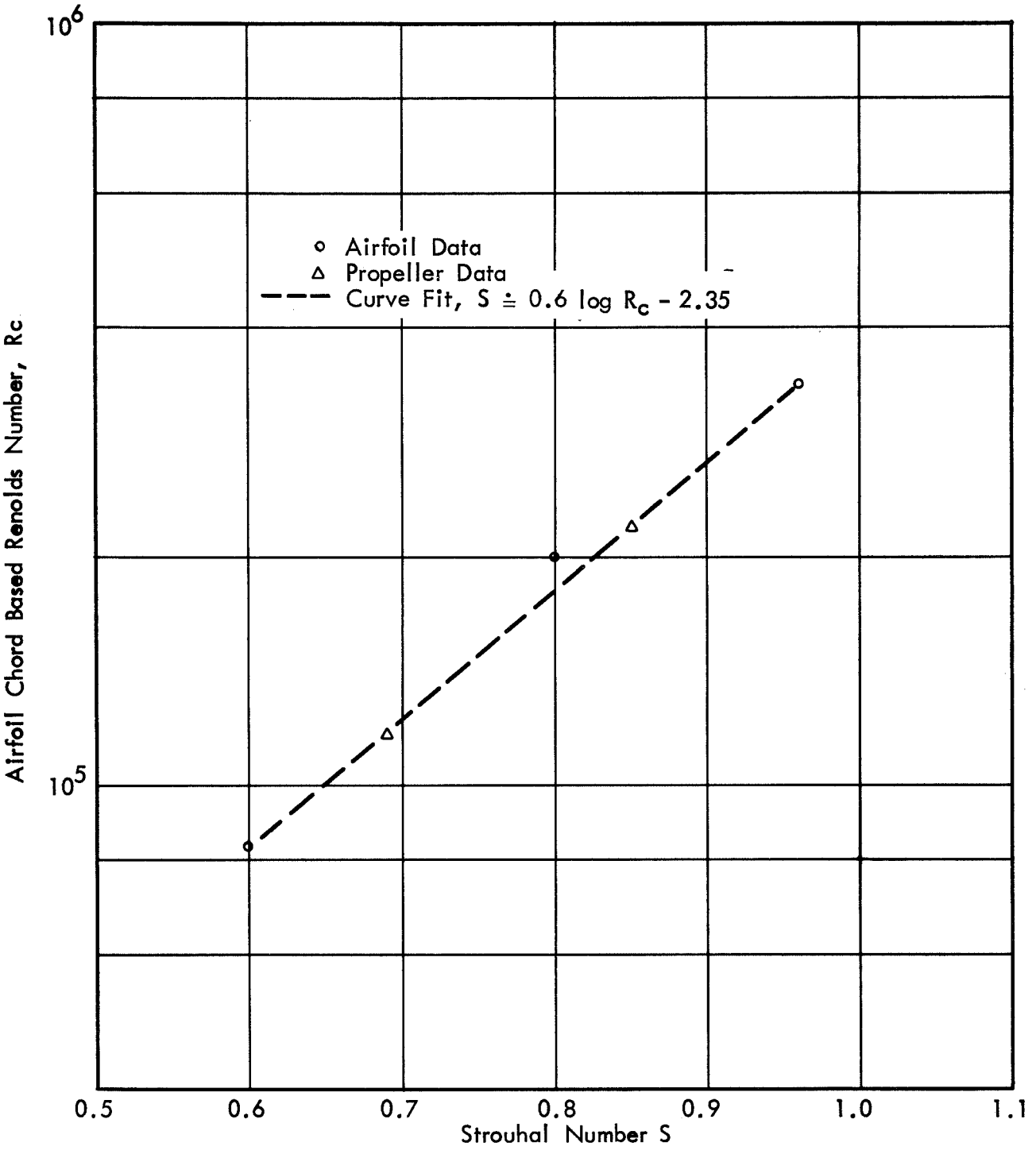

FIGURE 26. VARIATION OF STROUHAL NO. OF THE TONE WITH REYNOLDS NUMBER

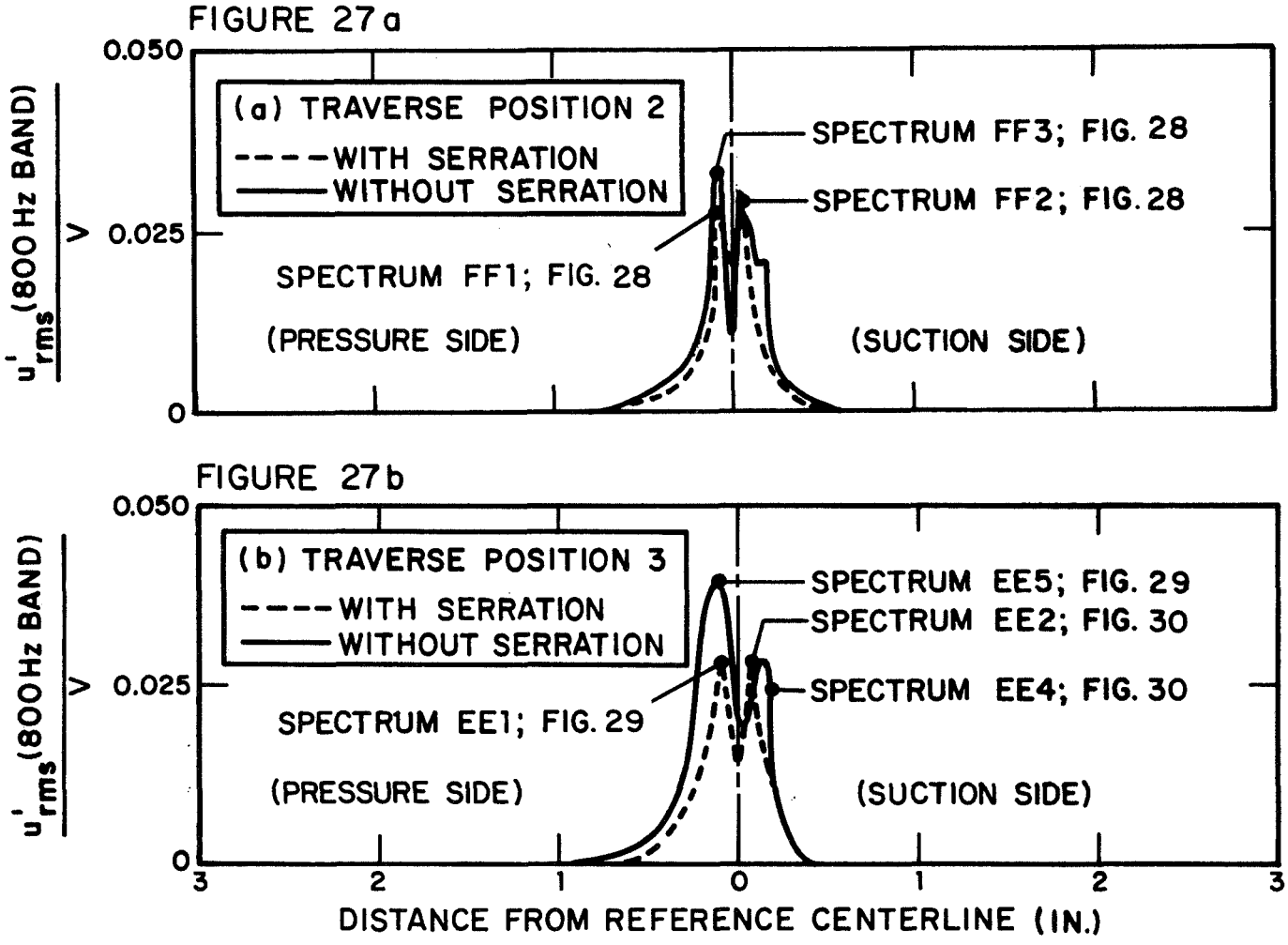

FIGURE 27. PROFILES OF UNSTEADY VELOCITY IN ACOUSTIC TONE BAND (800 Hz) IN VICINITY OF TRAILING EDGE; V = 60 FT/SEC (SEE FIGURE 33 FOR LOCATION OF TRAVERSE POSITIONS)

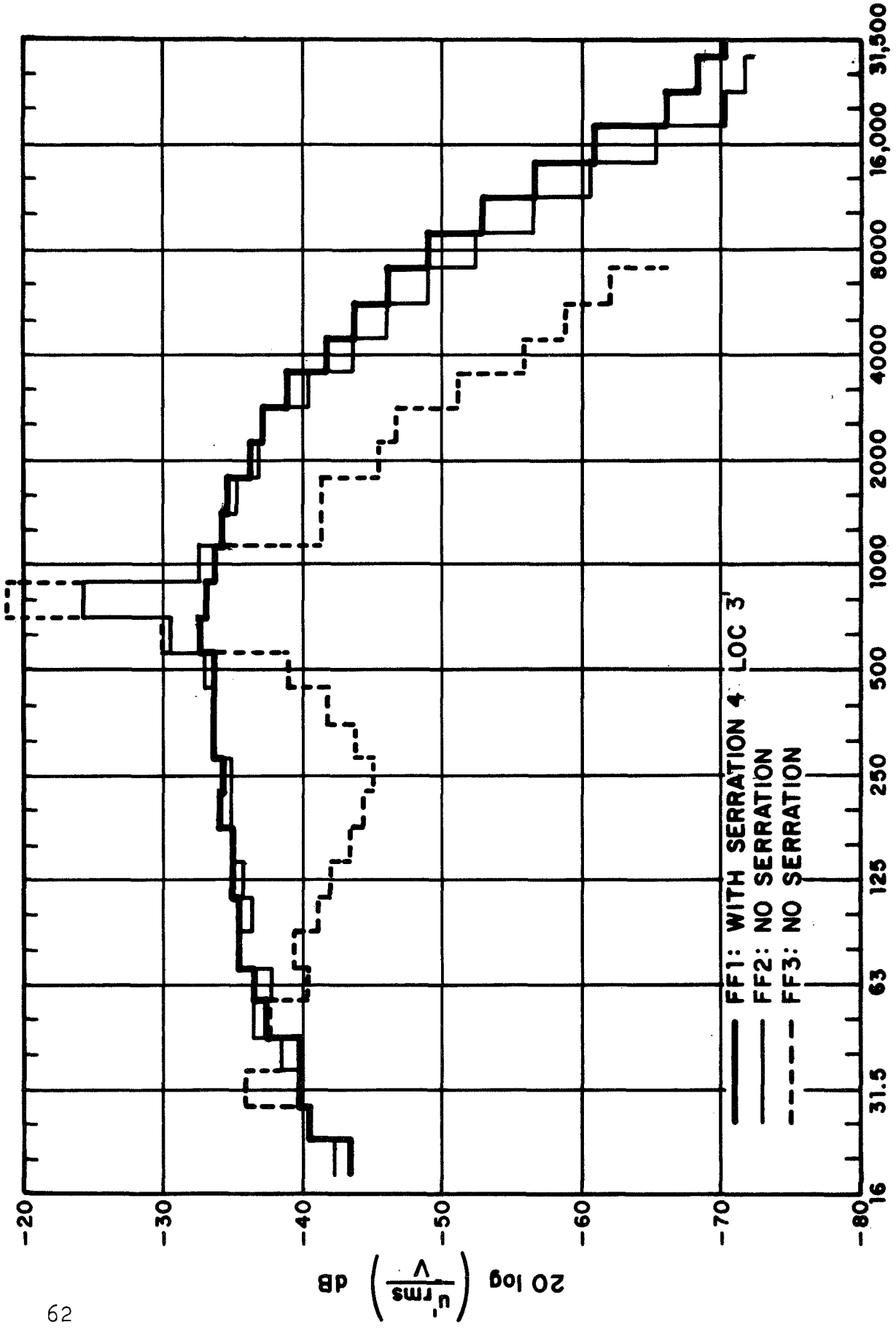

FIGURE 28. WAKE TURBULENCE, 0.1" BEHIND TRAILING EDGE (SEE FIGURE 27 FOR PROBE LOCATION) $\alpha = +4°$, V = 60 FT/SEC

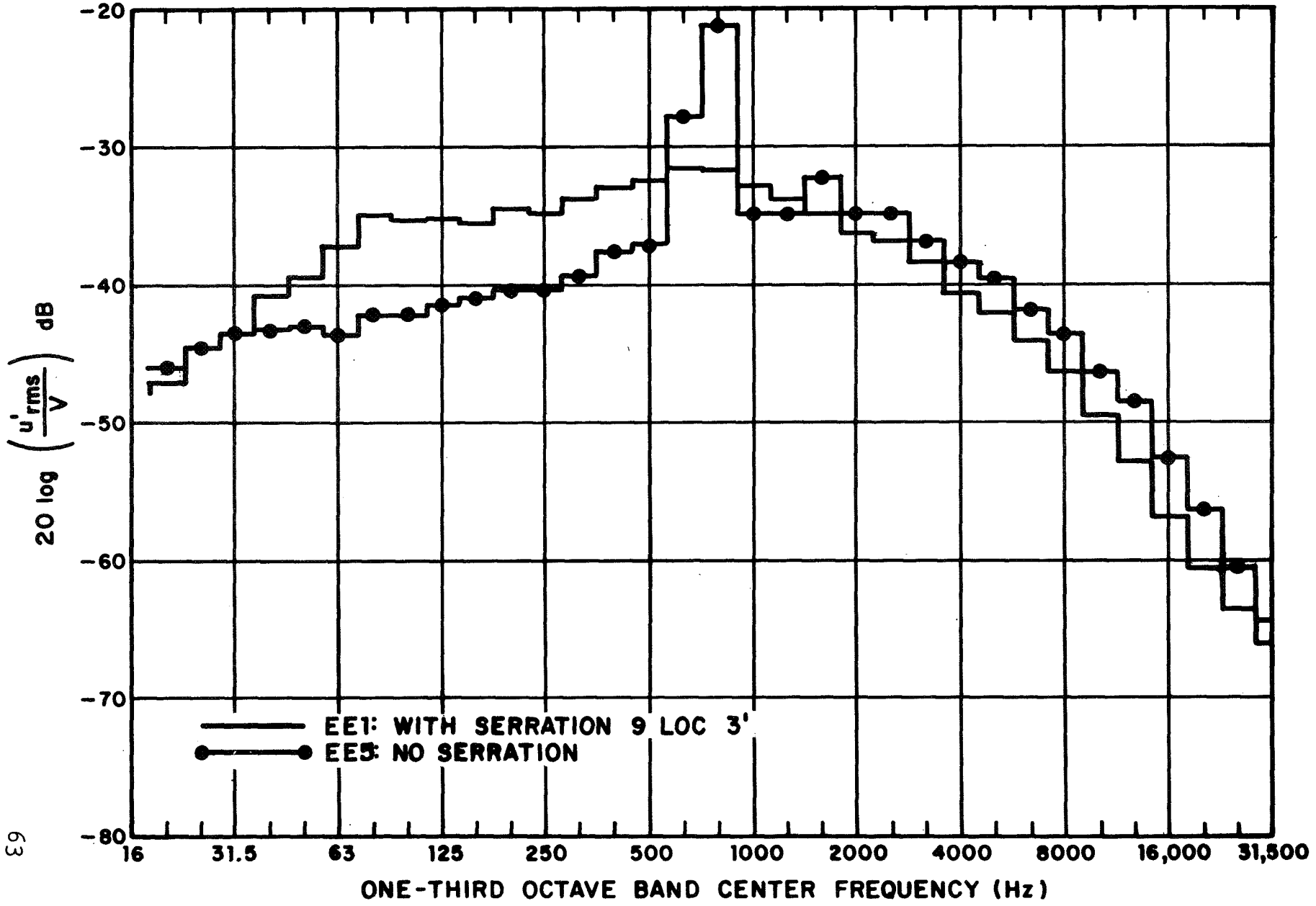

FIGURE 29. WAKE TURBULENCE 1" FROM TRAILING EDGE (SEE FIGURE 27 FOR PROBE LOCATION) $\alpha = +4^{\circ}$, V = 60 FT/SEC

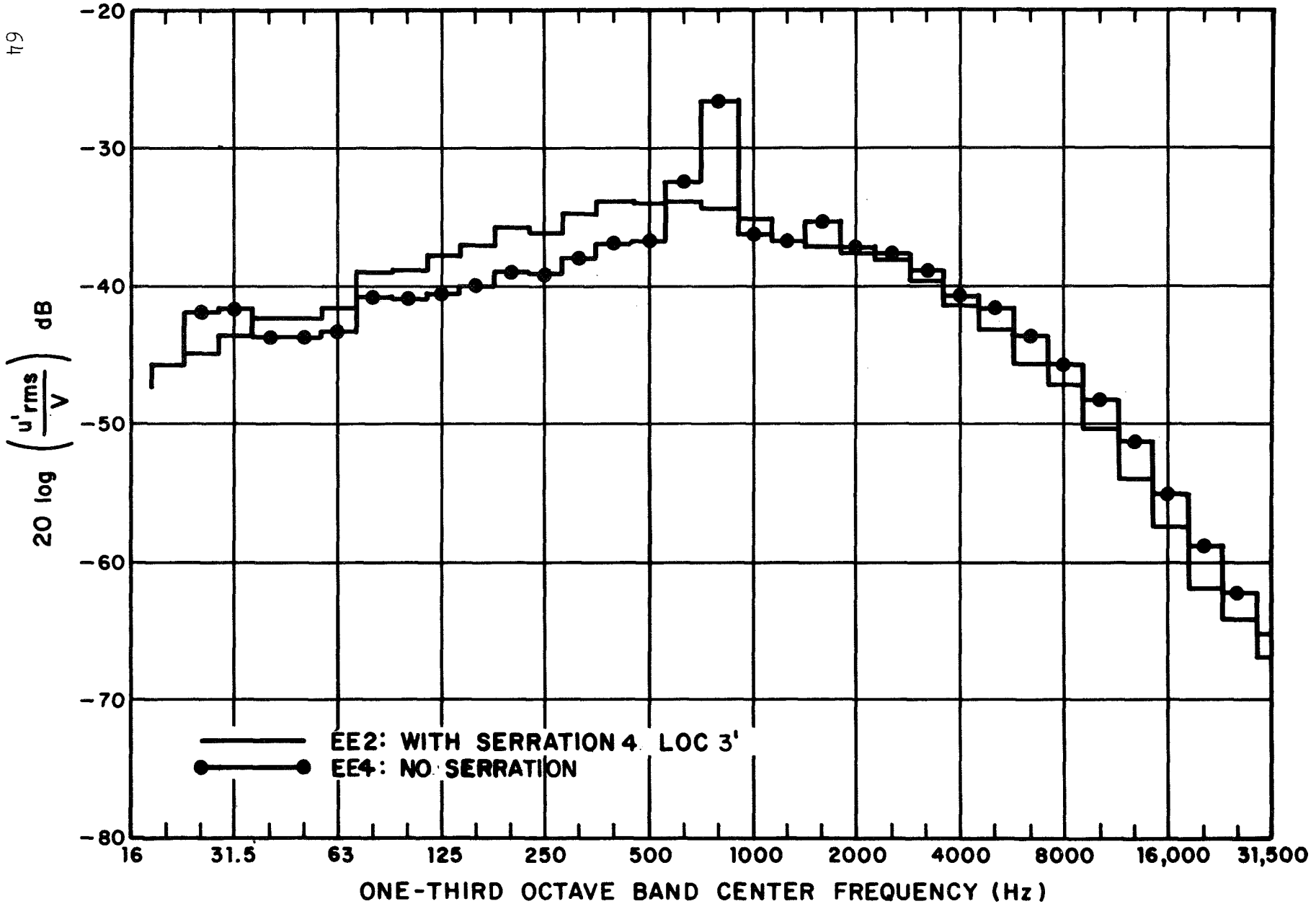

FIGURE 30. WAKE TURBULENCE 1" FROM TRAILING EDGE (SEE FIGURE 27 FOR PROBE LOCATION) $\alpha = +4^{\circ}$, V = 60 FT/SEC

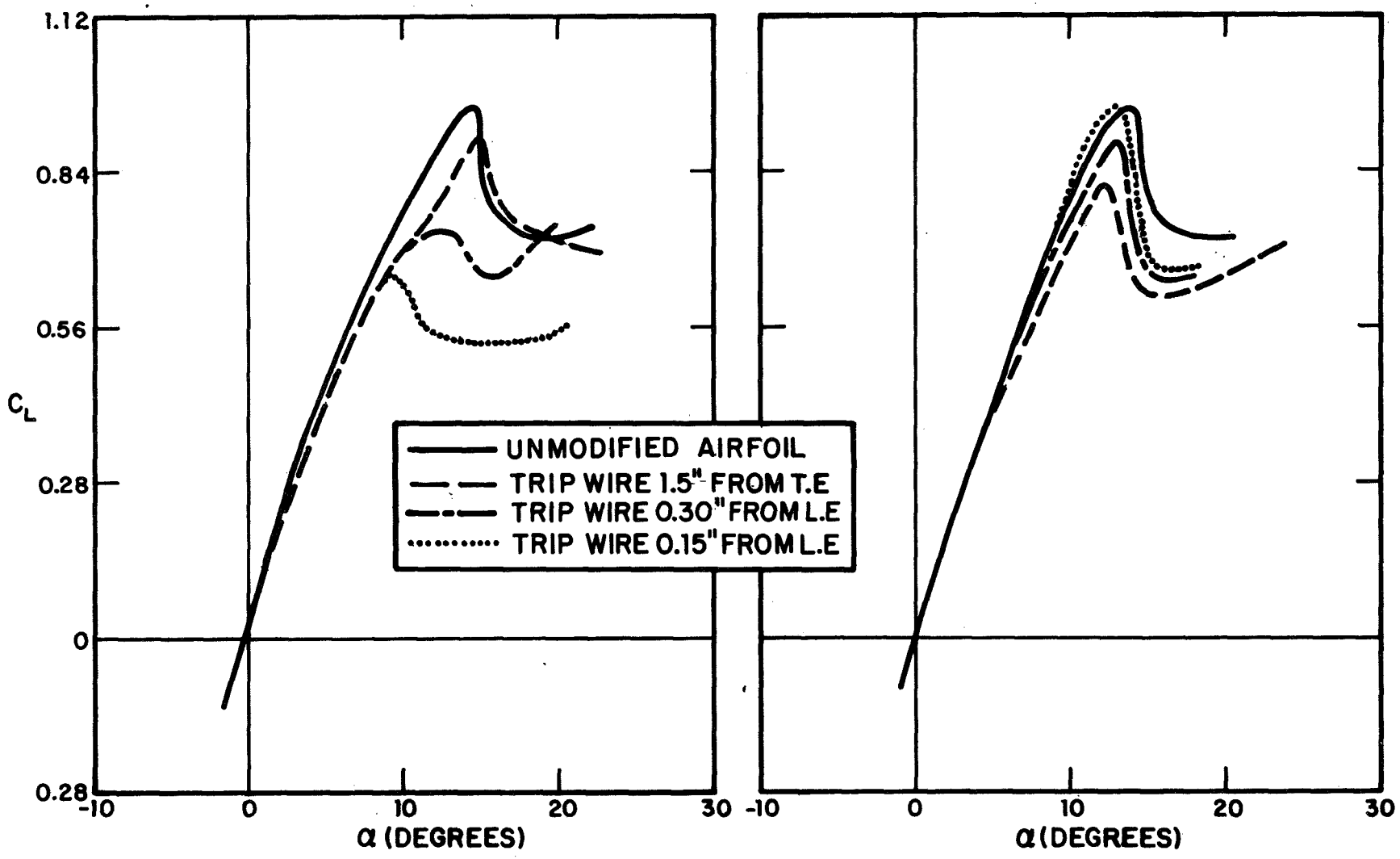

a. TRIP WIRE ON SUCTION SURFACE

b. TRIP WIRE ON PRESSURE SURFACE

FIGURE 31. EFFECT OF TRIP WIRE ON STEADY LIFT OF AIRFOIL

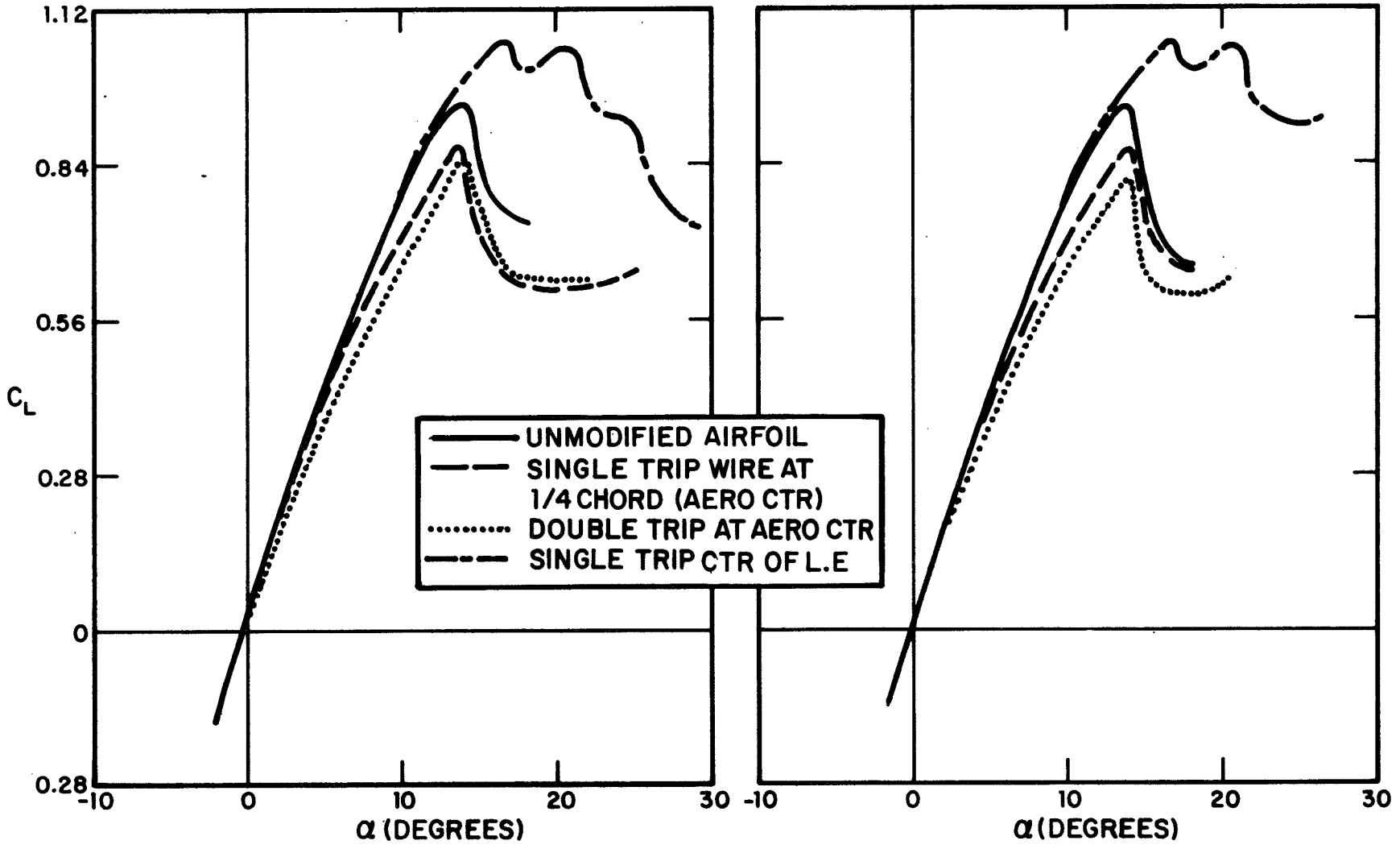

a. TRIP WIRE ON SUCTION SURFACE (WHERE APPLICABLE)

b. TRIP WIRE ON PRESSURE SIDE (WHERE APPLICABLE)

FIGURE 32. EFFECT OF TRIP WIRE(S) ON STEADY LIFT OF AIRFOIL

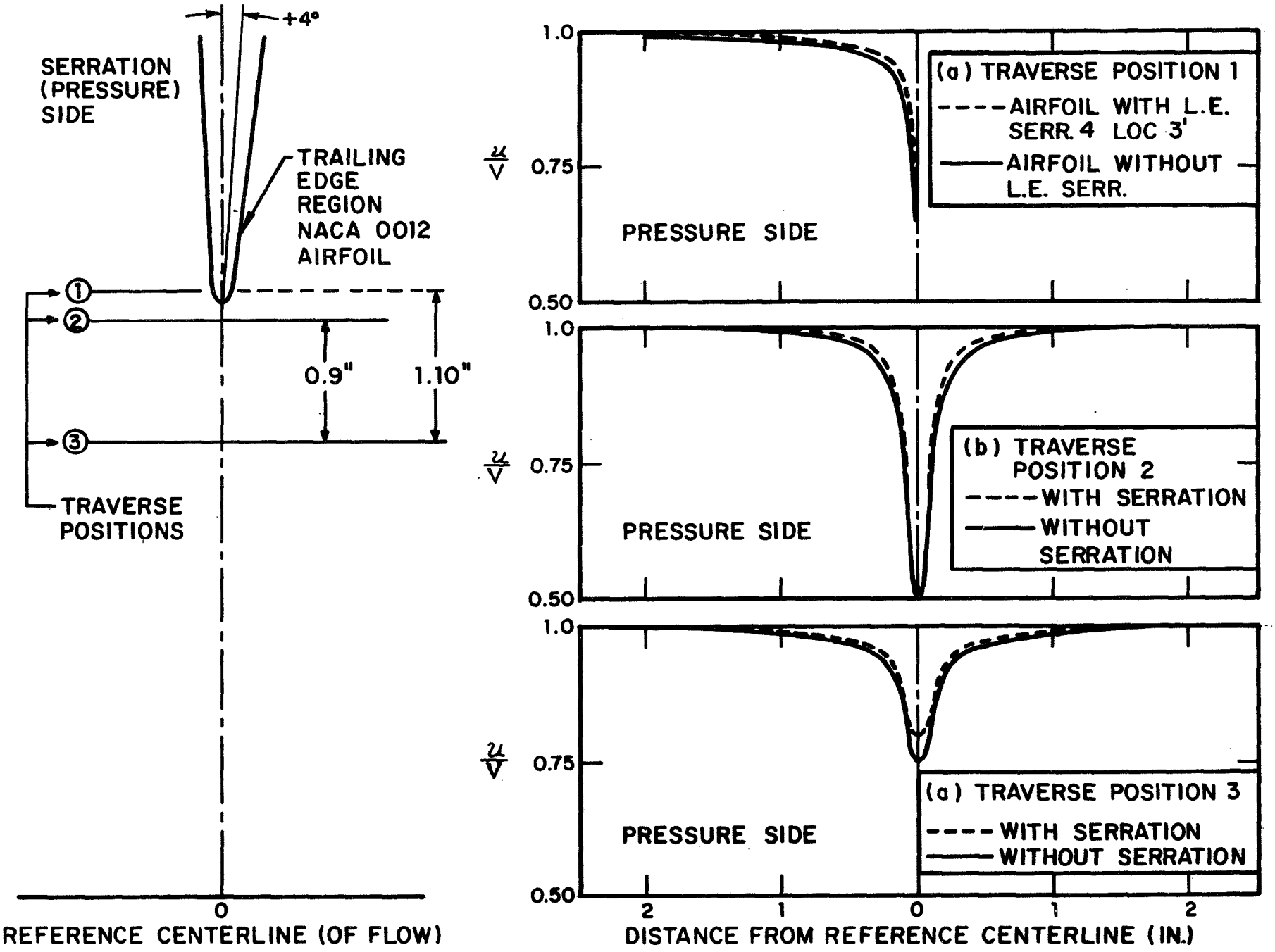

FIGURE 33. EFFECT OF SERRATION 4, LOC. 3' ON MEAN VELOCITY PROFILE IN VICINITY OF TRAILING EDGE

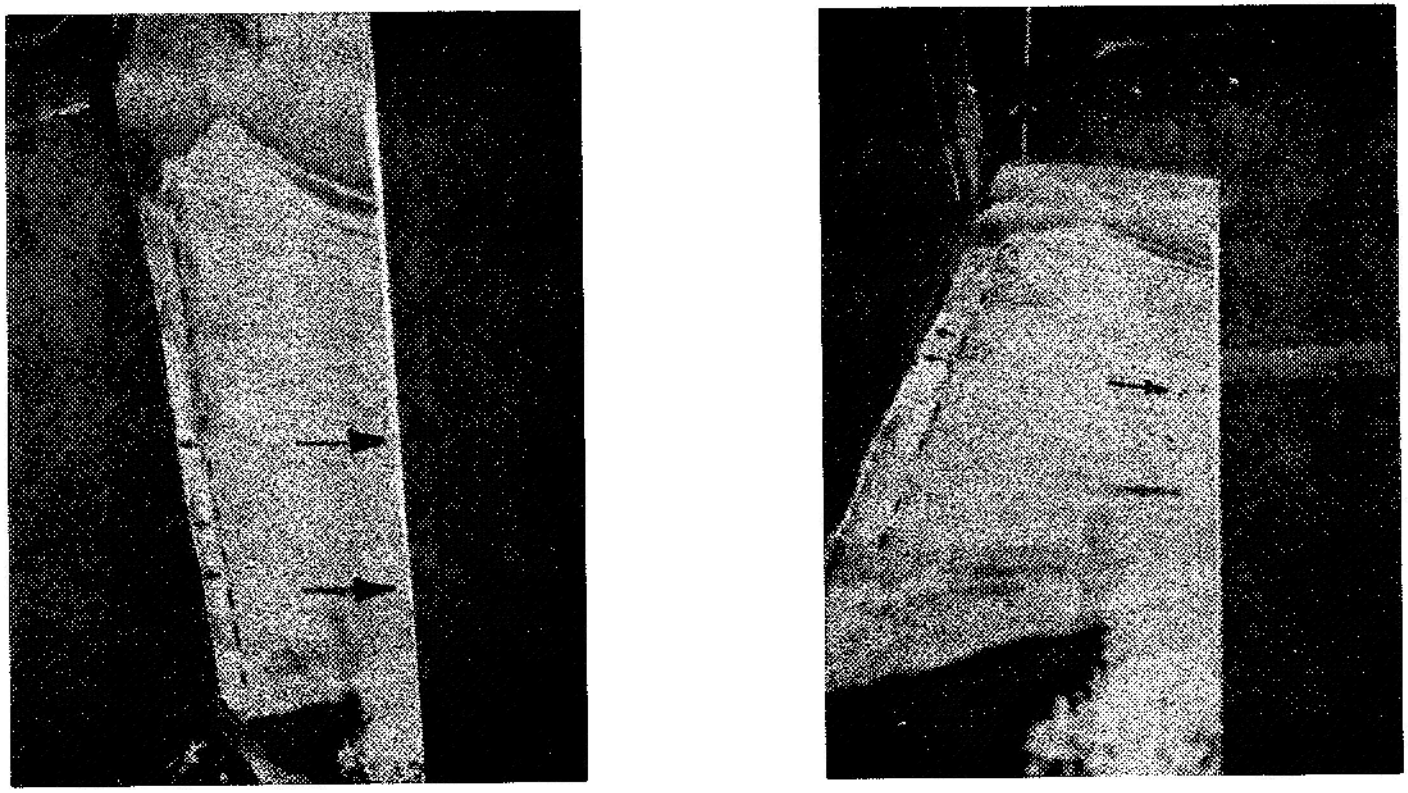

FIGURE 34. FLOW VISUALIZATION; NACA 0012 AIRFOIL; $\alpha = +5^{\circ}$ (Arrows Indicate Direction of Local Mean Flow); V = 60 ft/sec

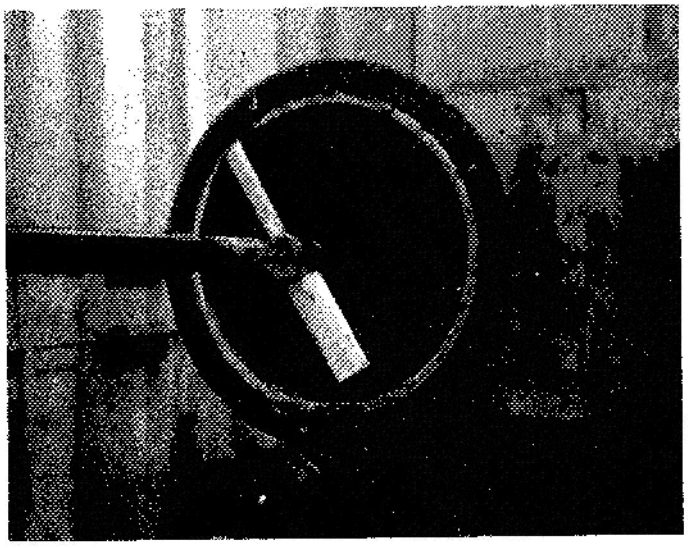

FIGURE 35a. PHOTOGRAPH OF PROPELLER MOUNTED ON SPINNER IN BBN QUIET WIND TUNNEL

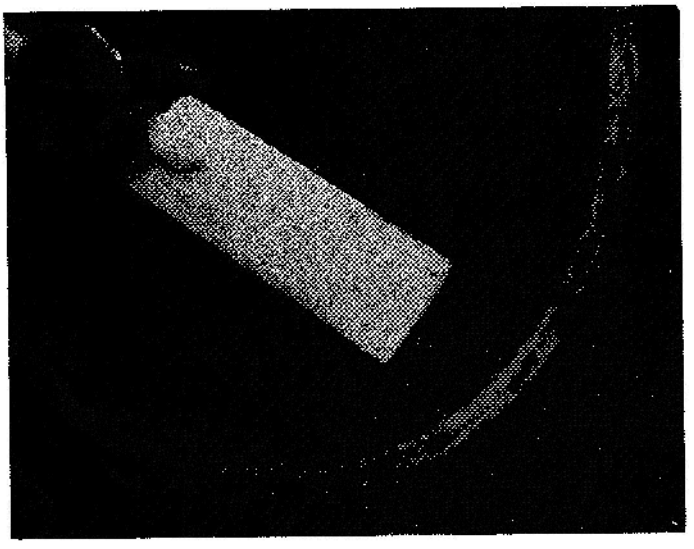

FIGURE 35b. PHOTOGRAPH OF PROPELLER AND SERRATION ATTACHED AT OUTER 1/4 SPAN; 14 IN. DIA., 2 IN. CHORD

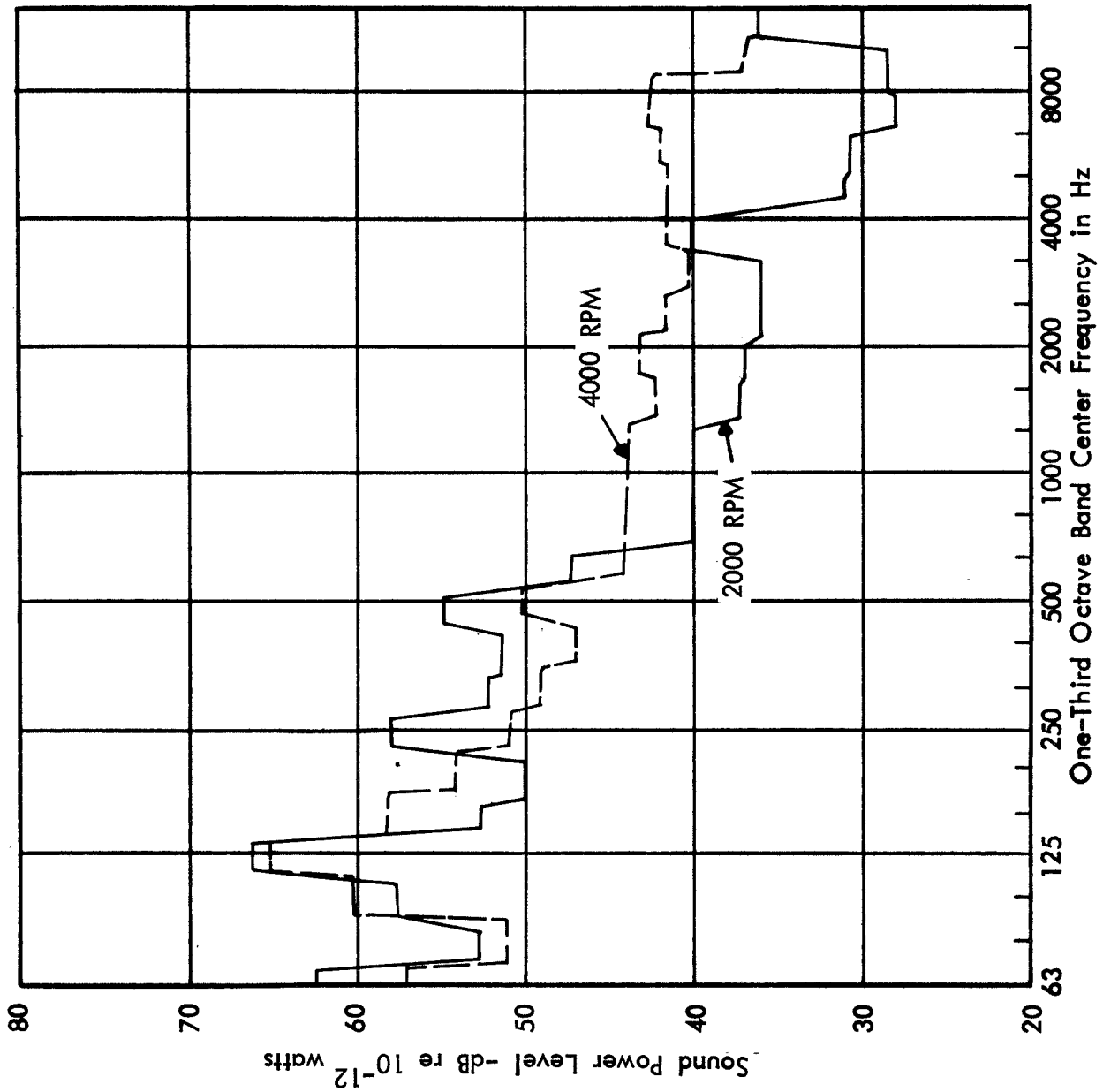

FIGURE 36. BACKGROUND SOUND POWER LEVEL WITH SPINNER ATTACHED AND BLADES REMOVED; V = 40 FT/SEC

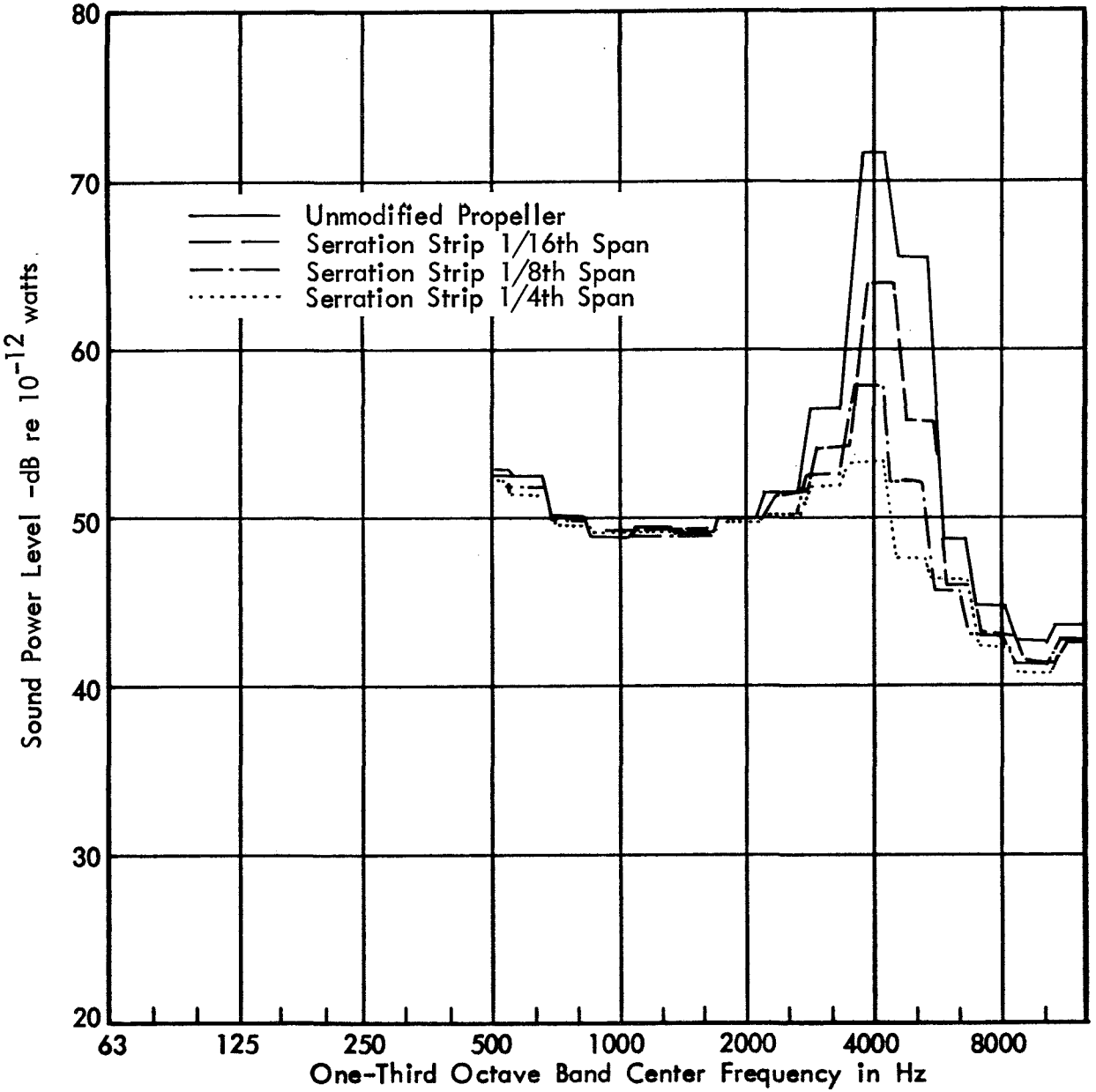

FIGURE 37. EFFECT OF VARYING SPANWISE LENGTH OF SERRATION 5, LOC 2' ON PROPELLER SOUND RADIATION; 2000 RPM, V = 40 FT/SEC, $\alpha_B = 20°$

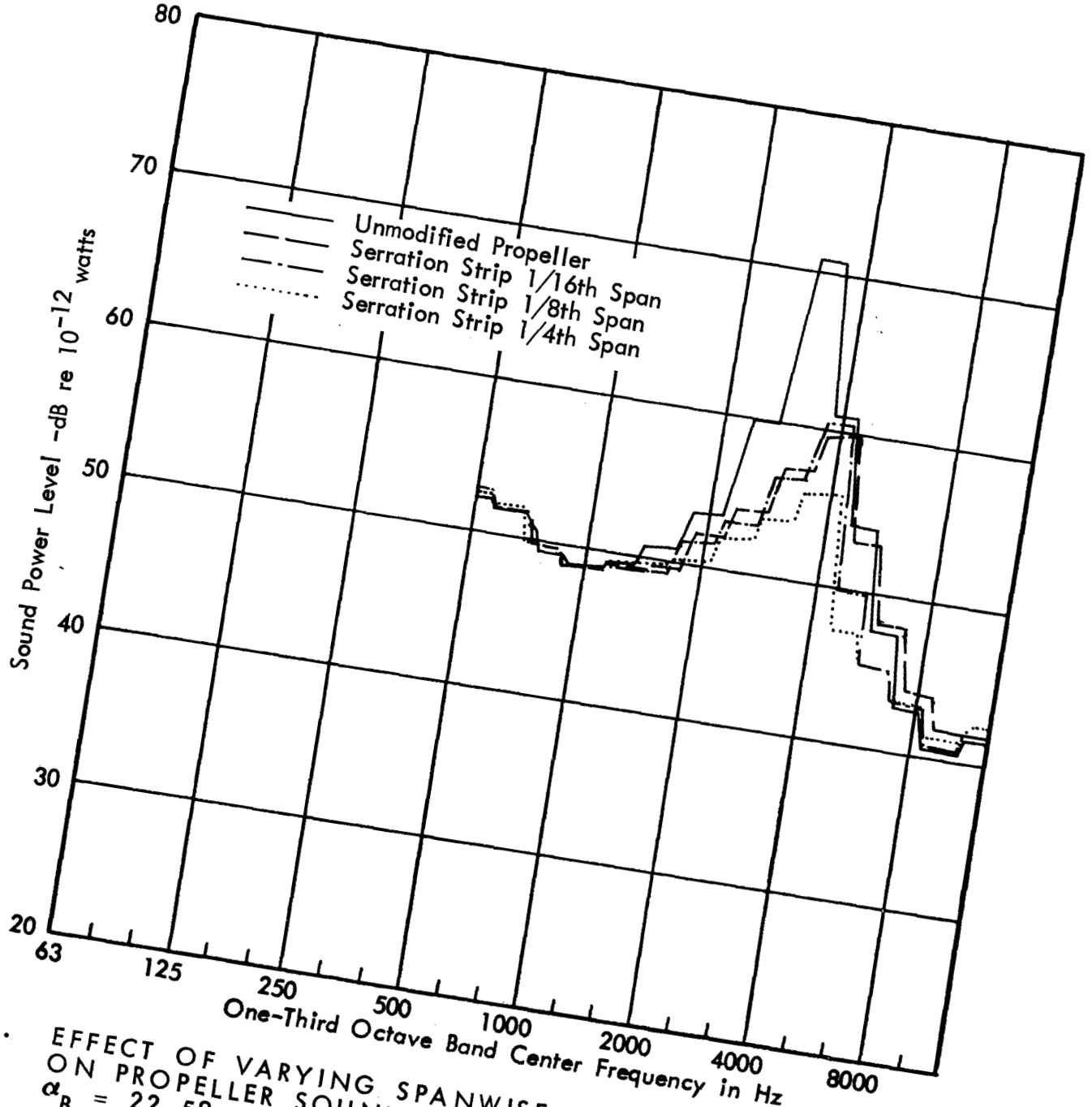

FIGURE 38. EFFECT OF VARYING SPANWISE LENGTH OF SERRATION 5, LOC 2' ON PROPELLER SOUND RADIATION; 2000 RPM, V = 40 FT/SEC, $\alpha_B = 22.5°$

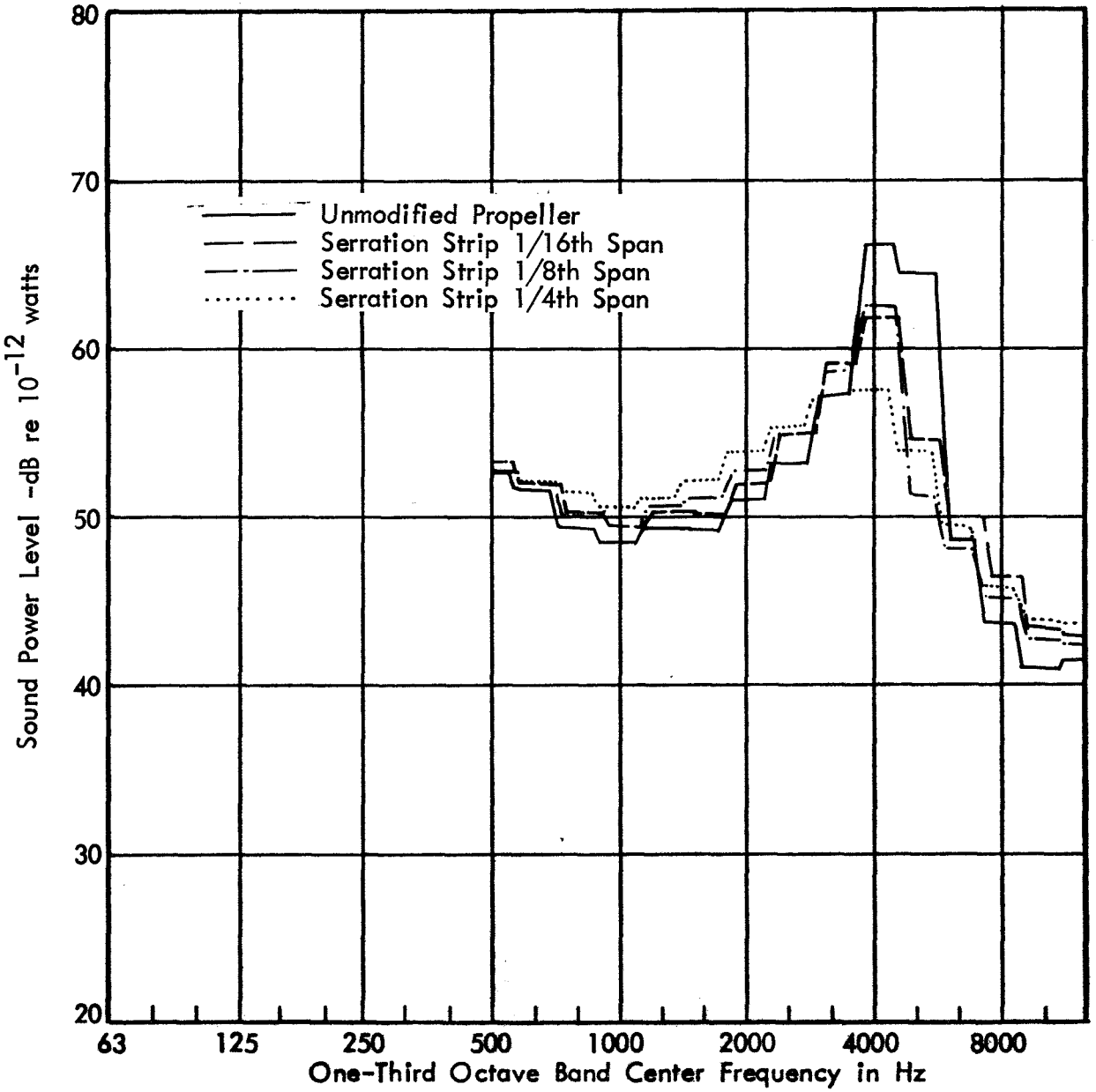

FIGURE 39. EFFECT OF VARYING SPANWISE LENGTH OF SERRATION 5, LOC 2' ON PROPELLER SOUND RADIATION; 2000 RPM, V = 40 FT/SEC, $\alpha_B = 25°$

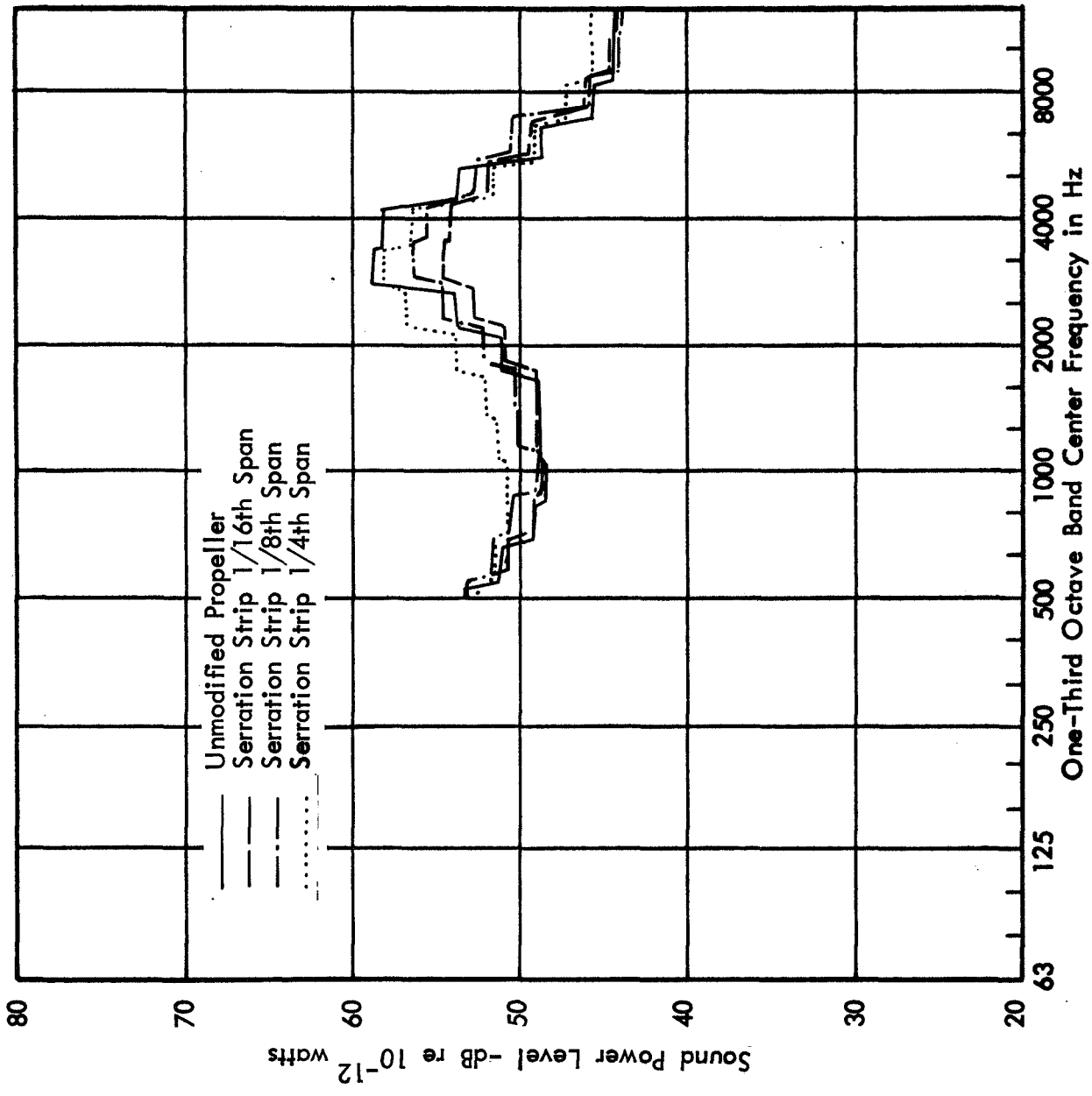

FIGURE 40. EFFECT OF VARYING SPANWISE LENGTH OF SERRATION 5', LOC 2' ON PROPELLER SOUND RADIATION; 2000 RPM, V = 40 FT/SEC, $\alpha_B = 27.5^\circ$

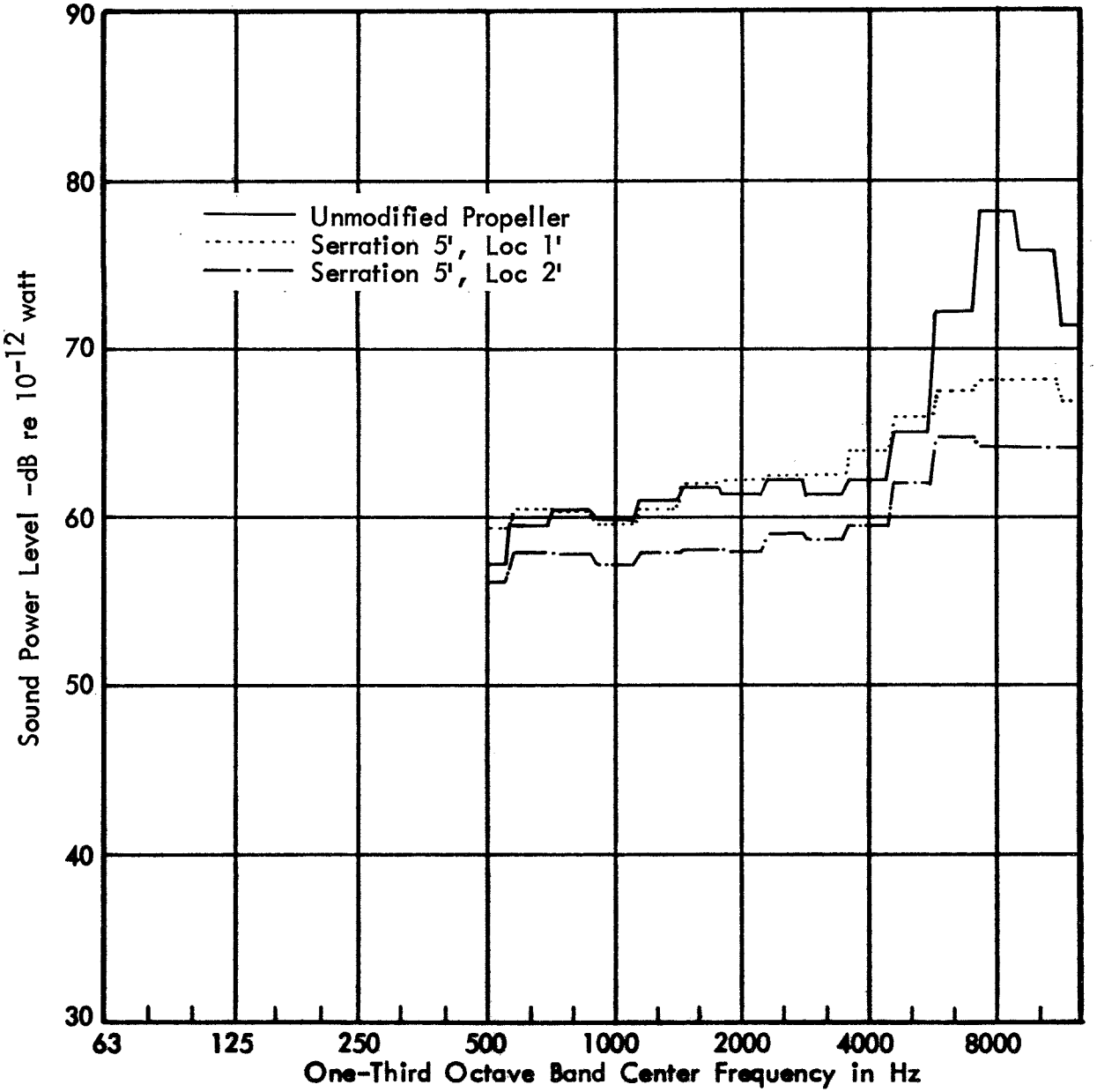

FIGURE 41. EFFECT OF SERRATION 5, LOC 1' AND 2' ON PROPELLER SOUND RADIATION; 4000 RPM, V = 40 FT/SEC, α_B = 17.5°

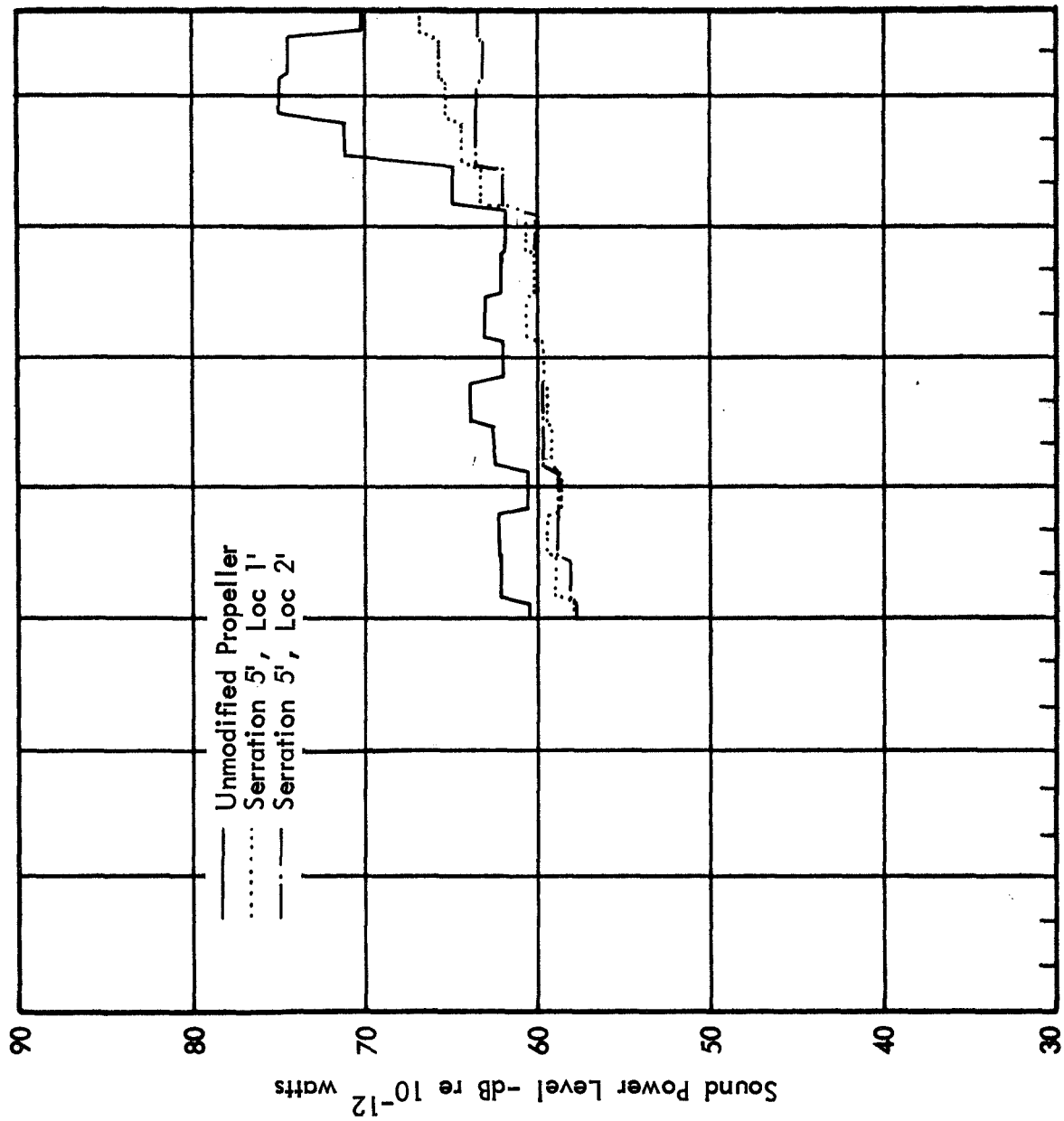

FIGURE 42. EFFECT OF SERRATION 5, LOC 1' AND 2' ON PROPELLER SOUND RADIATION; 4000 RPM, V = 40 FT/SEC, $\alpha_B = 20°$

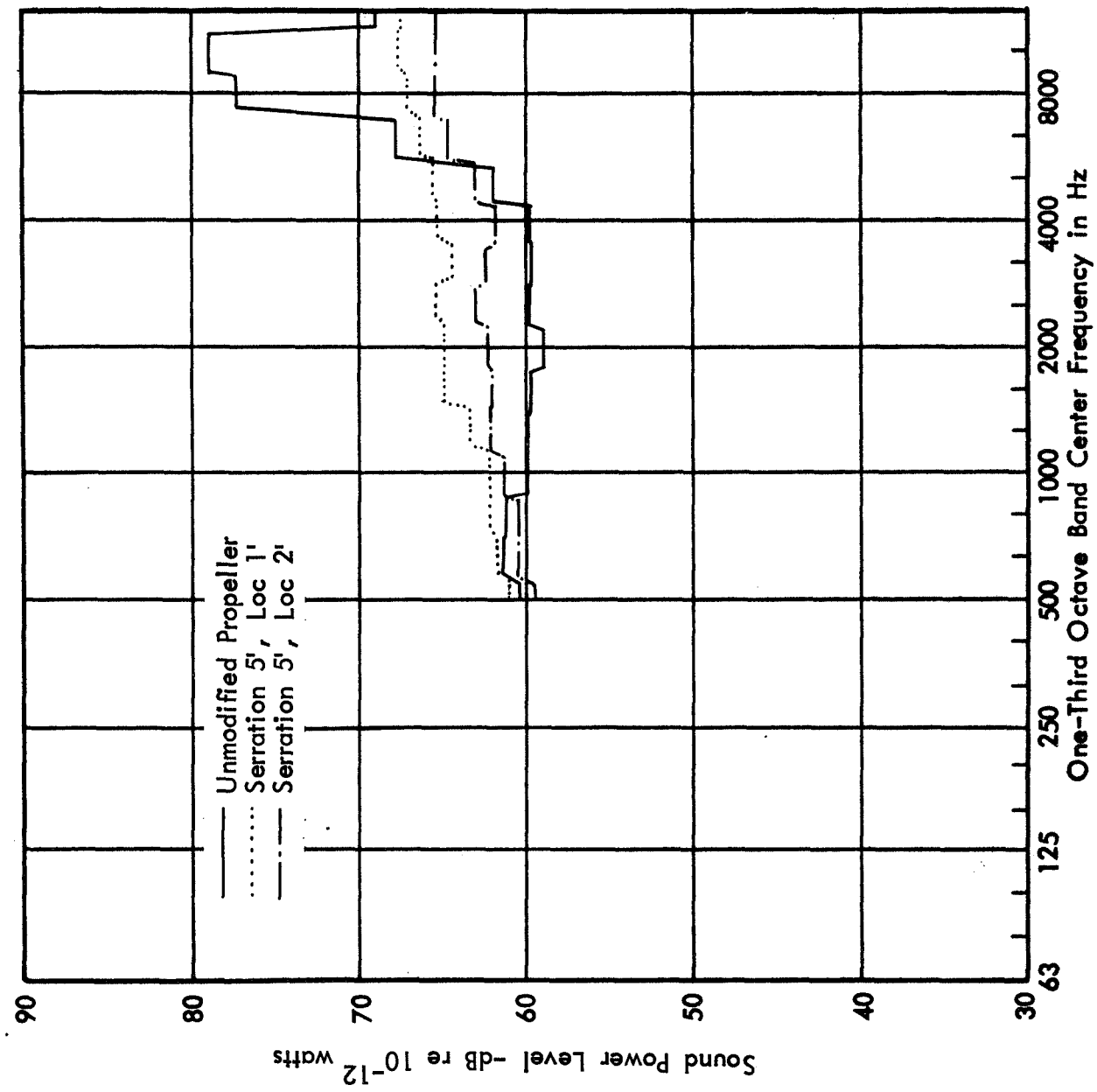

FIGURE 43. EFFECT OF SERRATION 5, LOC 1' AND 2' ON PROPELLER SOUND RADIATION; 4000 RPM, V = 40 FT/SEC, α_B = 22.5°

APPENDIX A

UCLA FREE-JET ANECHOIC FACILITY

The UCLA facility, which is designed to study jet noise, consists of a small subsonic jet exhausting into an anechoic room. A planview of the UCLA free-jet facility is shown in Fig. A-1. The airflow is passed through a water separator to remove possible condensed liquid. Upon exiting the water separator, the airflow enters a 20-ft muffler used to remove any extraneous noises produced by the various system control valves. The flow then enters the 1-1/2-in. diameter pipe which is oriented parallel to and 5-ft above the floor of the test room. The test chamber has mean dimensions of 21-ft long by 22-ft wide by 9-ft 6 in. high.

One of the first tasks undertaken in calibrating the UCLA facility was to determine the frequency response range of the facility. To accomplish this, we placed a broadband monopole sound source at the nozzle exit and recorded the decay in sound pressure level (SPL) in octave bands against distance from the source. We constructed the source by attaching a 1-ft long cardboard tube to a Stromberg-Carlson driver. Since the diameter of the tube was 1/2 in., the sound appeared as monopole at frequencies below 22,000 kHz.

The results of the tests are shown in Figs. A-2 and A-3. Experimental points are presented for only the 1 kHz and 16 kHz frequencies--results for frequencies intermediate between these are comparable. Figure A-2 represents data taken along the jet axis. Figure A-3 represents data taken at a 45° angle from the jet axis. In both cases the data indicate that the room is anechoic at these frequencies. A third set of data taken in a vertical direction from the source to the floor also showed a 6-dB loss per double distance. Thus, the data indicate that the room is sufficiently anechoic for our purposes.

To conduct the directivity experiments, we mounted a self-powered microphone boom, which rotates at a rate of 4.5 degrees per second, on a Bruel and Kjaer (B & K) Type 3921 turntable. This arrangement provides for continuous noise level measurements from 10 to 165 degrees relative to the jet exhaust axis.

A 1/2-in. B & K Type 4133 condenser microphone, covered with an Electrovoice windscreen, was used to traverse the radiation field along the microphone path. The output

of the microphone was fed through a high-pass filter and a B & K Type 2107 Frequency Analyzer (used as an amplifier) into an Ampex Model 600 tape recorder for later analysis. A high-pass filter removed the low-frequency "wind noise" which results when the microphone comes into direct contact with the jet exhaust at the beginning of its traverse. Also eliminated by the high-pass filter is that part of the acoustic signal for which the test chamber is not anechoic.

At the start of each traverse, a 1-kHz tone of approximately 1 sec duration was automatically recorded on the annotation track of the tape recorder from a Hewlett-Packard model 200AB audio oscillator. This tone was later used as a reference point for correlation of the noise signals with the angular location of the microphone. A schematic of the instrumentation system is shown in Fig. A-4.

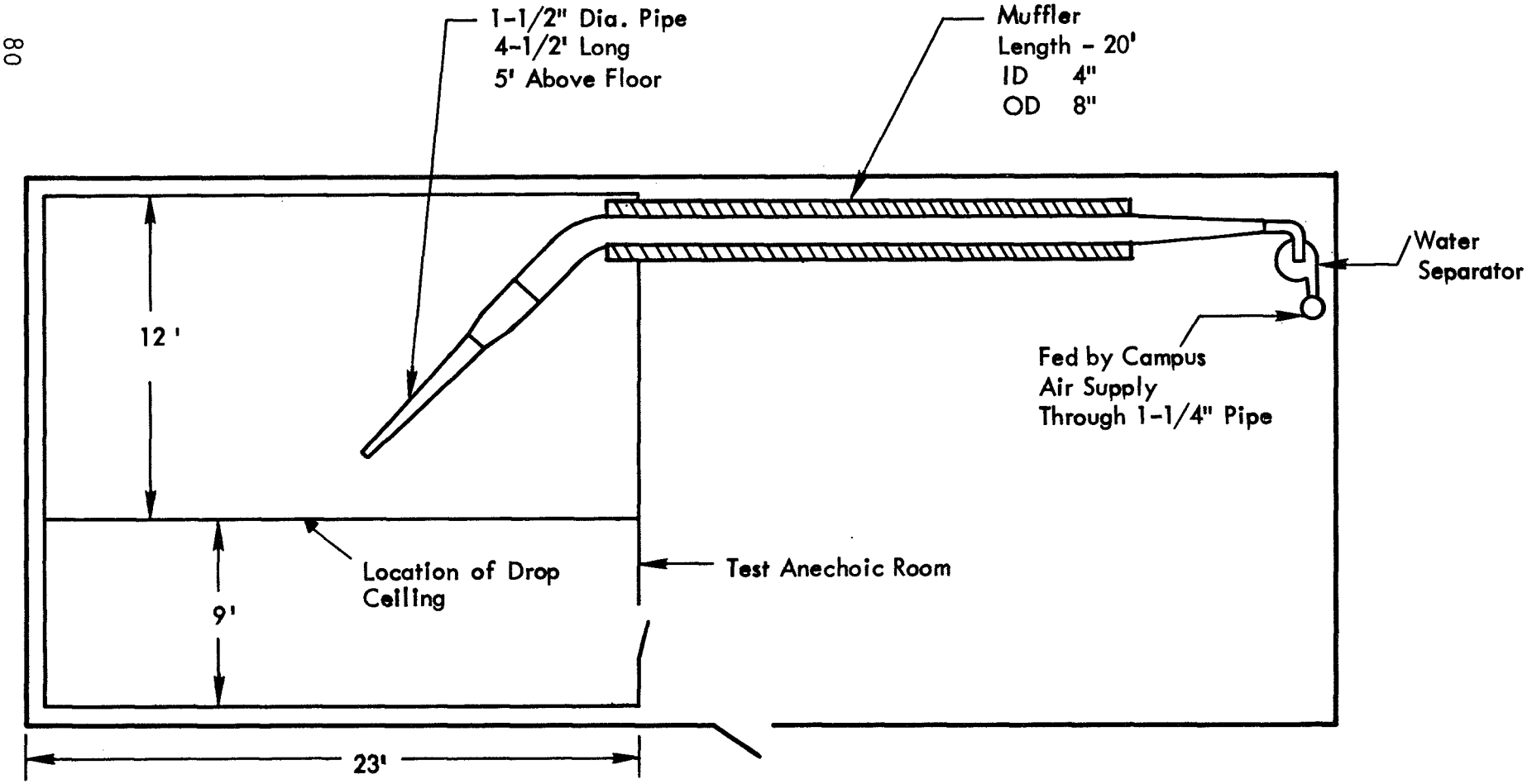

FIGURE A-1. SCHEMATIC OF UCLA JET FLOW FACILITY (PLANVIEW)

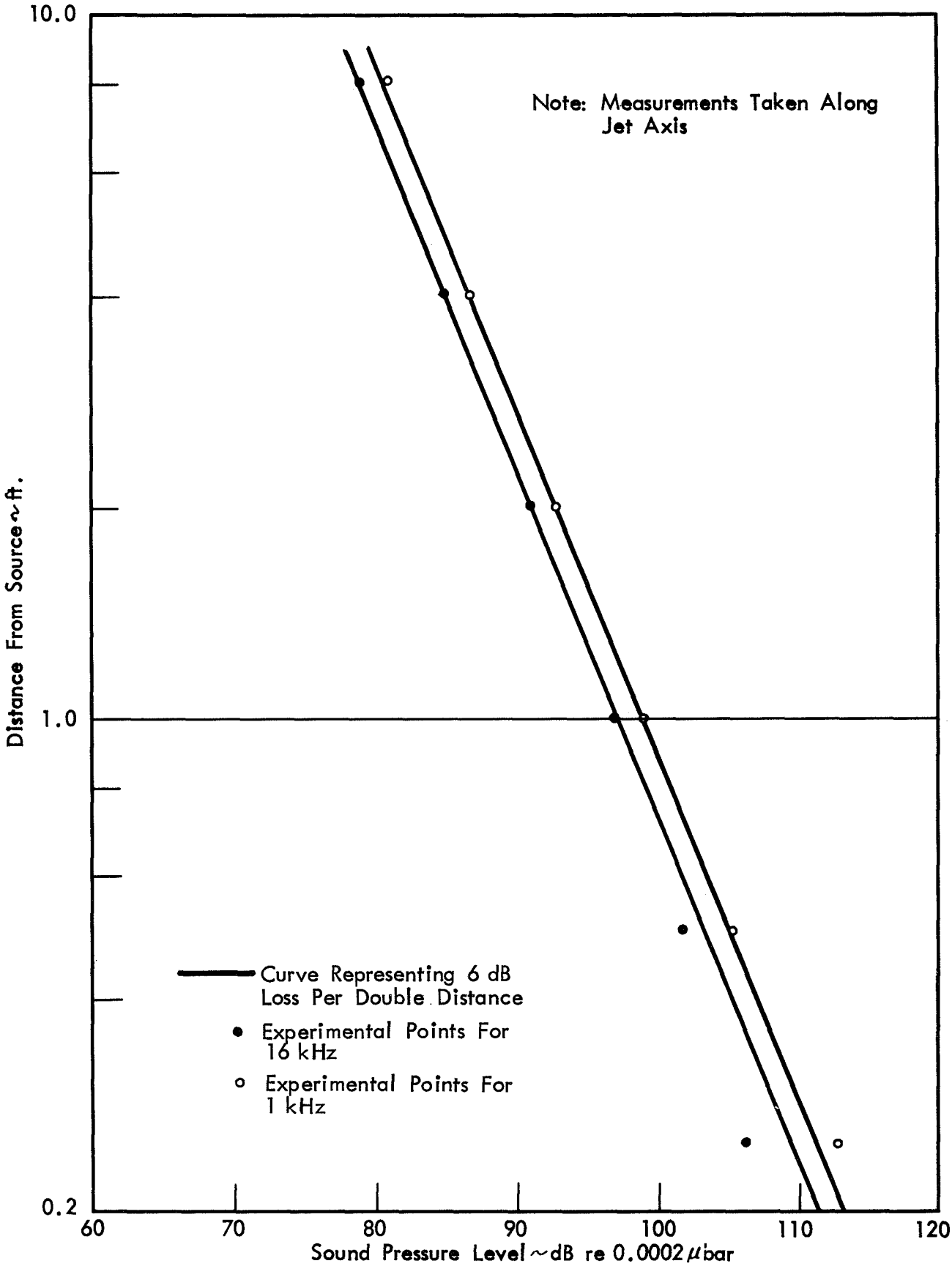

FIGURE A-2 EXPERIMENTAL CONFIRMATION THAT UCLA JET FLOW FACILITY IS ANECHOIC

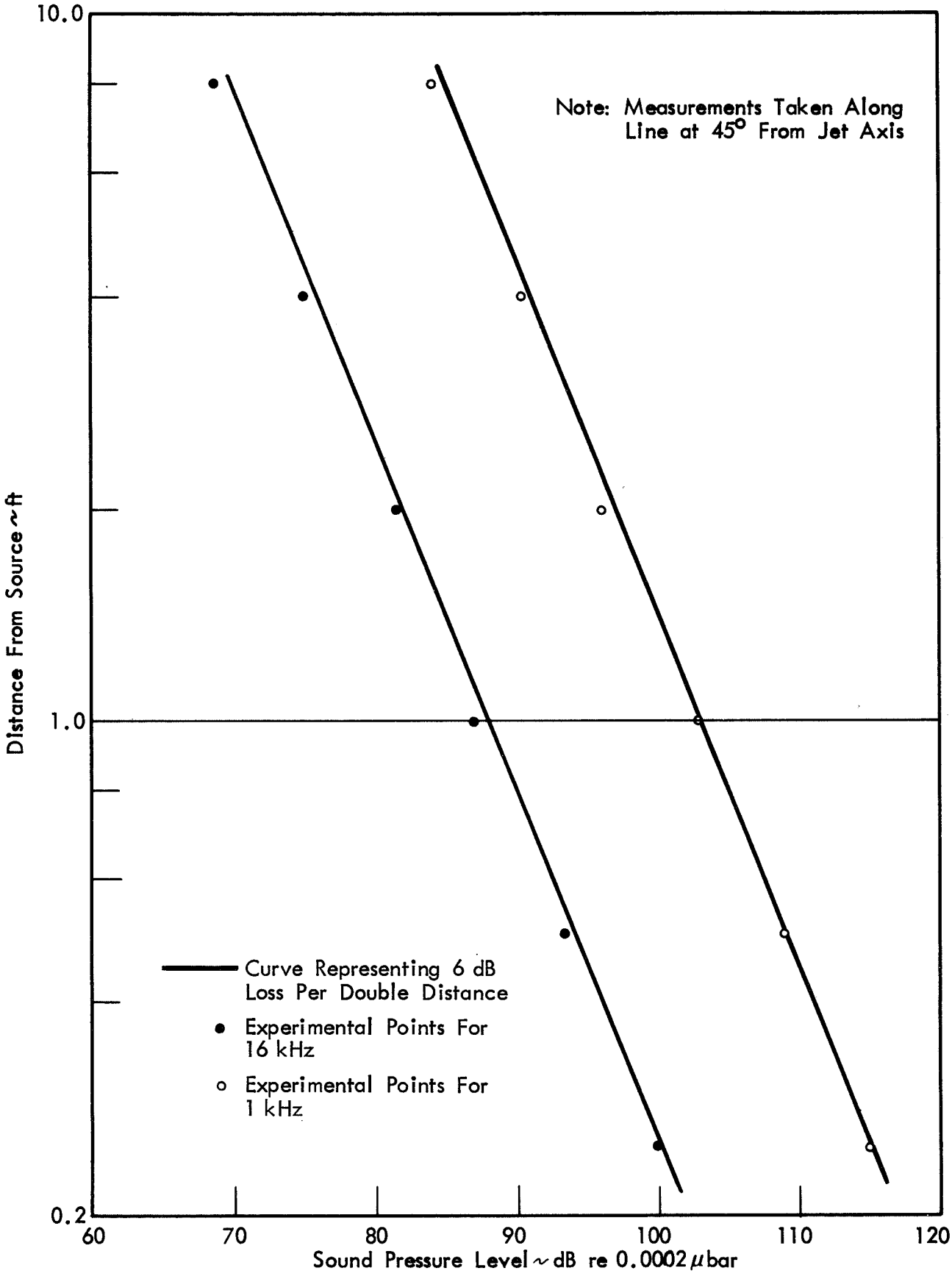

FIGURE A-3 EXPERIMENTAL CONFIRMATION THAT UCLA JET FLOW FACILITY IS ANECHOIC

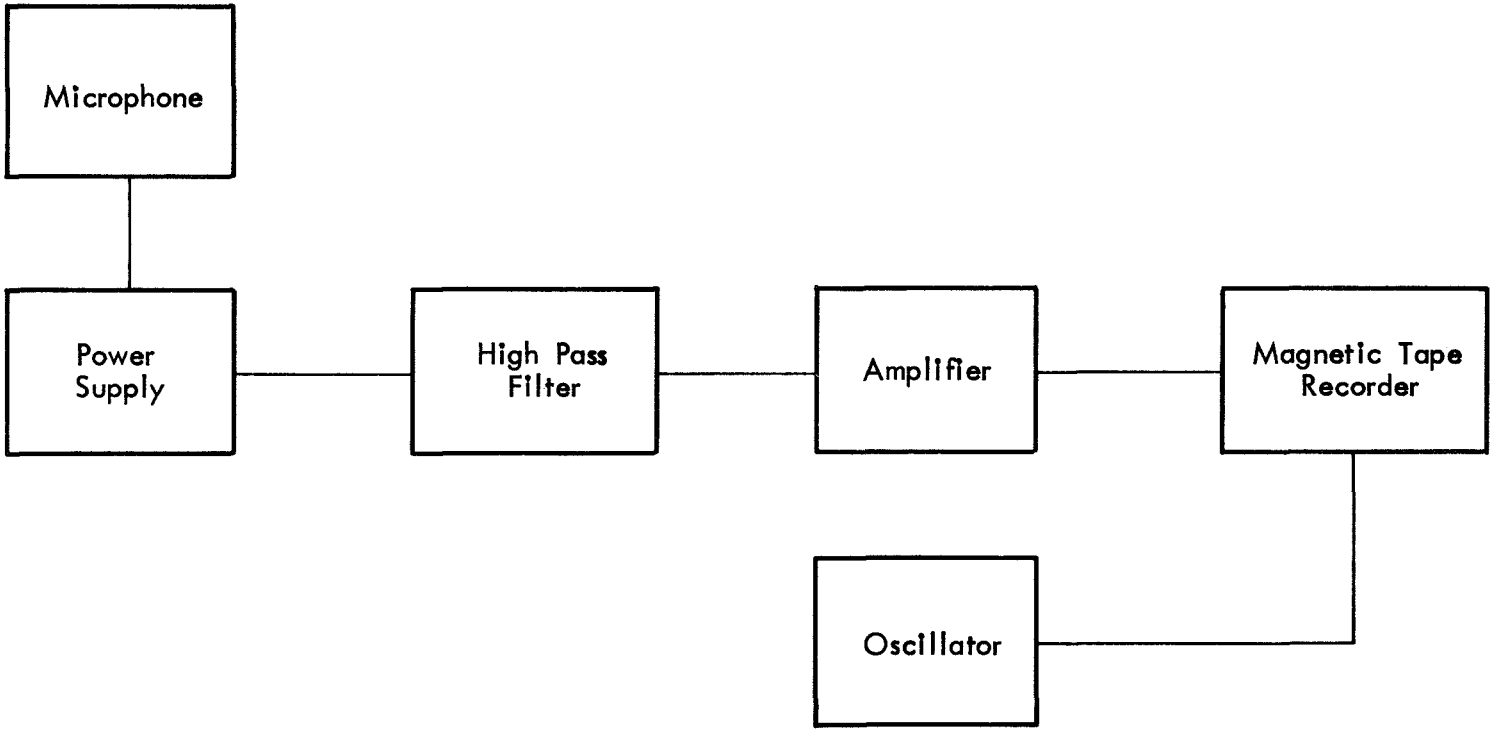

FIGURE A-4 SCHEMATIC OF NOISE MEASUREMENT SYSTEM

APPENDIX B

EXTENSION OF LIEPMANN'S MODEL TO PREDICT SOUND RADIATION FROM SMALL AIRFOILS IN TURBULENT FLOW

Liepmann's model analytically predicts the mean square lift fluctations imparted to a small, thin two-dimensional airfoil of chord c moving with velocity V through a turbulent fluid. The relationship between the fluctuating lift and the fluctuations in angle of attack induced by the turbulent fluid is given by unsteady thin airfoil theory.

Liepmann assumes that the turbulent fluid is homogeneous and isotropic and that the fluctuating instantaneous angle-of-attack (α) are given by

$$\alpha = \frac{w}{V} \quad , \tag{B-1}$$

where w represents the transverse (i.e., in the direction normal to the airfoil chord and span) velocity fluctuations. Equation (B-1) is valid as long as the fluctuations are small. Liepmann used the work of Sears [B-1] to connect the changes in angle-of-attack to the changes in lift for the case of an incident vertical velocity consisting of harmonic waves of angular frequency ω and wavelength $2\pi V/\omega$ given by

$$\frac{w(x,t)}{V} = \alpha_o e^{i\omega[t-x/V]} \quad , \tag{B-2}$$

where x corresponds to chordwise distance. Equation (B-2) assumes a fixed sinusoidal gust passing the airfoil at a velocity V. For this velocity distribution, Sears finds the following expression for the lift coefficient,

$$C_L(t) = 2\pi\alpha_o e^{i\omega t}\phi(k) \quad , \tag{B-3}$$

where $k = (\omega c/2V)$ is approximately the ratio of chord length to wavelength of the gust and $\phi(k)$ may be thought of as an admittance relating the forcing function $\alpha(t)$ to the response $C_L(t)$.

We assume that the turbulence pattern is frozen - i.e., that the convective rate of change is small compared to the local rate of change. Thus, the turbulent angle of attack will depend upon $t-(x/V)$ only, and Sears results can be applied.

With this assumption, Liepmann shows that the mean square lift coefficient may be written as

$$\langle C_L^2 \rangle = 4\pi^2 \int_0^\infty f(\omega) |\phi(k)|^2 d\omega \quad , \tag{B-4}$$

where $f(\omega)$ is the power spectrum of $\alpha(t)$ defined as

$$\langle \alpha^2 \rangle = \langle \frac{w^2}{V^2} \rangle = \int_0^\infty f(\omega) d\omega \tag{B-5}$$

and $|\phi(k)|^2$ is approximated by the simple expression

$$|\phi(k)|^2 \doteq \frac{1}{(1+2k)} \quad . \tag{B-6}$$

The power spectrum $f(\omega)$ is most conveniently determined from the Fourier transform of the autocorrelation function $R(\tau)$ of $\langle w^2 \rangle$. Experiments [B-2,B-3] show that in isotropic turbulence, $R(\tau)$ has very nearly the form

$$\langle w(t)w(t+\tau) \rangle = R(\tau) = \langle w^2 \rangle e^{-\frac{\tau V}{L}} [1-\frac{V\tau}{2L}] \quad . \tag{B-7}$$

Here, L is the so-called "scale of turbulence" and is defined by

$$LR(0) = \int_0^\infty R(x) dx \quad , \tag{B-8}$$

where $\tau = x/V$, which is valid for frozen turbulent flow, and

$$R(x) = \langle w^2 \rangle e^{-x/L} [1-\frac{x}{2L}] \quad . \tag{B-9}$$

$R(\tau)$ should have, by definition, a zero slope at $\tau=0$. An examination of $R(\tau)$ shows a nonzero slope which is inversely proportional to L, the characteristic length scale of the turbulent eddies. The autocorrelation function $R(\tau)$ describing a homogeneous isotropic turbulent flow really has two characteristic lengths, one being L, the "scale of turbulence" mentioned earlier, and the other a "microturbulent length", which is a measure of the size of the smallest eddy. The microturbulent length is proportional to $\sqrt{\nu/V}$, where ν is the kinematic viscosity of the fluid. Thus, the model developed above is not valid for small values of L.

The power spectrum $f(\omega)$ follows immediately by taking the Fourier transform of Eq. (B-7), yielding

$$f(\omega) = R\{\frac{2}{\pi}\int_0^\infty R(\tau)e^{i\omega\tau}d\tau\} \quad , \tag{B-10}$$

where R denotes the real part.

To apply Liepmann's analysis for predicting the airfoil sound radiation, we must determine the power spectrum of the time derivative of C_L, that is, $\langle\dot{C}_L^2\rangle$. The most direct way to determine $\langle\dot{C}_L^2\rangle$ is to determine first the power spectrum for $\langle\dot{\alpha}^2\rangle$ given by

$$\langle\dot{\alpha}^2\rangle = \frac{\langle\dot{w}^2\rangle}{V^2} = R''(\tau) \quad . \tag{B-11}$$

The power spectrum for $\langle\dot{\alpha}^2\rangle$, denoted by $g(\omega)$, is determined by taking the real part of the Fourier transform of $R''(\tau)$; that is,

$$g(\omega) = R\{\frac{2}{\pi}\int_0^\infty R''(\tau)e^{i\omega\tau}d\tau\} \tag{B-12}$$

Differentiating Eq. (B-7) twice with respect to the time delay and substituting into Eq. (B-12) yields

$$g(\omega) = \frac{V}{\pi L}\frac{\langle w^2\rangle}{V^2}\{\frac{3+5\left(\frac{\omega L}{V}\right)}{\left[1+\left(\frac{\omega L}{V}\right)^2\right]^2}\} \tag{B-13}$$

Substituting Eqs. (B-6) and (B-13) into the expression

$$\langle\dot{C}_L^2\rangle = \int_0^\infty g(\omega)|\phi(k)|^2 d\omega \quad , \tag{B-14}$$

and integrating yields

$$\langle\dot{C}_L^2\rangle = 4\frac{\langle w^2\rangle}{c^2}[\frac{\eta^2(4\eta+3\pi)}{4\pi(\eta^2+1)} + \frac{5\eta^2(1-\eta^2)}{4(\eta^2+1)^2} + \frac{(3\eta^2+5)}{\pi(\eta^2+1)^2}\eta^3\log\eta], \tag{B-15}$$

where $\eta = \frac{\pi c}{L}$.

The time derivative of the fluctuating lift $\dot{L}$ and lift coefficient C_L are related by the expression

$$\dot{L}(t) = \dot{C}_L(t) \cdot \frac{1}{2} \rho V^2 S \quad , \tag{B-16}$$

where ρ is the fluid density and S the airfoil surface area. The final expression for the sound radiated from a *small* airfoil in turbulent flow follows immediately by substituting Eq. (B-16) into Eq. (3) (Curle's point dipole sound equation) where $\dot{F} = \dot{L}$ yielding

$$\langle p^2 \rangle = \frac{\langle w^2 \rangle \rho^2 V^4 S^2}{16\pi^2 c^2 c_o^2 x^2} \left[\frac{\eta^2(4\eta+3\pi)}{4\pi(\eta^2+1)} + \frac{5\eta^2(1-\eta^2)}{4(\eta^2+1)^2} \right.$$

$$\left. + \frac{(3\eta^2+5)}{\pi(\eta^2+1)^2} \eta^3 \log \eta \right]. \tag{B-17}$$

REFERENCES

B-1. Sears, W. R.: Some Aspects of Nonstationary Airfoil Theory and Its Practical Applications. *J. Aero. Sci. 8*, no. 2, Feb. 1941, p. 104.

B-2. Dryden, H.L.: Turbulence Investigations at the National Bureau of Standards. Presented at International Congress of Applied Mechanics, Cambridge, England, 1938.

B-3. Liepmann, H. W.; Laufer, J; and Liepmann, K.: On The Spectrum of Isotropic Turbulence. NACA TN2473, 1951.

APPENDIX C

BBN QUIET WIND TUNNEL

The BBN wind tunnel is a low turbulence, low noise free-jet facility designed specifically to study low-speed aerodynamic noise phenomena. Vertical and plan views of the facility are shown in Fig. C-1. The facility operates in the "suction mode" (i.e., the blower lowers the pressure in the room), with air entering the room through a smoothly contoured converging nozzle having a 15-to-1 area contraction. The speed of the low turbulence core of the jet is variable between 20 and 120 fps in a 16-in. by 16-in. square cross-section or an 18-in. diameter round cross-section.

Surrounding the free-jet facility is a semireverberant room of approximately 3000 ft^3 with ceiling and one wall skewed to improve the uniformity of the reverberant sound field. The "cutoff frequency" of the room is 180 Hz (in 1/3-octave bands). Below this frequency, absolute sound measurements are not highly accurate, but meaningful *relative* measurements may be made. To achieve a space-averaged sound measurement, we mount the microphone on a pendulum which has a period of approximately 2 sec. The measured sound data has been found to be very repeatable.

A General Radio Model 1521 Real-Time Analyzer is used for directly recording spectra of sound power from a space-averaged measurement of mean square pressure (SPL). The GR Analyzer has a spectrum shaper which allows weighting of the individual 1/3-octave bands through a range of ±25 dB. An ILG fan is used as the known broadband sound power source, and the SPL measurements are appropriately weighted to give a direct 1/3-octave band plot in dB re 10^{-12} watts.

The flow speed is monitored by a standard pitot-static tube used with a Pace-Whittaker Model P7D differential-pressure sensor and a Hewlett-Packard Model 412A Vacuum Tube Voltmeter. The acoustic measurements are made with a B & K Model 4131 1-in. condenser microphone with random incidence corrector; the microphone connects into a B & K Model 2513 cathode follower and B & K Model 2801 power supply. A GR Model 1551B Sound Level Meter (variable gain) is used as a preamplifier.

Spectral data is obtained with a GR Model 1321 1/3-Octave Band Real-Time Analyzer. A 32-sec sampling period is used; thus, the sound measurements are repeatable

within ±0.5 dB in most bands. The spectra data are then immediately plotted on a BBN Plotamatic (TM) Model 800 X-Y plotter. A schematic of the noise measurement system is shown in Fig. C-2.

The fluctuating force and moment measurements were made with a six-degree-of-freedom, eight-component force balance designed and built by BBN. A unique technique employed by BBN's transducer development group to isolate force direction results in mechanical crosstalk between force-sensing elements of less than 1%.

The force balance is mounted on a massive vibration-isolated turntable and outputs of the individual sensing elements are amplified by D.C.-differential amplifiers having variable gain of up to 2000:1. The outputs of the various channels are combined to give lift, drag, etc. through use of a sum-and-difference amplifier. Both steady-state and fluctuating output signals are plotted on a BBN Model 800 Plotomatic X-Y Plotter. Spectral measurements are obtained with the General Radio Model 1521 1/3-Octave Band Real-Time Analyzer.

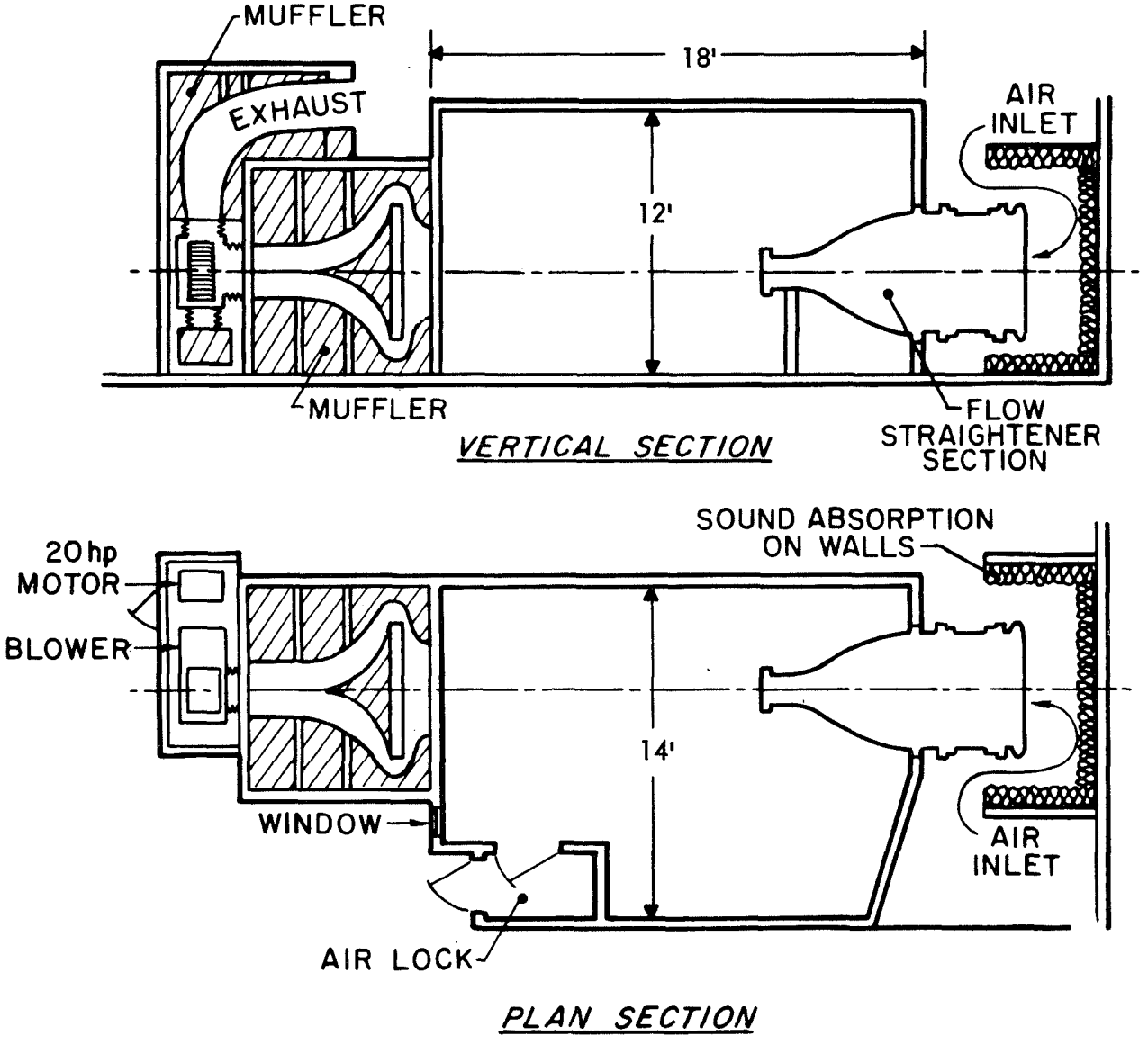

FIGURE C-1. SCHEMATIC OF BBN QUIET WIND TUNNEL

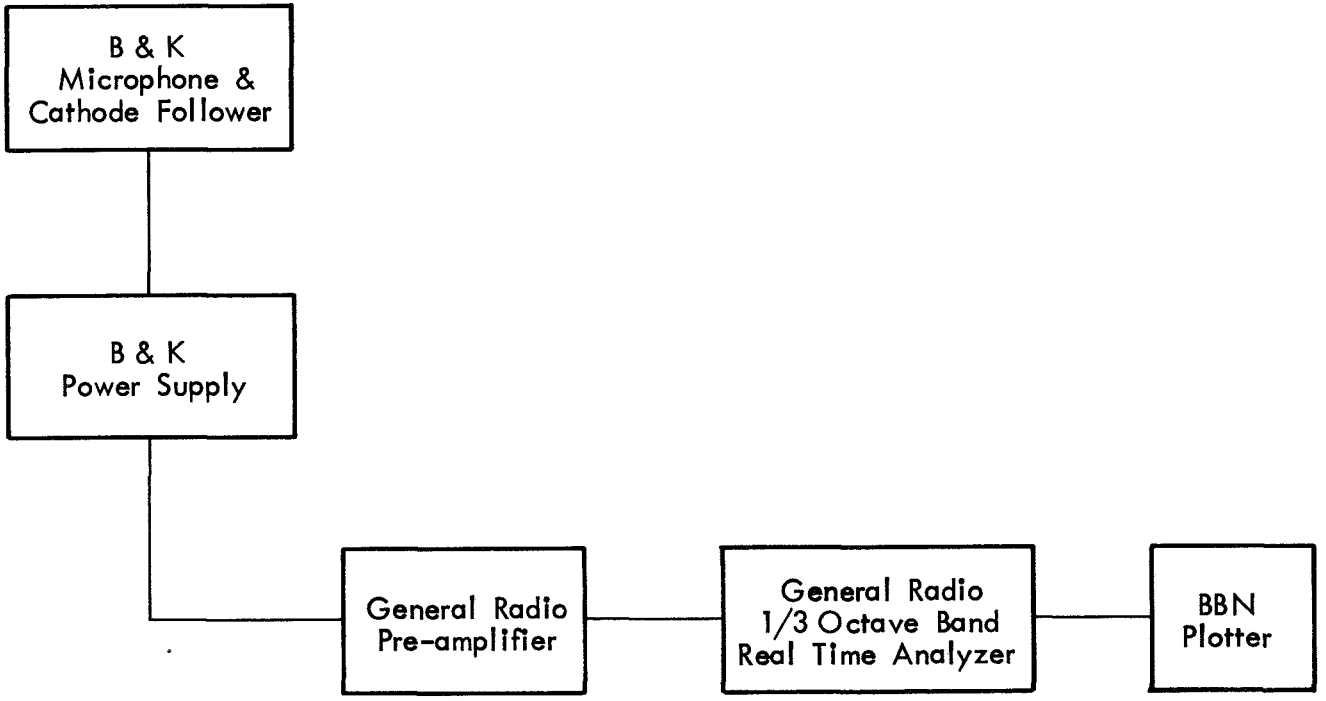

FIGURE C-2. SCHEMATIC OF NOISE MEASUREMENT SYSTEM